REPORT 1359

THIN AIRFOIL THEORY BASED ON APPROXIMATE SOLUTION OF THE TRANSONIC FLOW EQUATION [1]

By JOHN R. SPREITER and ALBERTA Y. ALKSNE

SUMMARY

The present paper describes a method for the approximate solution of the nonlinear equations of transonic small disturbance theory. Although the solutions are nonlinear, the analysis is sufficiently simple that results are obtained in closed analytic form for a large and significant class of nonlifting airfoils. Application to two-dimensional flows with free-stream Mach number near 1 leads, for instance, to general expressions for the determination of the pressure distribution on an airfoil of specified geometry and for the shape of an airfoil having a prescribed pressure distribution and gives, furthermore, the correct variation of pressure with Mach number at Mach number 1. For flows that are subsonic everywhere, the method yields a pressure-correction formula that is more accurate than the Prandtl-Glauert rule and compares favorably with existing higher approximations. For flows that are supersonic everywhere, the method yields the equivalent, in transonic approximation, of simple wave theory. Results obtained by application of these general expressions are shown to correspond closely to existing solutions and to experimental data for a wide variety of airfoils.

INTRODUCTION

The difficulty of solving the nonlinear equations of motion of a compressible inviscid gas has led to widespread use of approximate methods in the practical solution of the problems of airfoil theory. The simplest and most versatile approximate method is that based on a complete linearization of the equations and stems from the pioneering work of Munk, Prandtl, Glauert, Ackeret, and others (see refs. 1 and 2 for a résumé). Although this linear theory of compressible flow has been extensively developed in recent years and is widely used in aeronautical applications, it has two limitations that are of significance in the present discussion. First, linearized theory gives only a first approximation that is correct for airfoils of small thickness ratio. This limitation is, in some respects, of continually diminishing significance as the aeronautical engineer is forced to use thin wings and slender bodies to avoid heavy penalties in wave drag. If the airfoil is not sufficiently thin, however, corrections are necessary and higher order theories have been developed to fill the need (see ref. 3 for a résumé). Second, and more important for the present discussion, linearized theory requires, in general, that the Mach number be sufficiently removed from unity that the flow is either purely subsonic or purely supersonic. If both subsonic and supersonic velocities occur in different parts of a single flow field, the flow is said to be transonic and the results of neither linear theory nor the existing higher order theories are, even qualitatively, in agreement with the experimentally observed flows.

Transonic flows have been studied successfully by consideration of a simplified, although still nonlinear, theory that was originally conceived in an effort to provide a useful first approximation for the pressures and forces on thin wings and slender bodies in inviscid flows with free-stream Mach number very near unity (see ref. 4 for a short résumé). More recent developments described in references 5, 6, 7, 8, and elsewhere have shown that the useful range of this theory can be extended to include subsonic and supersonic flows if slightly different approximations are employed in the derivation of the fundamental equations. Although the resulting theory is commonly designated as transonic small disturbance theory, or more briefly as transonic flow theory, it is actually a unified theory for subsonic, supersonic, or transonic flow around thin wings and slender bodies, and is moreover, the simplest theory proposed to date that is capable of yielding reliable results throughout that Mach number range.

This formulation of transonic flow theory provides a set of equations that differs from that of linear theory by the addition of one nonlinear term in the differential equation for the perturbation potential and in the shock relation. If the flow is purely subsonic or purely supersonic, solutions of the equations of transonic flow theory can be sought by application of existing methods for approximating the solutions of the exact equations of compressible inviscid flow. If the flow is transonic, however, the results obtained by application of these methods are at wide variance with those observed experimentally and it is necessary to devise new and appropriate methods of solution. Although methods of the successive approximation type have recently been developed that can be applied to transonic flows (e. g., refs. 9 and 10), the principal method that has been employed in the theoretical analysis of such flows involves the use of the hodograph transformation by means of which the nonlinear equation for the perturbation potential is transformed into a linear differential equation of mixed elliptic-hyperbolic type, the Tricomi equation. Although the resulting boundary-value problem is still very difficult to solve, this method has been applied with considerable success in the study of transonic flow around wedge and flat-plate airfoils and a

[1] Supersedes NACA TN 3970 by John R. Spreiter and Alberta Y. Alksne, 1957.

number of specific results have been given in recent years by Guderley and Yoshihara, Vincenti and Wagoner, Cole, and others (see ref. 11 for a résumé). Extension of this method to permit calculation of transonic flows around arbitrary airfoils with curved boundaries appears, however, to be a difficult task.

The present analysis is based on a novel method of approximation that avoids most of the difficulties of existing procedures while still preserving much of the nonlinear effects in the solution. Sufficient simplicity is gained by restricting attention to surface pressures and to flows that are either purely subsonic, purely supersonic, or have a free-stream Mach number near 1, that results can be obtained in closed analytical form for both the direct problem of calculating the pressure distribution on an airfoil of given shape, and the inverse problem of calculating the shape of an airfoil associated with a given pressure distribution. Inasmuch as the magnitude of the errors introduced by use of the approximation procedures is not evaluated in all cases by mathematical considerations, the usefulness and accuracy of the results are demonstrated by the calculation of the pressure distribution and drag for many different airfoil shapes and by comparison with existing theoretical and experimental results.

Of the theoretical results available for comparison, only two are exact. They are the simple-wave solution for supersonic flows without shock waves, and the variation of pressure with Mach number at Mach number 1. The present method yields both of these results exactly within the framework of transonic small disturbance theory.

Although the existing results mentioned above for wedge airfoils at Mach number 1 contain certain approximations beyond those implicit in the use of the equations of transonic flow theory, the influence of these approximations appears to be minor and the results are generally considered to be very nearly exact solutions of these equations. The present method produces results for this case that are in substantial agreement with these previous theoretical results. In contrast to the hodograph methods, the necessary steps are sufficiently simple, moreover, that results can also be obtained for sonic and near sonic flow around arbitrary airfoils with curved boundaries. Since previous theoretical information for such cases is meager, comparisons are made with a large number of experimental results. In general, the theoretical results found by application of the present method lie within the range of experimental scatter of the data.

In the subsonic range, no exact solutions are available for flow around a thin airfoil. Comparisons are made, therefore, with pressure correction formulas, such as that of Kármán-Tsien, and with higher approximations obtained by iteration methods.

A simple heuristic account of the general method and extensive discussion of the results are contained in the main text. Additional details concerning the underlying basis for the general procedures are contained in the Appendix.

PRINCIPAL SYMBOLS

a	speed of sound
a_∞	speed of sound in the free stream
C_p	pressure coefficient, $\frac{p-p_\infty}{\frac{\rho_\infty}{2}U_\infty^2}$
$\overline{C}_p$	$\frac{[M_\infty^2(\gamma+1)]^{1/3}}{\tau^{2/3}}C_p$
c	chord
c_d	section pressure drag coefficient, $\frac{d}{\frac{\rho_\infty}{2}U_\infty^2 c}$
$\overline{c}_d$	$\frac{[M_\infty^2(\gamma+1)]^{1/3}}{\tau^{5/3}}c_d$
d	pressure drag
k	$\frac{M_\infty^2(\gamma+1)}{U_\infty}$
M	local Mach number
M_∞	free-stream Mach number
n	exponent in the relations for airfoil ordinates given by equations (56) and (61)
p	static pressure
p_∞	free-stream static pressure
q	resultant local velocity
t	maximum thickness of profile
U_∞	free-stream velocity
u,w	perturbation velocity components parallel to x and z axes, respectively
u_E	value of u obtained by solution of equation (21)
u_H	value of u obtained by solution of equation (8)
u_P	value of u obtained by solution of equation (39)
X	value of x at which parabolic and hyperbolic solutions are joined
x,z	Cartesian coordinates where x extends in the direction of the free-stream velocity
x^*	value of x at which the local velocity is sonic
Z	ordinates of the upper surface of the airfoil
Γ	gamma function
γ	ratio of specific heats, for air $\gamma=1.4$
θ	semiapex angle of wedge airfoil
Λ	pressure gradient, $\frac{dC_p}{d(x/c)}$
λ_E	$1-M_\infty^2-ku$
λ_H	M_∞^2-1+ku
λ_P	$k\frac{\partial u}{\partial x}$
ξ_∞	$\frac{M_\infty^2-1}{[M_\infty^2(\gamma+1)\tau]^{2/3}}$
ρ_∞	free-stream density of air
τ	thickness ratio, t/c
φ	perturbation velocity potential

SUBSCRIPTS

cr	values associated with critical Mach number
i	values associated with incompressible flow or with $M_\infty=0$
L	values given by linearized compressible flow theory

$M_\infty=1$ values associated with $M_\infty=1$
Z_{max} values associated with maximum ordinate of airfoil
$\xi_\infty=0$ values associated with $\xi_\infty=0$, or with $M_\infty=1$

FUNDAMENTAL EQUATIONS AND BOUNDARY CONDITIONS

Consider the steady flow of an inviscid compressible gas past an arbitrary thin symmetrical nonlifting airfoil, and introduce Cartesian coordinates x and z with the x axis parallel to the direction of the free-stream, as illustrated in figure 1.

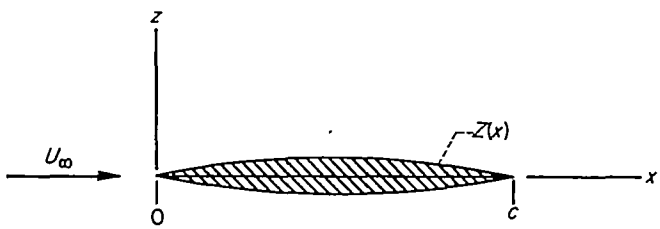

FIGURE 1.—View of airfoil and coordinate system.

Let the free-stream velocity and density be U_∞ and ρ_∞, the perturbation potential be φ, and the perturbation velocity components parallel to the x and z axes be φ_x, or u, and φ_z, or w, where the subscript indicates differentiation. The boundary conditions require that the perturbation velocities vanish at infinity, and that the flow be tangential to the wing surface. The first condition indicates that φ is constant at infinity. The latter condition can be approximated for thin wings by

$$(\varphi_z)_{z=0}=U_\infty \frac{dZ}{dx} \tag{1}$$

where Z represents the ordinates of the airfoil upper surface. The pressure coefficient C_p is likewise approximated to first order by

$$C_p\equiv\frac{p-p_\infty}{\frac{\rho_\infty}{2}U_\infty^2}=-2\frac{\varphi_x}{U_\infty}=-2\frac{u}{U_\infty} \tag{2}$$

These relations are familiar from linear theory, but apply equally for transonic thin airfoil theory. The differential equation for φ is not the same as in linear theory, however, but is

$$\left(1-M_\infty^2-M_\infty^2\frac{\gamma+1}{U_\infty}\varphi_x\right)\varphi_{xx}+\varphi_{zz}=0 \tag{3}$$

where M_∞ is the Mach number of the undisturbed flow and γ is the ratio of specific heats (1.4 for air). It is useful to note that the coefficient of φ_{xx} corresponds, in the present approximation, to $1-M^2$ where M is the local Mach number.

Knowledge of methods for obtaining solutions of equation (3) is meager, not only because the equation is nonlinear, but because it can change type (elliptic, hyperbolic), depending on the value of M_∞ and φ_x. This change of type is an essential feature of transonic flow, since subsonic flows are represented by elliptic equations and supersonic flows by hyperbolic equations. If both types of flow occur in a single flow field, it is apparent that the differential equation must change type. In the present case, the type of the equation is recognized by the sign of the total coefficient of φ_{xx}, as follows:

$$\left.\begin{array}{ll}>0 & \text{elliptic (subsonic)}\\ <0 & \text{hyperbolic (supersonic)}\end{array}\right\}\quad 1-M_\infty^2-M_\infty^2\frac{\gamma+1}{U_\infty}\varphi_x \tag{4}$$

An important quantity in the discussion of compressible flows is the critical pressure coefficient $C_{p_{cr}}$ associated with the local occurrence of sonic velocity. The appropriate relation is found by combination of equation (2) and the relation obtained by equating the coefficient of φ_{xx} in equation (3) to zero, and is

$$C_{p_{cr}}=-\frac{2(1-M_\infty^2)}{M_\infty^2(\gamma+1)} \tag{5}$$

In transonic and supersonic flows, it is also necessary, in general, to provide an additional equation for the discontinuous changes in velocity that occur at shock surfaces. The necessary equations, when simplified to the form consistent with the approximations of transonic flow theory, reduce to

$$\left.\begin{array}{l}\left[1-M_\infty^2-M_\infty^2\frac{\gamma+1}{U_\infty}\left(\frac{u_a+u_b}{2}\right)\right](u_a-u_b)^2+(w_a-w_b)^2=0\\ \varphi_a=\varphi_b\end{array}\right\} \tag{6}$$

where the subscripts a and b refer to the values on the two sides of the shock surface. With the exception of the Appendix and minor references in the main text, equation (6) is not employed explicitly in the following analysis and discussion because attention is confined to (a) purely subsonic flows in which no shocks occur, (b) purely supersonic flows in which shock waves can be approximated with good accuracy by isentropic compressions, and (c) flows with free-stream Mach number near 1 in which the shock waves are situated either downstream or far upstream of the airfoil.

The remainder of the present paper is concerned with the approximate solution of the preceding equations and with comparison of the results obtained in specific applications with existing theoretical and experimental results. Purely supersonic flows are discussed first because the method of approximation yields the exact equivalent, in transonic approximation, of simple wave theory. Purely subsonic flows are discussed next because of the close relationship between the results for this and the preceding case. Flows with free-stream Mach number near 1 are treated last.

SUPERSONIC FLOWS

APPROXIMATE SOLUTION OF EQUATIONS

It is convenient in the analysis of supersonic flows to introduce the symbol λ_H as an abbreviation for the negative of the coefficient of φ_{xx}

$$\lambda_H=M_\infty^2-1+M_\infty^2\frac{\gamma+1}{U_\infty}\varphi_x=M_\infty^2-1+ku>0 \tag{7}$$

and rewrite equation (3) in the form:

$$-\lambda_H\varphi_{xx}+\varphi_{zz}=0 \tag{8}$$

It is now assumed that λ_H is neither zero nor infinite and that it varies sufficiently slowly that its derivatives can be disregarded so that it can be considered, temporarily, as a constant. At this stage, the problem is equivalent to that encountered in linearized supersonic airfoil theory (it is identical if λ_H is replaced by M_∞^2-1) and the solution u_H at the airfoil surface is

$$u_H=-\frac{U_\infty}{\sqrt{\lambda_H}}\frac{dZ}{dx} \tag{9}$$

Differentiation yields

$$\frac{du_H}{dx}=-\frac{U_\infty}{\sqrt{\lambda_H}}\frac{d^2Z}{dx^2} \tag{10}$$

If, now, M_∞^2-1+ku is restored in place of λ_H so that, in effect, the local value for λ_H is used at each point and the subscript H on u is dropped, equation (10) becomes

$$\frac{du}{dx}=-\frac{U_\infty}{\sqrt{M_\infty^2-1+ku}}\frac{d^2Z}{dx^2} \tag{11}$$

It is immediately apparent that a certain degree of arbitrariness is displayed in the preceding steps and that different results will be obtained depending, for instance, on whether M_∞^2-1+ku is substituted for λ_H in equation (10) as above, or in equation (9), or in other equations obtained by further differentiation or integration of equation (9). It is shown in the Appendix, however, that the error involved in the preceding steps can be assessed exactly by examination of the remainder terms that have been omitted in writing equations (9) and (10). The advisability of using equation (11) is assured by the fact that the error is shown to vanish, in the absence of shock waves, if λ_H is replaced by M_∞^2-1+ku in equation (10), but not in equation (9). This conclusion becomes immediately evident, furthermore, upon recognition of the fact that equation (11) is the counterpart, in transonic small disturbance theory, of a fundamental differential equation that occurs in the analysis of Prandtl-Meyer and simple wave flows (see, e. g., ref. 12, p. 87 or ref. 13, pp. 190 and 212). Equation (11) is a nonlinear ordinary differential equation for u that can be solved easily by separation of variables. The result is

$$\frac{2}{3k}\left(M_\infty^2-1+ku\right)^{3/2}=-U_\infty\frac{dZ}{dx}+C \tag{12}$$

where C is a constant of integration. In applications of equation (12) to flows that are supersonic everywhere, perhaps the most logical method for the evaluation of this constant is to use the expression between u and dZ/dx provided at the leading edge by the transonic approximation to the shock relation, that is by equation (6) with u_a and w_a equated to zero, u_b to $(u)_{x=0}$, and w_b to $U_\infty(dZ/dx)_{x=0}$. The result given by equation (12) with C evaluated in this way corresponds, to the degree of approximation afforded by use of transonic small disturbance theory, to shock-expansion theory. An alternative procedure that leads to a somewhat simpler result possessing very nearly equal accuracy is to evaluate C by use of the result indicated by equation (9) that $u=0$ where $dZ/dx=0$ for any nonsingular λ_H thus

$$C=\frac{2}{3k}(M_\infty^2-1)^{3/2} \tag{13}$$

whence

$$u=\frac{1}{k}\left\{-(M_\infty^2-1)+\left[(M_\infty^2-1)^{3/2}-\frac{3}{2}kU_\infty\frac{dZ}{dx}\right]^{2/3}\right\} \tag{14}$$

The corresponding relation for the pressure coefficient C_p is obtained by combination of equations (2) and (14), and is

$$C_p=\frac{2}{M_\infty^2(\gamma+1)}\left\{(M_\infty^2-1)-\left[(M_\infty^2-1)^{3/2}-\frac{3}{2}M_\infty^2(\gamma+1)\frac{dZ}{dx}\right]^{2/3}\right\} \tag{15}$$

It should be noted that the restriction to supersonic flow imposed in the evaluation of C and in the inequality of equation (7) requires that equation (15) is to be applied only to cases for which the quantity in square brackets, that is, $[(M_\infty^2-1)^{3/2}-(3/2)M_\infty^2(\gamma+1)\ (dZ/dx)]$, is positive.

COMPARISON WITH EXISTING HIGHER APPROXIMATIONS

Equation (15) is recognized, by comparison with equation (3-15) of reference 3, page 387,[2] as the precise equivalent, in the transonic small disturbance approximation, of simple wave theory for the surface pressure on an airfoil in supersonic flow. Exact simple wave theory is known, moreover, to be perfectly adequate for all practical purposes up to a Mach number of 3, which is considerably in excess of the present range of interest. Within this Mach number range, the results obtained by use of simple wave theory are almost identical with those obtained by use of shock-expansion theory. Comparisons of the variations of C_p with dZ/dx indicated by exact simple wave theory and by equation (15) are shown in figure 2 for several Mach numbers from 1 to 2. As might be anticipated, the two sets of results are in close agreement for Mach numbers near 1, and differ by an increasing amount with increasing Mach number.

Although the necessary calculations are very easy to accomplish in any given case, simple wave theory is not always used in actual practice. Many calculations are based on linear theory or Busemann's second-order theory. Consequently, an additional set of graphs is shown in figure 3 in which the curves of figure 2 are repeated together with the corresponding curves calculated by use of first- and second-order theory. No comparisons are shown for $M_\infty=1$ because the latter theories indicate infinite pressures. It can be seen that equation (15) furnishes a better approximation than linear theory throughout the entire range of variables shown on figure 3 and a better approximation than second-order theory for Mach numbers less than about 1.4. It can be

[2] Comparison discloses that the quantity $M_\infty^2(\gamma+1)$ that appears in equation (15) is represented by $\gamma+1$ in equation (3-15) of reference 3. The difference is associated with a corresponding difference in the coefficient k of the nonlinear term of equation (3). Although the two coefficients are identical at $M_\infty=1$, and might appear to be equally consistent with the other assumptions of transonic flow theory, it has been shown in references 5, 6, 7, 8, and elsewhere that the approximation obtained by use of $M_\infty^2(\gamma+1)$ is much the better of the two for Mach numbers other than 1.

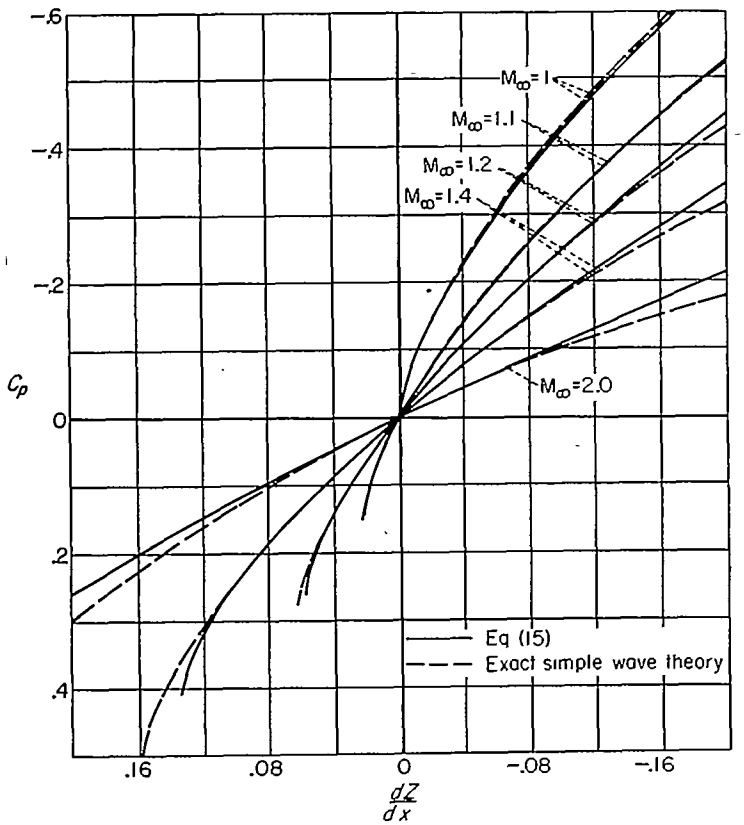

FIGURE 2.—Comparison of results indicated by present theory and by exact simple wave theory.

seen that second-order theory furnishes a very poor approximation for C_p at Mach numbers approaching unity.

In order to explore this behavior further, two additional curves labeled "third order" and "fourth order," calculated using the formulas of references 14 and 15,[3] are included on the graph of figure 3, even though they must be interpreted in a somewhat more restricted sense than the other curves. To be more precise, the third-order curve is restricted to airfoils for which dZ/dx is zero at the leading edge, and the fourth-order curve to airfoils for which both dZ/dx and d^2Z/dx^2 are zero there. It is clear from this sketch that the accuracy of second-order theory at Mach numbers near unity is not improved by addition of higher order terms. The explanation resides in the fact that the larger values of $|dZ/dx|$ shown on the graphs of figure 3 exceed the radius of convergence of the power series expansion for C_p for all but the highest Mach number shown. With the noted restrictions on the leading edge, the higher order results of figure 3 are equivalent to the first few terms of a power series expansion, in terms of dZ/dx, of the expression for C_p indicated by exact simple wave theory. The radius of convergence of the series depends, of course, on the Mach number and is given by the value of $|dZ/dx|$ associated with the occurrence of sonic flow or, in terms of the curves shown on figures 2 and 3, with the termination of the left end of the exact curve. The failure of higher order theories at negative dZ/dx is thus of purely mathematical origin and has no direct physical significance.

[3] Attention of those who refer to reference 15 is called to the fact that the first term appearing in the fourth-order coefficient a_4 of equation (29) should be 2/3 rather than 1/3. This term is written correctly in the numerical example given in equation (135).

ADDITIONAL PROPERTIES OF APPROXIMATE SOLUTION

Equation (15) has some additional interesting properties worth noting. Of the two major components of the right-hand side, the first is recognized upon comparison with equation (5) as the expression for $C_{p_{cr}}$. Since the remaining term is zero when $C_p=C_{p_{cr}}$, it follows that the expression for the critical value for dZ/dx associated with the occurrence of sonic velocity at a given Mach number M_∞ is

$$\left(\frac{dZ}{dx}\right)_{cr}=\frac{2(M_\infty^2-1)^{3/4}}{3M_\infty^2(\gamma+1)} \tag{16}$$

It follows, furthermore, that a curve representing the variation of C_p with M_∞ for a given dZ/dx, and hence a given point on the airfoil, approaches infinite slope as C_p approaches $C_{p_{cr}}$.

An alternative form for equation (15) that is useful for some purposes is the following which expresses C_p in terms of the linear-theory solution C_{p_L} rather than dZ/dx.

$$C_p=\frac{2(M_\infty^2-1)}{M_\infty^2(\gamma+1)}\left\{1-\left[1-\frac{3}{4}\frac{M_\infty^2(\gamma+1)}{M_\infty^2-1}C_{p_L}\right]^{4/3}\right\} \tag{17}$$

where

$$C_{p_L}=\frac{2}{\sqrt{M_\infty^2-1}}\frac{dZ}{dx}$$

This relation can be written in somewhat more concise form if expressed in terms of the transonic similarity parameters $\overline{C}_p$ and ξ_∞, thus

$$\overline{C}_p=2\xi_\infty\left[1-\left(1-\frac{3}{4}\frac{\overline{C}_{p_L}}{\xi_\infty}\right)^{4/3}\right] \tag{18}$$

where

$$\overline{C}_p\equiv\frac{[M_\infty^2(\gamma+1)]^{1/4}}{\tau^{3/4}}C_p, \qquad \xi_\infty\equiv\frac{M_\infty^2-1}{[M_\infty^2(\gamma+1)\tau]^{3/4}}$$

and τ refers to the thickness ratio. Critical values for $\overline{C}_p$ and $\overline{C}_{p_L}$ corresponding to the local occurrence of sonic velocity are easily recognized to be the following:

$$\overline{C}_{p_{cr}}=2\xi_\infty, \qquad \overline{C}_{p_{L_{cr}}}=\frac{4}{3}\xi_\infty \tag{19}$$

SUBSONIC FLOWS

APPROXIMATE SOLUTION OF EQUATIONS

The procedure described in the preceding section will now be applied to the analysis of subsonic flows. Thus, introduce the symbol λ_E as an abbreviation for the coefficient of φ_{xx}

$$\lambda_E=1-M_\infty^2-M_\infty^2\frac{\gamma+1}{U_\infty}\varphi_x=1-M_\infty^2-ku>0 \tag{20}$$

and rewrite equation (3) as follows:

$$\lambda_E\varphi_{xx}+\varphi_{zz}=0 \tag{21}$$

If it is again assumed that λ_E is neither zero nor infinite and that it varies sufficiently slowly that its derivatives can be disregarded, the problem is equivalent to that encountered

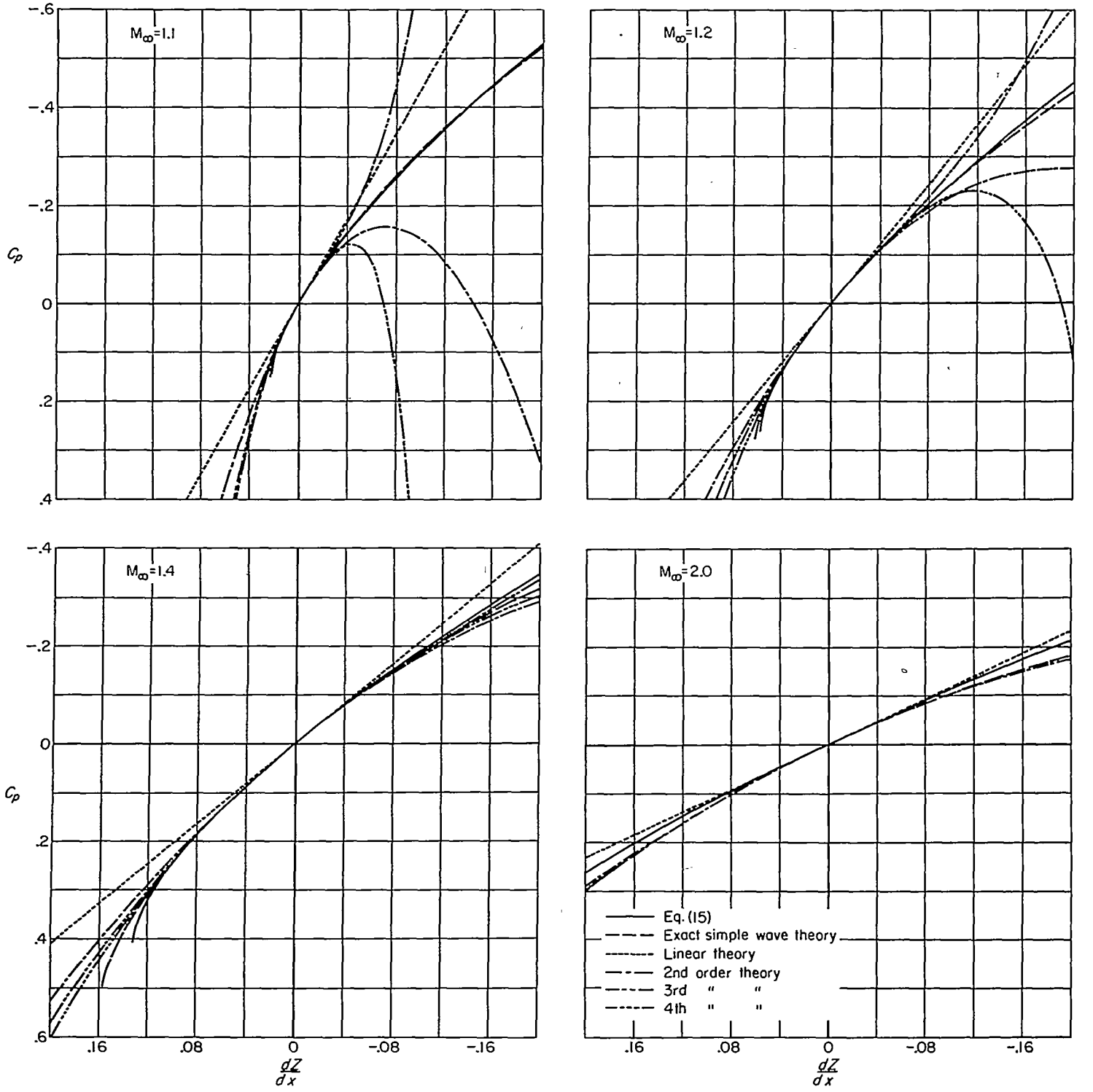

FIGURE 3.—Comparison of results indicated by present theory and by the method of successive approximations for supersonic flow.

in linearized subsonic airfoil theory and the solution u_E at the airfoil surface is

$$u_E=\frac{U_\infty}{\pi\sqrt{\lambda_E}}\int_0^c\frac{dZ/d\xi}{x-\xi}\,d\xi=\frac{u_i}{\sqrt{\lambda_E}} \tag{22}$$

where the subscript i refers to the values for $M_\infty=0$. Differentiation yields

$$\frac{du_E}{dx}=\frac{1}{\sqrt{\lambda_E}}\frac{du_i}{dx} \tag{23}$$

If, in the same manner as described for the supersonic case, $1-M_\infty^2-ku$ is restored in place of λ_E so that, in effect, the local value for λ_E is used at each point, and the subscript E on u is dropped, equation (23) becomes

$$\frac{du}{dx}=\frac{1}{\sqrt{1-M_\infty^2-ku}}\frac{du_i}{dx} \tag{24}$$

As in the previous discussion of supersonic flows, the error terms are omitted in writing the preceding relations, but are included in a more complete presentation of the equations

given in the Appendix. Once again, the resulting relation is a nonlinear ordinary differential equation that can be solved readily by separation of variables

$$-\frac{2}{3k}(1-M_\infty^2-ku)^{3/2}=u_t+C \tag{25}$$

In applications to flows that are subsonic everywhere, the constant of integration C is evaluated by use of the result indicated by equation (22) that $u=0$ where $u_t=0$ for any nonsingular λ_E, thus

$$C=-\frac{2}{3k}(1-M_\infty^2)^{3/2} \tag{26}$$

In this way, the following relation is obtained between u and u_t

$$u=\frac{1}{k}\left\{1-M_\infty^2-\left[(1-M_\infty^2)^{3/2}-\frac{3}{2}ku_t\right]^{2/3}\right\} \tag{27}$$

The corresponding relation for the pressure coefficient C_p is obtained by combination of equations (2) and (27) and is [4]

$$C_p=-\frac{2}{M_\infty^2(\gamma+1)}\left\{(1-M_\infty^2)-\left[(1-M_\infty^2)^{3/2}+\frac{3}{4}M_\infty^2(\gamma+1)C_{p_t}\right]^{2/3}\right\} \tag{28}$$

where

$$C_{p_t}=-2\frac{u_t}{U_\infty}=-\frac{2}{\pi}\int_0^c\frac{dZ/d\xi}{x-\xi}d\xi$$

In the same way as noted for supersonic flows following equation (15), the restriction to subsonic flow imposed in the evaluation of C and by the inequality of equation (20) requires that equation (28) be applied only to cases where the quantity in the square bracket is positive.

This result possesses several simple, but interesting, properties. First of all, the leading term of an expansion of equation (28) in a series involving ascending powers of C_{p_t} is precisely the familiar Prandtl-Glauert rule of linearized subsonic compressible flow theory

$$C_{p_L}=\frac{C_{p_t}}{\sqrt{1-M_\infty^2}} \tag{29}$$

The coefficients of succeeding terms, however, do not agree with those given by the method of successive approximation. Next, the first of the two major components of the right-hand member of equation (28) is recognized, just as in the supersonic case, as the expression for the critical pressure coefficient $C_{p_{cr}}$. Since the remaining term is zero when $C_p=C_{p_{cr}}$, it follows that the expression for the critical value for C_{p_t} associated with the occurrence of sonic velocity at a given Mach number M_∞ is

$$C_{p_{t_{cr}}}=-\frac{4}{3}\frac{(1-M_\infty^2)^{3/2}}{M_\infty^2(\gamma+1)} \tag{30}$$

[4] Attention is called to the fact that this same relation, except for replacement of $M_\infty^2(\gamma+1)$ by $\gamma+1$ for the same reasons as noted in footnote 2, has been found independently by Kusukawa by application of the WKB method of approximation to the equations of transonic flow theory. This result, together with a number of applications, is published in the September 1957 issue of the Journal of the Physical Society of Japan.

It may be noted that this value is just two-thirds of that obtained by use of equation (5) together with the Prandtl-Glauert rule. It follows, furthermore, that a curve illustrating the variation of C_p with M_∞ for a given C_{p_t}, and hence a given point on the airfoil surface, approaches infinite slope as C_p approaches $C_{p_{cr}}$. This latter behavior signifies that a power series expansion of the result will only converge for Mach numbers less than the critical. Last, the following result is obtained if equation (28) is expressed in terms of the subsonic linear theory solution C_{p_L} rather than C_{p_t}

$$C_p=\frac{-2(1-M_\infty^2)}{M_\infty^2(\gamma+1)}\left\{1-\left[1+\frac{3}{4}\frac{M_\infty^2(\gamma+1)}{1-M_\infty^2}C_{p_L}\right]^{2/3}\right\} \tag{31}$$

where

$$C_{p_L}=\frac{C_{p_t}}{\sqrt{1-M_\infty^2}}$$

Note that the relation between C_p and C_{p_L} indicated by equation (31) for subsonic flows is precisely the same as given by equation (17) for supersonic flows. It follows immediately that the corresponding expression in terms of the transonic similarity parameters $\overline{C}_p$ and ξ_∞ given by equation (18) applies to subsonic, as well as supersonic flows. In order to illustrate the nature of the results indicated by equation (18), a plot of the variation of $\overline{C}_p$ with ξ_∞ for various $C_{p_L}\sqrt{|\xi_\infty|}$ is shown in figure 4. Although the remarkable symmetry about $\xi_\infty=0$ is a consequence of expressing the results in terms of the transonic similarity parameters, the general symmetry remains, although in somewhat distorted form, when C_p is plotted as a function of M_∞ for constant $C_{p_L}\sqrt{|1-M_\infty^2|}$. Such a plot is shown in figure 5.

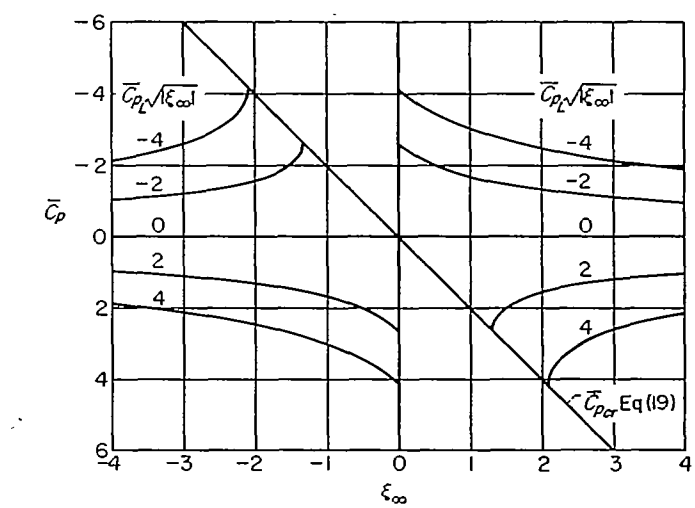

FIGURE 4.—Variation of reduced pressure coefficient, $\overline{C}_p$, with the similarity parameter, ξ_∞, for various values of $\overline{C}_{p_L}\sqrt{|\xi_\infty|}$.

COMPARISON WITH EXISTING HIGHER APPROXIMATIONS

The remainder of the present section on subsonic flows is concerned with an evaluation of the degree of accuracy achieved by use of equation (28). This discussion is handicapped somewhat by the fact that all other theories for subsonic flows around airfoils are also approximate and that no exact solutions are known. Perhaps the most widely

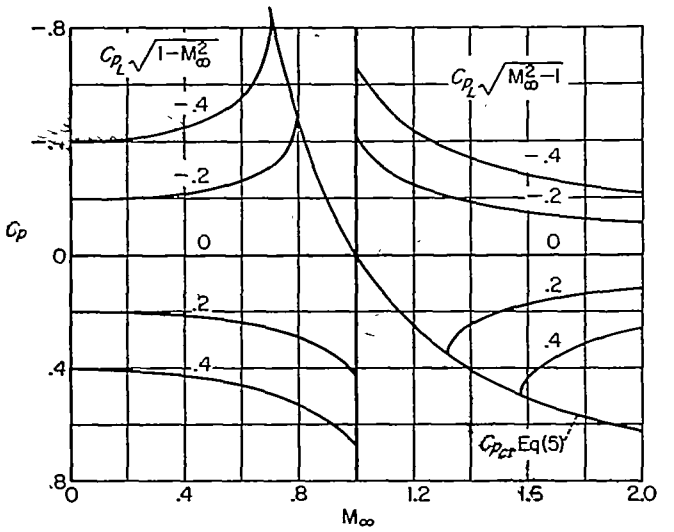

FIGURE 5.—Variation of C_p with M_∞ for various values of $C_{p_L}\sqrt{|M_\infty^2-1|}$.

used higher approximation is the Kármán-Tsien rule. (See refs. 3 and 16 for a résumé.) Although the traditional derivation of the Kármán-Tsien rule is based on the hodograph method, it is not without interest to observe that the Kármán-Tsien rule can be obtained by use of the present procedures together with the three assumptions introduced in the original derivation. These are: (a) that γ can be approximated by -1 in the expression for the speed of sound, (b) that the perturbation velocities are small, and (c) that the Mach number can be considered small in the evaluation of additional effects of compressibility beyond those indicated by linear theory. The starting point is equation (3) with the coefficient of φ_{xx} replaced by the approximate relation for $1-M^2$, where M is the local Mach number, afforded by use of assumptions (a) and (b). The necessary relation can be derived from the energy equation

$$\frac{a^2}{\gamma-1}+\frac{q^2}{2}=\frac{a_\infty^2}{\gamma-1}+\frac{U_\infty^2}{2} \tag{32}$$

where

$$q^2=(U_\infty+u)^2+w^2$$

by setting $\gamma=-1$, whence

$$a^2=a_\infty^2-U_\infty^2+q^2$$

and

$$1-M^2=1-\frac{q^2}{a^2}=\frac{1-M_\infty^2}{1-M_\infty^2+M_\infty^2(q^2/U_\infty^2)}\approx\frac{1-M_\infty^2}{1+2M_\infty^2(u/U_\infty)} \tag{33}$$

Note that this approximation does not permit the attainment of $M=1$ with finite q/U_∞ and with M_∞ different from unity. Substitution of this relation for $1-M^2$ in place of λ_E in equation (23) and integration yields

$$\sqrt{1+2M_\infty^2(u/U_\infty)}=\frac{M_\infty^2}{\sqrt{1-M_\infty^2}}\frac{u_t}{U_\infty}+C \tag{34}$$

The constant of integration is again evaluated by setting $u=0$ where $u_t=0$, whence C equals unity. Solution for u and introduction of the relation between u and C_p given by equation (2) yields

$$C_p=\frac{C_{p_t}}{\sqrt{1-M_\infty^2}}\left(1-\frac{M_\infty^2}{4\sqrt{1-M_\infty^2}}C_{p_t}\right)\approx\frac{C_{p_t}}{\sqrt{1-M_\infty^2}+(1/4)M_\infty^2C_{p_t}} \tag{35}$$

Replacement of M_∞^2 in the second term in the denominator by $2(1-\sqrt{1-M_\infty^2})$ is consistent with assumption (c) and leads directly to the familiar expression for the Kármán-Tsien rule

$$C_p=\frac{C_{p_t}}{\sqrt{1-M_\infty^2}+(1-\sqrt{1-M_\infty^2})(C_{p_t}/2)} \tag{36}$$

This rule, in common with the Prandtl-Glauert rule and the present result given in equation (28), is termed a pressure correction formula because C_p is given in terms of C_{p_t} and M_∞ with no further dependence on airfoil shape. A comparison of the variations of C_p with M_∞ indicated by these three relations is shown in figure 6. A great many other pressure-correction formulas having widely varying properties have also been proposed in recent years. One that yields results in closer agreement with equation (28) than the Prandtl-Glauert or the Kármán-Tsien rule has been given by Garrick and Kaplan in reference 17. A curve illustrating their results is included on figure 6.

A second important method that has been used to obtain higher approximations for subsonic pressure distributions on thin airfoils is the method of successive approximation in which the solution is expressed in a power series in thickness ratio. In this method, the first term is the result given by linear theory, and the coefficients of successive terms are determined by iteration. Higher approximations cannot be expressed in terms of C_{p_t} and M_∞ in such a simple and uni-

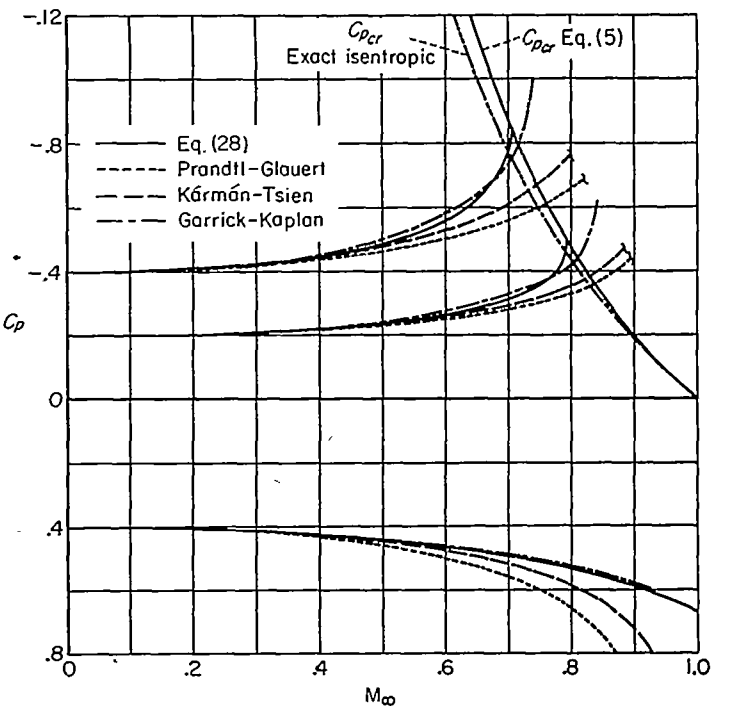

FIGURE 6.—Comparison of results indicated by present theory and by various pressure correction formulas for subsonic flow.

versal manner as with the pressure-correction formulas, but depend on the airfoil shape in a more explicit manner. Although a relatively simple and general procedure for the evaluation of the second approximation has recently been given by Van Dyke (ref. 18), the determination of the third approximation has been accomplished for only a few special shapes. One of these is the nonlifting symmetrical circular-arc section for which the second approximation has been given by Hantzsche and Wendt (ref. 19) and the third approximation by Asaka (refs. 20, 21, and 22).[5] Figure 7 shows a comparison of the variations of C_p with M_∞ at the midpoint of such an airfoil having a thickness ratio τ of 0.10, as indicated by equation (28) and by the first, second, and third approximations. It can be seen that the results obtained by use of equation (28) are identical to those given by the first approximation (or linear theory) for small Mach numbers, but depart therefrom with increasing Mach number and are much closer to the higher approximations for Mach numbers near the critical. It should be noted that the curves labeled first, second, and third order represent the results indicated by successive approximations to the solution of the exact equation for inviscid compressible flow. It is also of interest to compare the results indicated by equation (28) with those indicated by successive approximations to the solution of the simplified equations of transonic small disturbance theory. The latter results can be calculated by use of the following expression, which is readily derived from Asaka's result by taking the limiting form consistent with the approximations of transonic flow theory:

$$C_p=-\frac{8}{\pi}\frac{\tau}{\sqrt{1-M_\infty^2}}-\left(\frac{10}{\pi^2}-\frac{1}{2}\right)\frac{(\gamma+1)M_\infty^2}{(1-M_\infty^2)^2}\tau^2-$$

$$\left[\frac{1}{\pi}\left(-\frac{281}{108}+\frac{7}{6}ln2\right)+\frac{1}{\pi^3}\left(\frac{292}{9}+4.908\right)\right]\frac{(\gamma+1)^2M_\infty^4}{(1-M_\infty^2)^{7/2}}\tau^3+\ldots$$

$$=-2.5465\frac{\tau}{\sqrt{1-M_\infty^2}}-0.5132\frac{(\gamma+1)M_\infty^2}{(1-M_\infty^2)^2}\tau^2-$$

$$0.6339\frac{(\gamma+1)^2M_\infty^4}{(1-M_\infty^2)^{7/2}}\tau^3+\ldots \qquad (37)$$

It can be seen that the curve in figure 8 indicated by equation (28) is somewhat higher than even that representing the third approximation, but evaluation of its accuracy remains difficult because neither the exact solution nor an upper bound for the results is provided by the classical method of successive approximation. Attention is called to the fact that recent developments in transonic flow theory permit the establishment of an upper bound by application of an alternative method of successive approximation that involves the solution of quadratic, rather than linear, equations at each step of the iteration process. This process, based on the methods employed in reference 9. is described in the Appendix, and additional results are given for the specific case considered in figure 8.

[5] The results for the third approximation given in the present report differ from those obtainable directly from the expressions given in either reference 20 or 21 and 22 due to the correction of some misprints. These corrections have been verified by correspondence with the author, and are published in the January 1958 issue of the Journal of the Physical Society of Japan.

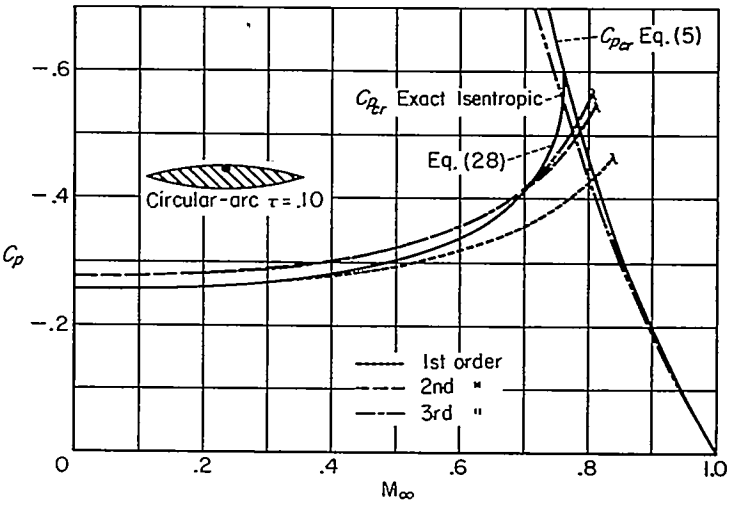

FIGURE 7.—Comparison of the variation of C_p with M_∞ at the midpoint of a circular-arc airfoil, as indicated by present theory and by application of the method of successive approximations to the exact equations for inviscid subsonic flow.

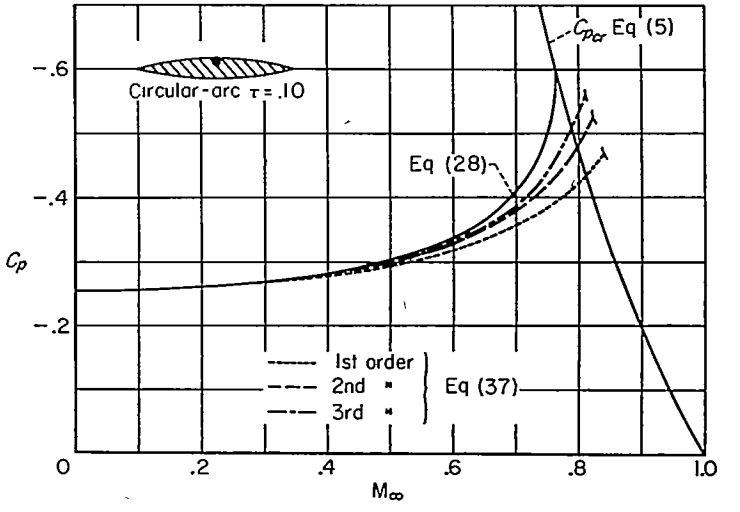

FIGURE 8.—Comparison of the variation of C_p with M_∞ at the midpoint of a circular-arc airfoil in subsonic flow, as indicated by present theory and by application of the method of successive approximations to the transonic equation.

FLOWS WITH FREE-STREAM MACH NUMBER NEAR 1

The analyses of supersonic and subsonic flows given in the preceding sections have started by introduction of a symbol λ for the coefficient of φ_{xx} and the assumption that λ is nonsingular and varies sufficiently slowly that it can be regarded as a constant in the initial stages of the analysis. Since the results so obtained terminate if $\lambda=0$, or physically if sonic velocity occurs in the flow field, it is immediately clear that some change is necessary to study flows with free-stream Mach number near 1 where the transition from subsonic to supersonic flow is an essential feature. The technique adopted is to introduce the symbol λ_P as an abbreviation for the coefficient of φ_x rather than φ_{xx}, thus

$$\lambda_P=M_\infty^2\frac{\gamma+1}{U_\infty}\varphi_{xx}=k\frac{\partial u}{\partial x} \qquad (38)$$

whence equation (3) may be written as follows:

$$\varphi_{xx}-\lambda_P\varphi_x=-(1-M_\infty^2)\varphi_{xx}=f_P \qquad (39)$$

If attention is confined to flows with free-stream Mach number 1 so that the right-hand side of equation (39) vanishes and if λ_P is replaced by a constant, the resulting relation given by equation (39) is a linear partial differential equation of parabolic type that is familiar from the study of one-dimensional unsteady conduction of heat. If approximate solutions for flows with free-stream Mach number 1 are sought in this way, the analysis proceeds through considerations that are generally applied to parabolic differential equations, and is, in some sense, intermediate between the mixed elliptic-hyperbolic type of the transonic equation. The idea of using the equation for heat conduction for the study of transonic flows in this way is not new, but apparently originated with Oswatitsch, who suggested it to Behrbohm for the analysis of internal flows of nozzles (refs. 23 and 24) The same idea has been applied more recently by Oswatitsch and Keune (refs. 25, 26, and 27) to calculate the flow around the forepart of slender bodies of revolution at free-stream Mach number 1, and they have shown that the results are in remarkable agreement with those measured on the front half of a circular-arc body of revolution. Although the parameter λ_P is regarded throughout as a constant, and various means are proposed for the selection of an appropriate value, it develops that the numerical result for the pressures on the forward part of typical smooth bodies of revolution depends so slightly on the actual choice that almost any reasonable value can be used for λ_P.

If flows with free-stream Mach number different from unity are considered so that the right-hand side of equation (39) remains, and if λ_P is again replaced by a constant, the resulting differential equation is linear and is of elliptic or hyperbolic type depending on whether the free-stream Mach number, rather than the local Mach number, is less than or greater than unity. Maeder and Thommen (ref. 28) have suggested that this linearized equation, or its counterpart in three dimensions, be applied, together with a new and arbitrary rule for the selection of a value for λ_P, to calculate the pressure distribution on complete bodies of revolution and on airfoils in two-dimensional flows. The selection of an appropriate value for λ_P is much more critical for these problems than for those discussed originally by Oswatitsch and Keune, however, and the replacement of λ_P by a constant results not only in serious loss of accuracy in many applications, but also in loss of certain essential general features of the solution. In general, results obtained by replacing λ_P, or $\partial u/\partial x$, with a constant appear to be remarkably accurate if the resulting values calculated for $\partial u/\partial x$ are, indeed, nearly constant over most of the chord. If, on the other hand, $\partial u/\partial x$ varies substantially over the chord, no choice of a single value for λ_P will suffice to provide a useful result. This point is developed further in the course of the following discussion and in the Appendix. Some criticisms of the above procedure, although principally from a different point of view, have appeared in a note by Miles (ref. 29).

In the present analysis, it is assumed once again that λ_P is nonsingular and that it varies sufficiently slowly that it can be considered as a constant in the initial stages of the analysis in which a nonlinear ordinary differential equation is established for u on the airfoil surface. The final result for u is determined by integration of this differential equation and restores, to a large degree, the effects of the variation of λ_P along the chord. The result for the first stage of the analysis requires the solution of equation (39) subject to the boundary conditions given in equation (1) and can be obtained by application of standard procedures. The solution has two distinct forms depending on the sign of λ_P. The form associated with positive λ_P is appropriate for application to regions where the flow is accelerating, whereas that associated with negative λ_P may be appropriate for application to regions where the flow is decelerating. The analysis of accelerating flow will be developed first. The direct problem in which the airfoil shape is specified and the pressure distribution is sought, and the inverse problem in which the pressure distribution is specified and the associated airfoil shape is sought are discussed for each case.

ACCELERATING FLOWS, DIRECT PROBLEMS

Approximate solution of equations for arbitrary airfoil shape.—A relation for u at the airfoil surface derived by consideration of equation (39) with positive λ_P, the boundary conditions stated in equation (1), and the form of Green's theorem associated with the left side of equation (39) (see Appendix) is

$$u_P=-\frac{U_\infty}{\sqrt{\pi\lambda_P}}\frac{d}{dx}\int_0^x\frac{dZ/d\xi}{\sqrt{x-\xi}}d\xi-\frac{1}{\lambda_P}\frac{\partial}{\partial x}\int_{-\infty}^{+\infty}d\zeta\int_{-\infty}^{x}\sigma_P f_P d\xi$$
$$=-\frac{U_\infty}{\sqrt{\pi\lambda_P}}\left[\left(\frac{dZ}{dx}\right)_{x=0}\frac{1}{\sqrt{x}}+\int_0^x\frac{d^2Z/d\xi^2}{\sqrt{x-\xi}}d\xi\right]-$$
$$\frac{1}{\lambda_P}\frac{\partial}{\partial x}\int_{-\infty}^{+\infty}d\zeta\int_{-\infty}^{x}\sigma_P f_P d\xi \qquad (40)$$

where

$$f_P=-(1-M_\infty^2)\varphi_{\xi\xi},\ \sigma_P=\sqrt{\frac{\lambda_P}{4\pi(x-\xi)}}\,e^{\left[-\frac{\lambda_P(x-\xi)^2}{4(x-\xi)}\right]}$$

The two alternative expressions for u_P are completely equivalent. The first is more concise and will be used in the following equations, but the second is often somewhat simpler to evaluate. If the free-stream Mach number is unity, the double integral vanishes and u_P can be calculated directly. The result so obtained corresponds to that found by application of Maeder and Thommen's proposal of reference 28. (It should be noted, however, that the general expression for φ given in reference 28 is incorrect owing to improper treatment of plus and minus signs.)

If the free-stream Mach number is not unity, equation (40) is an integral equation, and it might appear that little progress toward a solution has been made. If attention is confined to the vicinity of the airfoil and to Mach numbers near unity, however, it is only necessary to approximate $\varphi_{\xi\xi}$ well locally and it is sufficient to substitute λ_P/k for $\varphi_{\xi\xi}$ or $\partial u/\partial\xi$ in the double integral. The integral can then be evaluated and the following relationship results:

$$u_P=\frac{(1-M_\infty^2)U_\infty}{M_\infty^2(\gamma+1)}-\frac{U_\infty}{\sqrt{\pi\lambda_P}}\frac{d}{dx}\int_0^x\frac{dZ/d\xi}{\sqrt{x-\xi}}d\xi \qquad (41)$$

If, once again, ku_x is restored in place of λ_P so that, in effect, the local value is used at each point, and the subscript P on

u is dropped, a simple nonlinear ordinary differential equation is obtained for u

$$u=\frac{(1-M_\infty^2)U_\infty}{M_\infty^2(\gamma+1)}-\frac{U_\infty}{\sqrt{\pi k(du/dx)}}\frac{d}{dx}\int_0^x\frac{dZ/d\xi}{\sqrt{x-\xi}}d\xi \tag{42}$$

Equation (42) can be written in the following form upon rearranging the terms and squaring both sides.

$$\left[u-\frac{(1-M_\infty^2)U_\infty}{M_\infty^2(\gamma+1)}\right]^2\frac{du}{dx}=\frac{U_\infty^3}{\pi M_\infty^2(\gamma+1)}\left(\frac{d}{dx}\int_0^x\frac{dZ/d\xi}{\sqrt{x-\xi}}d\xi\right)^2 \tag{43}$$

As in the other cases, equation (43) can be solved readily by separation of variables, and the constant of integration can be evaluated by introduction of the additional condition that equation (41) provides the correct location $x=x^*$ for the sonic point, or point where $u=(1-M_\infty^2)U_\infty/M_\infty^2(\gamma+1)$. The result is

$$\left[u-\frac{(1-M_\infty^2)U_\infty}{M_\infty^2(\gamma+1)}\right]^3=\frac{3U_\infty^3}{\pi M_\infty^2(\gamma+1)}\int_{x^*}^x\left(\frac{d}{dx_1}\int_0^{x_1}\frac{dZ/d\xi}{\sqrt{x_1-\xi}}d\xi\right)^2dx_1 \tag{44}$$

where x^* is the value for x for which

$$\frac{d}{dx}\int_0^x\frac{dZ/d\xi}{\sqrt{x-\xi}}d\xi=0 \tag{45}$$

This method of evaluation of the constant of integration is completely analogous to that employed in the analysis of subsonic and supersonic flows, and is necessary in the analysis of flows with free-stream Mach number near 1 in order to avoid infinite pressure gradients at the point of sonic velocity on smooth airfoils. This method, moreover, provides a mechanism for the introduction of direct upstream dependence on airfoil shape in the subsonic region, and its exclusion in the supersonic region. The corresponding relation for the pressure coefficient C_p is obtained by combination of equations (2) and (44) and is

$$C_p=\frac{-2(1-M_\infty^2)}{M_\infty^2(\gamma+1)}-2\left[\frac{3}{\pi M_\infty^2(\gamma+1)}\int_{x^*}^x\left(\frac{d}{dx_1}\int_0^{x_1}\frac{dZ/d\xi}{\sqrt{x_1-\xi}}d\xi\right)^2dx_1\right]^{1/3} \tag{46}$$

An alternative expression in terms of the transonic similarity parameter is

$$\overline{C}_p\equiv\frac{[M_\infty^2(\gamma+1)]^{1/3}}{\tau^{2/3}}C_p=2\xi_\infty-2\left\{\frac{3}{\pi}\int_{x^*}^x\left[\frac{d}{dx_1}\int_0^{x_1}\frac{d(Z/\tau)/d\xi}{\sqrt{x_1-\xi}}d\xi\right]^2dx_1\right\}^{1/3}=2\xi_\infty+\overline{C}_{p_{\xi_\infty=0}} \tag{47}$$

The variation of C_p with ξ_∞ expressed by equation (47) is exact, within the approximation of transonic small disturbance theory, for flows with free-stream Mach numbers very near unity, and is associated with the fact that the local Mach number distribution on an airfoil is independent of the free-stream Mach number at values of the latter near unity. This phenomenon has been discussed previously in references 30, 31, 6, and elsewhere.

Once C_p is known, the pressure drag d can be readily calculated by use of the following relation

$$c_d\equiv\frac{d}{\frac{\rho_\infty}{2}U_\infty^2c}\equiv\frac{2}{c}\int_0^c C_p\frac{dZ}{dx}dx \tag{48}$$

Application to single-wedge airfoils.—Sufficient theoretical and experimental results are available at the present time to provide considerable insight into the accuracy and usefulness of equation (46) or (47). The shape for which the greatest amount of information is available is the single-wedge profile for which both theoretical and experimental pressure distributions are available. Thus, consider a single-wedge profile of maximum thickness t and chord $c/2$ as illustrated in figure 9. The ordinates of the airfoil upper surface are

$$\left.\begin{aligned}Z=t\frac{x}{c}=\tau x \quad &\text{for } 0<x<c/2\\ Z=t/2=\tau c/2 \ &\text{for } x>c/2\end{aligned}\right\} \tag{49}$$

and the semiapex angle θ is equal, to the order of accuracy of thin airfoil theory, to τ. Substitution of equation (49) for Z into equations (45) and (46) provides that the sonic point is at the shoulder ($x^*=c/2$) and that the pressure distribution on the surface of the wedge at free-stream Mach numbers near 1 is

$$\overline{C}_p\equiv\frac{[M_\infty^2(\gamma+1)]^{1/3}}{\tau^{2/3}}C_p=2\xi_\infty-2\left(\frac{3}{\pi}\ln\frac{x}{c/2}\right)^{1/3} \tag{50}$$

A plot of the results for Mach number 1 is shown in figure 10 together with the corresponding theoretical results given by Guderley and Yoshihara in reference 32. Although some approximations are introduced in the course of the latter analysis, the results are generally regarded as virtually an exact solution of the equations of transonic small disturbance

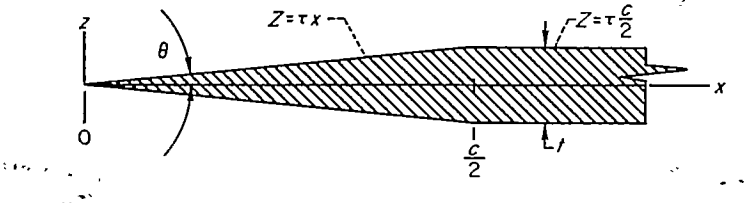

FIGURE 9.—View of single-wedge airfoil and principal dimensions.

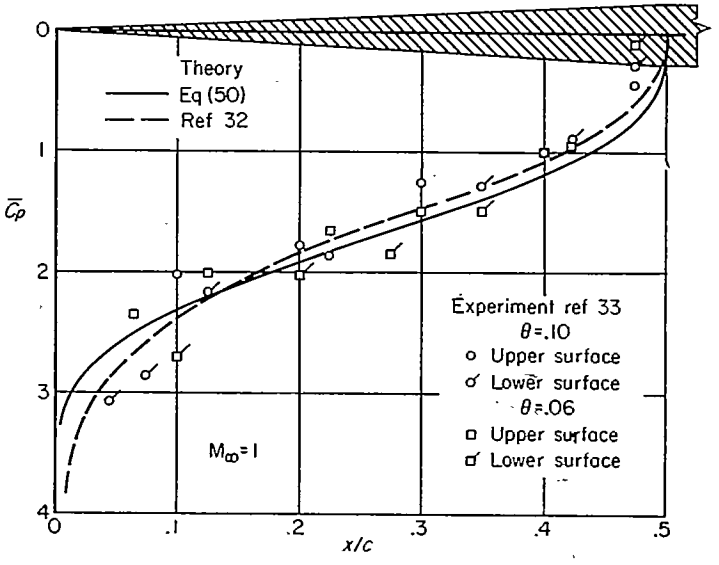

FIGURE 10.—Theoretical and experimental pressure distributions for single-wedge airfoils at free-stream Mach number 1.

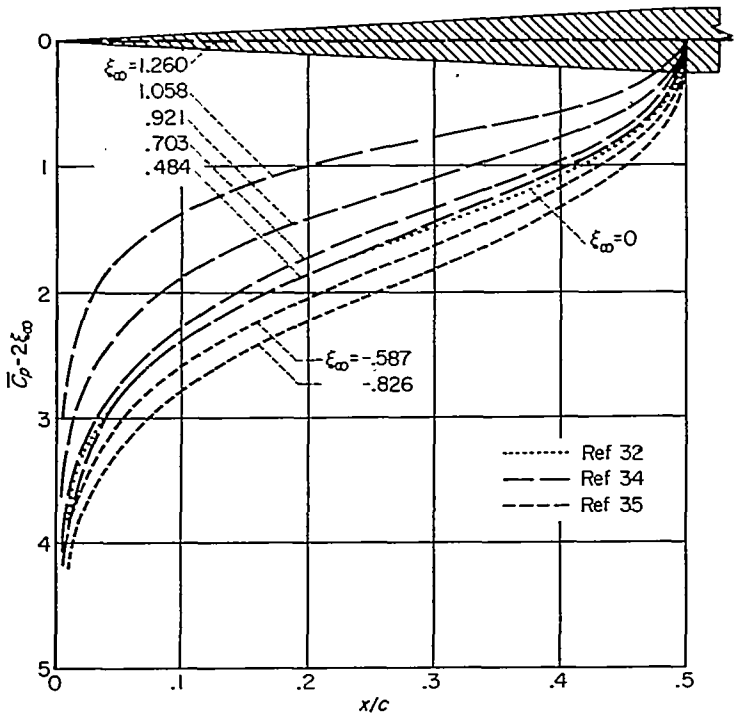

FIGURE 11.—Summary of other theoretical results for transonic flow past single-wedge airfoils.

theory. Also included in figure 10 are experimental results for $M_\infty=1$ obtained in the Langley annular transonic wind tunnel and reported by Habel, Henderson, and Miller in reference 33.

Since the comparisons shown in figure 10 indicate that equation (50) provides an approximate solution for the pressure distribution on a single-wedge profile at $M_\infty=1$ that is probably satisfactory for most purposes, and since the variation of $\overline{C}_p$ with ξ_∞ given by equation (47) or (50) is exact, within the framework of transonic small disturbance theory, at $M_\infty=1$, the principal question remaining in the evaluation of the degree of approximation afforded by use of equation (50) is to define the range of ξ_∞, or Mach number, over which it applies. Accordingly, figure 11 has been prepared to summarize the results given previously by Guderley and Yoshihara for Mach number 1 (ref. 32), by Vincenti and Wagoner for Mach numbers slightly greater than unity (ref. 34), and by Yoshihara for Mach numbers slightly less than unity (ref. 35). The latter two sets of results were obtained by lengthy numerical calculations and, together with the results for Mach number 1, are generally regarded as being very close to those that would be given by exact solutions of the equations of transonic small disturbance theory. The results are plotted in terms of $\overline{C}_p-2\xi_\infty$ so that the pressure distributions for Mach numbers very near unity should determine a single line. It can be seen that the variation of $\overline{C}_p$ with ξ_∞ indicated by equation (47) or (50) holds until the absolute value of ξ_∞ is nearly one-half. At greater values, the results begin to tend toward those associated with purely subsonic or purely supersonic flows, and equations (47) and (50) are no longer applicable.

Experimental measurements of the flow around single-wedge profiles at free-stream Mach numbers both less than and greater than unity have been made by Liepmann and Bryson and reported in references 30 and 31. Results were obtained for three different profiles having semiapex angles of 4½°, 7½°, and 10°. Plots of the experimental pressure distributions for the test Mach numbers closest to unity for each profile are shown in figure 12 together with the theoretical pressure distribution calculated by use of equation (50). Additional experimental data for other Mach numbers are not included on figure 12 since those shown are already for values of ξ_∞ that are somewhat outside the range of validity of equation (50). Only the theoretical results given by equation (50) are included since examination of the data reveals that these results differ less from the theoretical results shown on figure 11, for Mach numbers near unity, than the experimental curves differ from either set of theoretical curves, or even than the experimental curves differ among themselves. Perhaps the most prominent discrepancy is that which occurs near the shoulder. Theory indicates that sonic velocity ($\overline{C}_p-2\xi_\infty=0$) occurs at the shoulder, whereas the experimental data, particularly that of Liepmann and Bryson, consistently indicate that sonic velocity occurs forward of the shoulder. It is interesting to observe that this discrepancy is greatest for the thinnest airfoil tested.

The foregoing results may be contrasted with those obtained by direct use of equation (41) in which case $\overline{C}_p-2\xi_\infty$

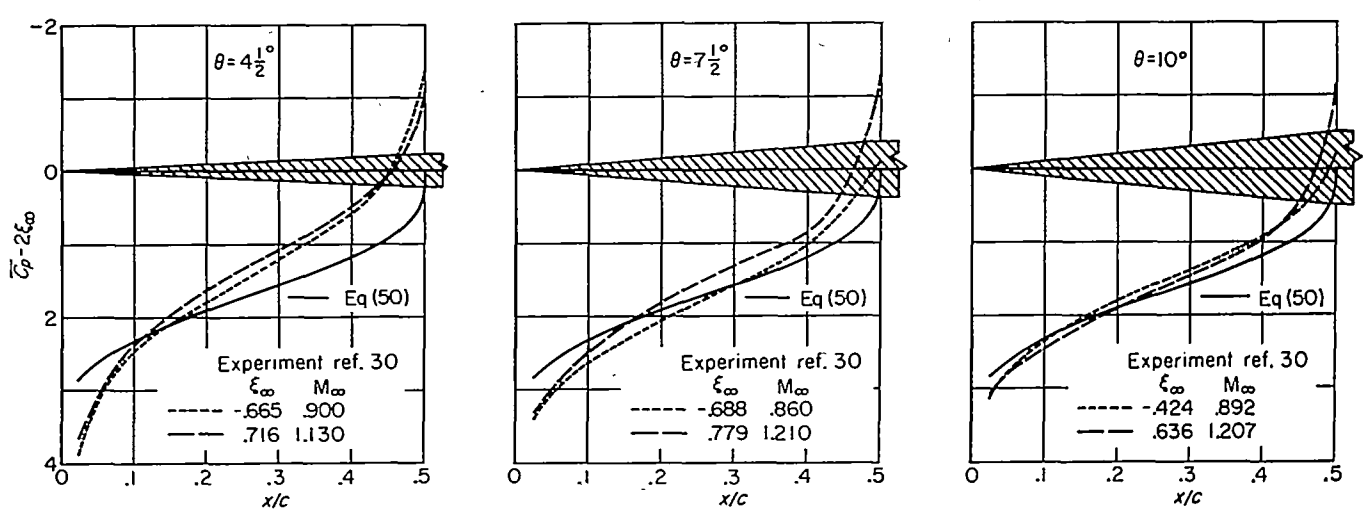

FIGURE 12.—Theoretical and experimental pressure distributions for three single-wedge airfoils at free-stream Mach numbers near 1.

is found to be proportional to $1/\sqrt{\lambda_P x}$. It is clear from this comparison that there is no constant with which λ_P can be replaced that would provide a satisfactory solution for the pressure distribution on a single-wedge airfoil at free-stream Mach numbers near unity.

The pressure drag of single-wedge profiles at Mach numbers near 1 can be found easily by integration of equation (48) with the relations given by equations (49) and (50) substituted for Z and C_p. The result is

$$\frac{[M_\infty^2(\gamma+1)]^{1/3}c_d}{\tau^{5/3}} \equiv \bar{c}_d = 2\xi_\infty + 2\left(\frac{3}{\pi}\right)^{1/3}\Gamma\left(\frac{4}{3}\right) = 2\xi_\infty + 1.758 \quad (51)$$

where Γ represents the gamma function. This result compares very favorably with the value of 1.75 for $\xi_\infty = 0$, or Mach number 1, given by Cole in reference 36 as that obtained by numerical integration of the pressure distribution given by Guderley and Yoshihara in reference 32. Cole's own theory for the drag of a single-wedge airfoil at high subsonic speeds, which is fundamentally somewhat less accurate than Guderley and Yoshihara's theory, gives the value 1.67 for $\xi_\infty = 0$.

Application to biconvex circular-arc airfoils.—In addition to data for three single-wedge profiles, Bryson also gives in reference 30 experimental results for transonic flow around the front half of an 8.8-percent thick biconvex circular-arc airfoil followed by a straight section as illustrated in figure 13. Since the pressure distribution on the curved portion

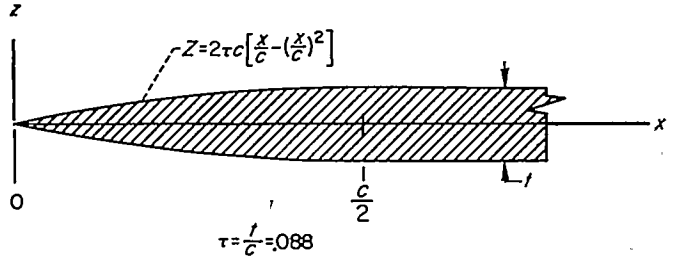

FIGURE 13.—View of a half-circular-arc airfoil and principal dimensions.

of this profile is the same at Mach numbers near unity as that on the front half of a complete circular-arc airfoil having the same thickness ratio, and additional experimental data are available for the latter airfoil although for other thickness ratios, the following analysis is developed for a complete biconvex circular-arc airfoil. It is moreover sufficient, in thin airfoil theory, to approximate the ordinates Z for a circular-arc airfoil by those for a parabolic-arc airfoil, thus

$$\frac{Z}{c} = 2\tau\left[\frac{x}{c}-\left(\frac{x}{c}\right)^2\right] \quad (52)$$

where τ is the thickness ratio as indicated in figure 14. Substitution of this relation for Z into equations (45) and (47) yields the following result for the pressure distribution on the airfoil surface.

$$\bar{C}_p \equiv \frac{[M_\infty^2(\gamma+1)]^{1/3}}{\tau^{2/3}} C_p = 2\xi_\infty - 2\left\{\frac{12}{\pi}\left[ln\left(4\frac{x}{c}\right) - 8\frac{x}{c} + 8\left(\frac{x}{c}\right)^2 + \frac{3}{2}\right]\right\}^{1/3} \quad (53)$$

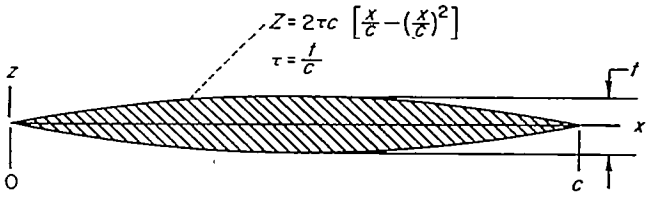

FIGURE 14.—View of a complete circular-arc airfoil and principal dimensions.

Figure 15 shows a comparison of the pressure distributions for Mach numbers near unity calculated by use of equation (53) with those obtained from Bryson's experiments with the half airfoil. As for the single-wedge profile, the results are again plotted in terms of $\bar{C}_p - 2\xi_\infty$ since experimental results are available only for Mach numbers somewhat different from unity. It can be seen by comparison of figures 12 and 15 that the theoretical and experimental results are in much better agreement for the front half of a circular-arc airfoil than for single-wedge profiles. Experimental pressure distributions for transonic flow past four complete biconvex circular-arc airfoils having thickness ratios of 6, 8, 10, and 12 percent have been given by Michel, Marchaud, and Le Gallo in reference 37. Their results for Mach number 1 are plotted in figure 16 together with the theoretical results calculated by use of equation (53). These results are presented in terms of $\bar{C}_p$ because transonic theory indicates that the pressure distributions for all four airfoils should then define a single curve independent of the thickness ratio. Results for Mach numbers other than unity are not included on this plot because the variation of $\bar{C}_p$ with ξ_∞ for small ξ_∞ indicated by equation (47) and subsequent relations is not only simple but is amply verified by the preceding comparisons

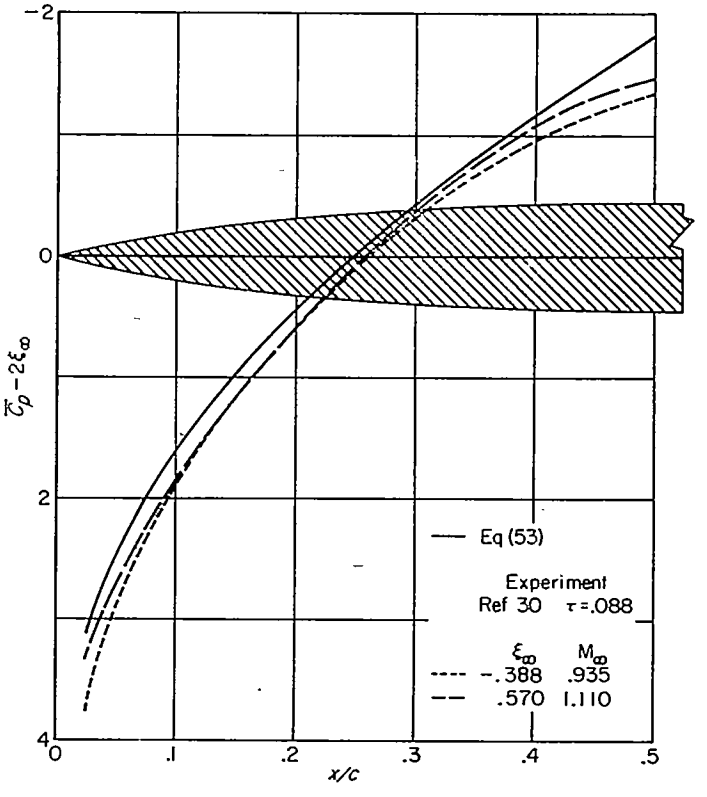

FIGURE 15.—Theoretical and experimental pressure distributions for half-circular-arc airfoils at free-stream Mach numbers near 1.

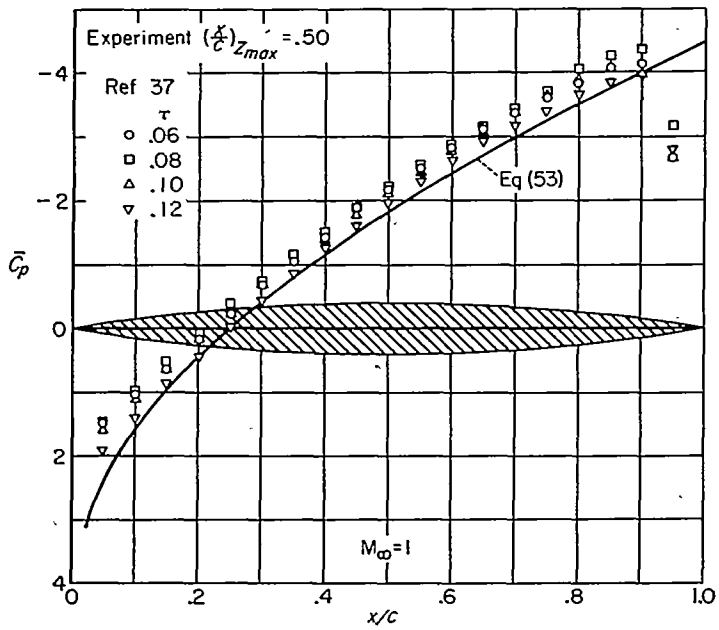

FIGURE 16.—Theoretical and experimental pressure distributions for circular-arc airfoils; $M_\infty=1$.

and by similar discussions elsewhere in the literature of transonic flow. It can be seen that the theoretical and experimental results are in substantial agreement. The most notable discrepancy is that found near the trailing edge, and can be attributed to flow separation induced by boundary-layer shock-wave interaction. It can also be seen that the agreement between theory and experiment is not so good for the complete airfoils, particularly the thinner ones, as for the half airfoil. Part of the discrepancy for the complete airfoils may possibly be attributed to the experimental technique in which the airfoil is simulated by a bump on the tunnel wall and is hence imbedded in the wall boundary layer. Some comments on this method of testing have been given recently by Carroll and Anderson in reference 38.

The pressure drag of circular-arc airfoils at Mach numbers near 1 has been found by numerical integration of equation (48) with the relations given by equations (52) and (53) substituted for Z and C_p and is

$$\frac{[M_\infty^2(\gamma+1)]^{1/3}c_d}{\tau^{5/3}}\equiv\bar{c}_d=4.77 \tag{54}$$

The pressure drag of the front half can be evaluated in the same way by changing the upper limit in equation (48) to $c/2$ and is

$$\bar{c}_d=2\xi_\infty+1.13 \tag{55}$$

The integrations required to determine the drag results given in equations (54) and (55) were evaluated numerically using Simpson's rule together with an analytic determination of the contribution of the region in the immediate vicinity of the leading-edge singularity. Sufficiently fine intervals were used that the resulting values are estimated to be accurate to within about one digit in the third significant figure, as judged by comparison with the results of similar calculations made with wider intervals. It is necessary to use very fine intervals, particularly near the nose, to achieve such accuracy, and intervals as small as $0.00005c$ were used in some cases.

Application to a family of airfoils having the point of maximum thickness displaced aft of the midchord station.—The primary object of this present section is to present some comparisons of calculated and measured pressure distributions at Mach number 1 on a number of specific airfoils that have the point of maximum thickness aft of the midchord station. The experimental data are from reference 39 by Michel, Marchaud, and Le Gallo, and are for members of the family of airfoils having ordinates given by

$$\frac{Z}{c}=A\left[\frac{x}{c}-\left(\frac{x}{c}\right)^n\right] \tag{56}$$

where A and n are constants for each airfoil and n is greater than unity. The values selected for A and n determine the thickness ratio τ and the location $(x/c)_{z_{max}}$ of the point of maximum thickness according to the relations

$$\left(\frac{x}{c}\right)_{z_{max}}=\left(\frac{1}{n}\right)^{\frac{1}{n-1}} \tag{57}$$

$$\tau=2A\left[\left(\frac{1}{n}\right)^{\frac{1}{n-1}}-\left(\frac{1}{n}\right)^{\frac{n}{n-1}}\right]=\frac{2A(n-1)}{n^{n/(n-1)}} \tag{58}$$

The biconvex circular-arc airfoils discussed in the preceding section are special cases of the present family that correspond to $n=2$. The point of maximum thickness is located forward or aft of the midchord station depending on whether n is less than or greater than 2. The particular airfoils tested by Michel, Marchaud, and Le Gallo are special cases that correspond to either $n=3.38$ or 6.05 and have the point of maximum thickness at 0.60 or 0.70 chord. As in the earlier work by the same investigators on biconvex circular-arc airfoils, the results were obtained by simulating the airfoil by a bump on the tunnel wall and are again subject to criticism regarding the influence of the wall boundary layer.

Substitution of equation (56) for Z into equations (45) and (46) yields the following result for the pressure distribution on the airfoil surface for Mach number near unity:

$$\bar{C}_p\equiv\frac{[M_\infty^2(\gamma+1)]^{1/3}}{\tau^{2/3}}C_p$$

$$=2\xi_\infty-2\left\{\frac{3}{4\pi}\left[\frac{n^{n/(n-1)}}{n-1}\right]^2\right\}^{1/3}\left\{\ln\frac{x}{c}-\right.$$

$$\left.\frac{2\sqrt{\pi}\Gamma(n+1)}{(n-1)\Gamma\left(n-\frac{1}{2}\right)}\left(\frac{x}{c}\right)^{n-1}+\frac{\pi[\Gamma(n+1)]^2}{2(n-1)\left[\Gamma\left(n-\frac{1}{2}\right)\right]^2}\left(\frac{x}{c}\right)^{2(n-1)}+\right.$$

$$\left.\frac{1}{n-1}\ln\frac{\sqrt{\pi}\Gamma(n+1)}{\Gamma\left(n-\frac{1}{2}\right)}+\frac{3}{2(n-1)}\right\}^{1/3} \tag{59}$$

where Γ represents the gamma function. If m is any positive integer greater than unity, the following relations are useful for evaluation of the gamma function:

$$\left.\begin{aligned} &\Gamma(m)=1\cdot2\cdot3\ldots(m-1)=(m-1)!, \qquad \Gamma(1/2)=\sqrt{\pi} \\ &\Gamma\left(m+\frac{1}{2}\right)=\sqrt{\pi}\,\frac{1}{2}\cdot\frac{3}{2}\cdot\frac{5}{2}\cdot\cdot\left(m-\frac{1}{2}\right), \qquad \Gamma\left(\frac{3}{2}\right)=\frac{\sqrt{\pi}}{2} \end{aligned}\right\} \quad (60)$$

Substitution of $n=2$ in equation (59) reproduces equation (53) for the pressure distribution on biconvex circular-arc airfoils as a special case. Equation (50) for the pressure distribution on a single-wedge airfoil can also be obtained as a limiting case by setting $n=\infty$ and noting that the chord of the wedge is designated here as c rather than $c/2$. Theoretical pressure distributions on the airfoils tested by Michel, Marchaud, and Le Gallo are obtained from equation (59) by substitution of the values 3.38 and 6.05 for n. Figures 17 and 18 show comparisons of the theoretical and experimental pressure distributions for $M_\infty=1$ for the two groups of airfoils. Except for the discrepancy near the trailing edge which can again be attributed to boundary-layer shock-wave interaction, it can be seen that the theoretical and experimental results are in at least qualitative agreement. Some differences occur, however, in the levels of the pressure distribution curves. Comparison with the results for the circular-arc airfoils shown in figure 16 reveals that the same trend is in evidence for those airfoils, although to a lesser degree, and that the difference between the theoretical and experimental results increases as the point of maximum thickness moves rearward. It is not clear at the present time whether this discrepancy is to be attributed principally to the shortcomings of the theoretical or the experimental results.

Application to a family of airfoils having the point of maximum thickness forward of midchord station.—The test program of Michel, Marchaud, and Le Gallo reported in reference 39 and discussed in the preceding section also included tests of each of the airfoils reversed in the wind

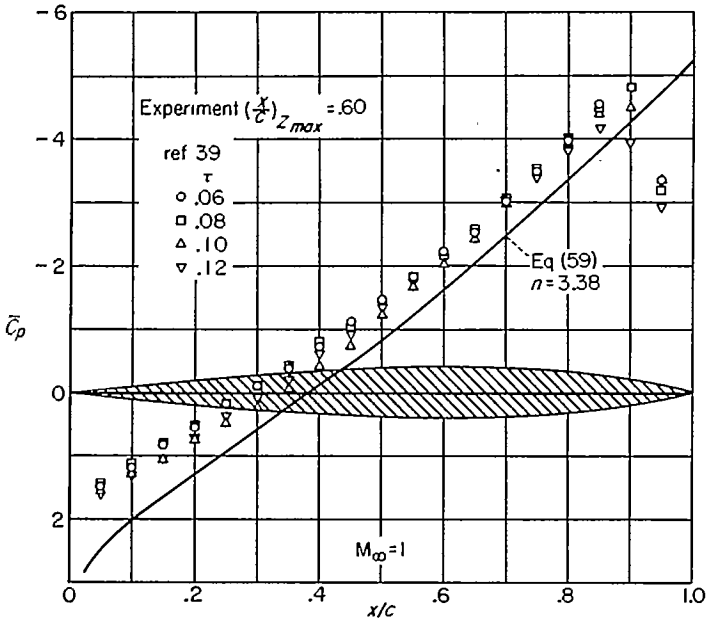

FIGURE 17.—Theoretical and experimental pressure distributions for airfoils having maximum thickness at 0.60 chord; $M_\infty=1$.

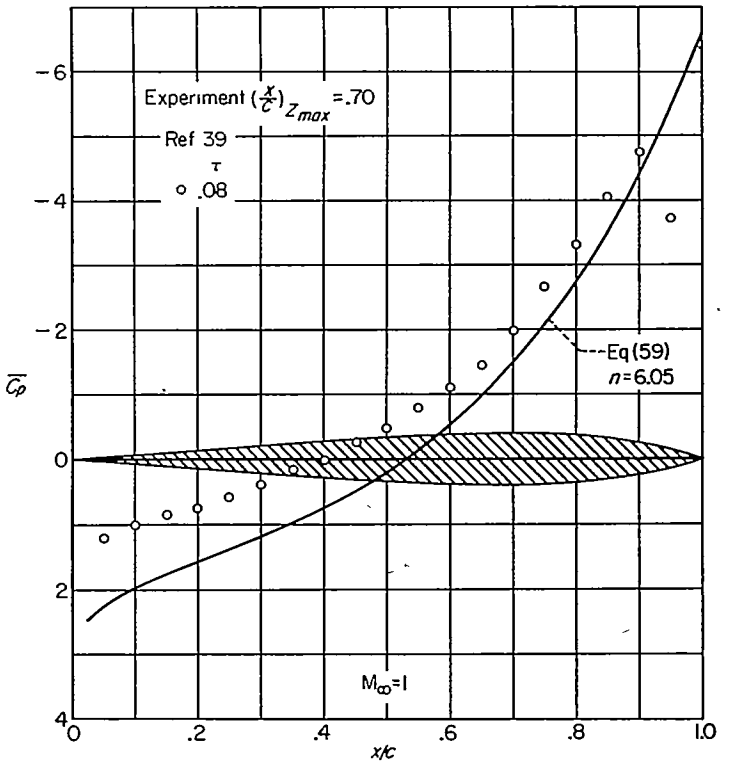

FIGURE 18.—Theoretical and experimental pressure distributions for airfoils having maximum thickness at 0.70 chord: $M_\infty=1$.

tunnel so that the point of maximum thickness is located forward of the midchord station. The particular airfoils tested are thus specific cases of the family of profiles described by equation (56) with x/c replaced by $1-(x/c)$; that is, the ordinates are

$$\frac{Z}{c}=A\left[1-\frac{x}{c}-\left(1-\frac{x}{c}\right)^n\right] \quad (61)$$

where A and n are again constants for each airfoil and n is greater than unity. The values selected for A and n determine the thickness ratio τ and the location $(x/c)_{Z_{max}}$ of the point of maximum thickness according to the relations

$$\left(1-\frac{x}{c}\right)_{Z_{max}}=\left(\frac{1}{n}\right)^{\frac{1}{n-1}} \quad (62)$$

$$\tau=\frac{2A(n-1)}{n^{n/(n-1)}} \quad (63)$$

Biconvex circular-arc airfoils are special cases of the present family that correspond to $n=2$. The point of maximum thickness is located forward or aft of the midchord station depending on whether n is greater or less than 2. The particular airfoils tested by Michel, Marchaud, and Le Gallo are special cases that correspond to either $n=3.38$ or 6.05 and have the point of maximum thickness at 0.40 or 0.30 chord.

Since the integrations encountered when equation (61) is substituted in equations (45) and (46) for the determination of C_p are more difficult than those encountered in any of

the preceding examples, no general formula will be given for arbitrary n. Two formulas of more restricted generality are given, however. One is applicable when n is any integer greater than unity, the other when n is one-half plus any positive integer. The first is

$$\bar{C}_p=2\xi_\infty-2\left[\frac{3}{4\pi}\left(\frac{n^{\frac{n}{n-1}}}{n-1}\right)^2\right]^{1/3}\left[\left\{(n-1)^2 ln\frac{x}{c}+2(n-1)\Gamma(n+1)\sqrt{\pi}\sum_{\nu=1}^{n-1}\frac{1}{\Gamma(n-\nu)\Gamma\left(\nu+\frac{1}{2}\right)}\frac{(-x/c)^\nu}{\nu}+[\Gamma(n+1)]^2\pi\sum_{\nu=1}^{n-1}\frac{1}{\Gamma(n-\nu)\Gamma\left(\nu+\frac{1}{2}\right)}\sum_{\mu=1}^{n-1}\frac{1}{\Gamma(n-\mu)\Gamma\left(\mu+\frac{1}{2}\right)}\frac{(-x/c)^{\nu+\mu}}{\nu+\mu}\right\}\Bigg|_{x^*}^{x}\right]^{1/3} \tag{64}$$

where the symbol $|_{x^*}^{x}$ is used to denote the difference between the preceding expression with first x and then x^* substituted for x, that is,

$$f(x)\Big|_{x^*}^{x}=f(x)-f(x^*)$$

where x^*, the location of the sonic point, is found from

$$n-1+\Gamma(n+1)\sqrt{\pi}\sum_{\nu=1}^{n-1}\frac{(-x^*/c)^\nu}{\Gamma(n-\nu)\Gamma\left(\nu+\frac{1}{2}\right)}=0$$

and Γ refers again to the gamma function. The second is

$$\bar{C}_p=2\xi_\infty-2\left[\frac{3}{4\pi}\left(\frac{n^{\frac{n}{n-1}}}{n-1}\right)^2\right]^{1/3}\left[\left\{(n-1)^2 ln\frac{x}{c}-\frac{B^2\left(1-\frac{x}{c}\right)^{2n-2}}{2n-2}\left(ln\frac{1+\sqrt{x/c}}{1-\sqrt{x/c}}\right)^2+\left[\left(1+\sqrt{\frac{x}{c}}\right)ln\left(1+\sqrt{\frac{x}{c}}\right)+\left(1-\sqrt{\frac{x}{c}}\right)ln\left(1-\sqrt{\frac{x}{c}}\right)\right]\left[-2n(n-1)+\frac{B^2\sqrt{\pi}}{n-1}F(2n-2)\right]+\left[\frac{x}{c}+\left(1+\frac{x}{c}\sqrt{\frac{x}{c}}\right)ln\left(1+\sqrt{\frac{x}{c}}\right)+\left(1-\frac{x}{c}\sqrt{\frac{x}{c}}\right)ln\left(1-\sqrt{\frac{x}{c}}\right)\right]\left[B^2\pi\sum_{\nu=1}^{n-\frac{3}{2}}\frac{F\left(n-\frac{1}{2}-\nu\right)F\left(n-\frac{3}{2}+\nu\right)}{n-1+\nu}\right]-\frac{2n(n-1)}{\sqrt{\pi}}\left(1-\frac{x}{c}\right)\sum_{\nu=1}^{n-\frac{3}{2}}\frac{\left(1-\frac{x}{c}\right)^{n-\frac{3}{2}-\nu}}{\left(n-\frac{1}{2}-\nu\right)F\left(n-\frac{1}{2}-\nu\right)}\left(\frac{1}{n-\frac{1}{2}-\nu}+\sqrt{\frac{x}{c}}\,ln\frac{1+\sqrt{x/c}}{1-\sqrt{x/c}}\right)+\frac{B^2}{n-1}\left(1-\frac{x}{c}\right)F(2n-2)\sum_{\nu=1}^{2n-3}\frac{\left(1-\frac{x}{c}\right)^{2n-3-\nu}}{(2n-2-\nu)F(2n-2-\nu)}\left(\frac{1}{2n-2-\nu}+\sqrt{\frac{x}{c}}\,ln\frac{1+\sqrt{x/c}}{1-\sqrt{x/c}}\right)+2B^2\sqrt{\pi}\left(1-\frac{x}{c}\right)\sum_{\nu=1}^{n-\frac{3}{2}}\frac{F\left(n-\frac{1}{2}-\nu\right)F\left(n-\frac{3}{2}+\nu\right)}{n-1+\nu}\sum_{\mu=1}^{n-\frac{5}{2}+\nu}\frac{\left(1-\frac{x}{c}\right)^{n-\frac{5}{2}+\nu-\mu}}{F\left(n-\frac{1}{2}+\nu-\mu\right)}\left[\frac{1}{n-\frac{3}{2}+\nu-\mu}-\frac{\left(1-\frac{x}{c}\right)}{n-\frac{1}{2}+\nu-\mu}+\frac{x}{c}\sqrt{\frac{x}{c}}\,ln\frac{1+\sqrt{x/c}}{1-\sqrt{x/c}}\right]+2(n-1)B\sqrt{\pi}\sum_{\nu=1}^{n-\frac{3}{2}}F\left(n-\frac{1}{2}-\nu\right)\frac{\left(1-\frac{x}{c}\right)^\nu}{\nu}-B^2\pi\sum_{\nu=1}^{n-\frac{3}{2}}F\left(n-\frac{1}{2}-\nu\right)\sum_{\mu=1}^{n-\frac{3}{2}}F\left(n-\frac{1}{2}-\mu\right)\left(1-\frac{x}{c}\right)^{\nu+\mu-1}\left[\frac{1}{\nu+\mu-1}-\frac{\left(1-\frac{x}{c}\right)}{\nu+\mu}\right]\right\}\Bigg|_{x^*}^{x}\right]^{1/3} \tag{65}$$

where $B=\dfrac{n}{\sqrt{\pi}F\left(n-\frac{1}{2}\right)}$, and $F(\zeta)=\dfrac{\Gamma(\zeta)}{\Gamma\left(\zeta+\frac{1}{2}\right)}$

Attention is called to the fact that ν and μ are positive integers so that when n=(3/2) all the summations drop out.

Again x^* is the location of the sonic point and it is found from

$$n-1-B\left(1-\frac{x^*}{c}\right)^{n-\frac{3}{2}}\sqrt{\frac{x^*}{c}}ln\frac{1+\sqrt{x^*/c}}{1-\sqrt{x^*/c}}-B\sum_{\nu=1}^{n-\frac{3}{2}}F\left(n-\frac{1}{2}-\nu\right)\frac{x^*}{c}\left(1-\frac{x^*}{c}\right)^{\nu-1}=0$$

Substitution of $n=2$ in equation (64) again reproduces equation (53) for the pressure distribution on biconvex circular-arc airfoils. Figures 19 and 20 show comparisons of the pressure distributions measured at Mach number 1.3 by Michel, Marchaud, and Le Gallo with those calculated by use of equations (64) and (65). The experimental results shown in sketch (s) are for airfoils that have the point of maximum thickness located at 0.40 chord corresponding to a value for n of 3.38. Since results could not be calculated analytically for this value for n, theoretical results are shown for both $n=3.0$ and $n=3.5$. The corresponding locations for the point of maximum thickness can be readily calculated using equation (62) and are 0.423 and 0.394 chord. Similarly, the experimental results shown in figure 20 are for an

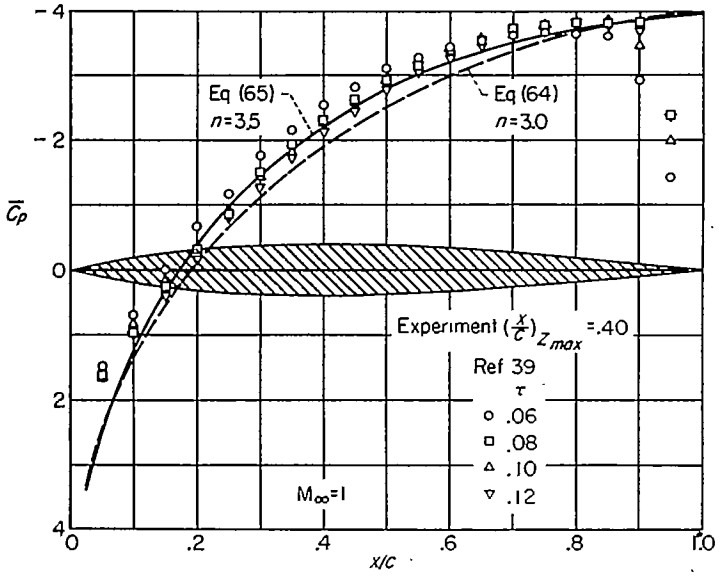

FIGURE 19.—Theoretical and experimental pressure distributions for airfoils having maximum thickness near 0.40 chord; $M_\infty=1$.

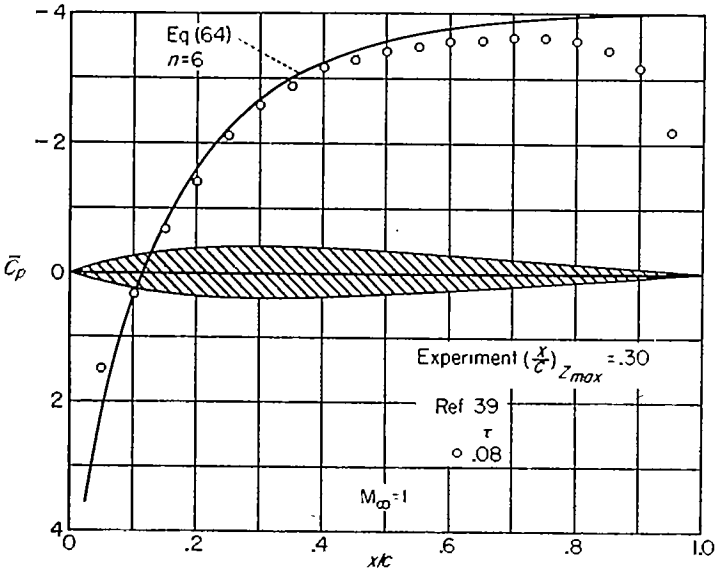

FIGURE 20.—Theoretical and experimental pressure distributions for airfoils having maximum thickness at 0.30 chord: $M_\infty=1$.

airfoil that has the point of maximum thickness located at 0.30 chord corresponding to a value for n of 6.05; whereas the theoretical results are for airfoils that have the point of maximum thickness located at 0.301 chord corresponding to a value for n of 6.00. These results continue the trend noted in the preceding section that the agreement between the present experimental and theoretical results improves as the location of the point of maximum thickness moves forward along the chord. The principal discrepancy remaining is, in fact, reduced to that near the trailing edge associated with boundary-layer shock-wave interaction, and is therefore beyond the scope of any inviscid theory.

ACCELERATING FLOWS, INVERSE PROBLEMS

Approximate solution of equations for given pressure distribution.—Although all of the preceding discussion is concerned with the calculation of the pressure distribution on an airfoil of specified geometry, an equally important problem in many engineering situations is the design of an airfoil to have a specified pressure distribution at a given Mach number. This poses no new problem in the analysis of purely subsonic or purely supersonic flows by the present methods because the specification of C_p permits the determination of C_{p_L} through application of equation (31) or (17), and the inversion problem is reduced to the familiar inversion problem of linear theory. The necessary relation for flows with free-stream Mach number near 1 can be derived from consideration of equation (42) as an integral equation in which u and du/dx are given and the unknown appears in the integrand of a definite integral. This equation can be inverted readily since it has the same form as the relation encountered in the solution of Abel's integral equation (see, e. g., ref. 40, pp. 483–484). The inversion thus has the form of Abel's integral equation, and is the following in the present application:

$$\frac{dZ}{dx}=-\frac{1}{U_\infty}\sqrt{\frac{k}{\pi}}\int_0^x\left[u-\frac{(1-M_\infty^2)U_\infty}{M_\infty^2(\gamma+1)}\right]\sqrt{\frac{du}{d\xi}}\frac{d\xi}{\sqrt{x-\xi}} \tag{66}$$

The desired relation for the ordinates $Z(x)$ of the airfoil can now be found by a second integration, and is the following if it is assumed that Z is zero at the leading edge ($x=0$).

$$Z=Z^*-\frac{1}{U_\infty}\sqrt{\frac{k}{\pi}}\int_{x^*}^x dx_1\int_0^{x_1}\left[u-\frac{(1-M_\infty^2)U_\infty}{M_\infty^2(\gamma+1)}\right]\sqrt{\frac{du}{d\xi}}\frac{d\xi}{\sqrt{x_1-\xi}}$$

$$=-\frac{1}{U_\infty}\sqrt{\frac{k}{\pi}}\int_0^x dx_1\int_0^{x_1}\left[u-\frac{(1-M_\infty^2)U_\infty}{M_\infty^2(\gamma+1)}\right]\sqrt{\frac{du}{d\xi}}\frac{d\xi}{\sqrt{x_1-\xi}} \tag{67}$$

where Z^* is the ordinate at the point x^* where u is zero. It is interesting to note that the two alternative expressions for Z lead to identical results although the apparent regions of dependence, as indicated by the limits on the integrals, are quite different. The same result expressed in terms of C_p or $\overline{C}_p$ is

$$Z=\frac{1}{2}\sqrt{\frac{M_\infty^2(\gamma+1)}{2\pi}}\int_0^x dx_1\int_0^{x_1}\left[C_p+\frac{2(1-M_\infty^2)}{M_\infty^2(\gamma+1)}\right]\sqrt{-\frac{dC_p}{d\xi}}\frac{d\xi}{\sqrt{x_1-\xi}} \tag{68}$$

or

$$Z=\frac{\tau}{2\sqrt{2\pi}}\int_0^x dx_1\int_0^{x_1}(\overline{C}_p-2\xi_\infty)\sqrt{-\frac{d\overline{C}_p}{d\xi}}\frac{d\xi}{\sqrt{x_1-\xi}} \tag{69}$$

A simple application or check of these relations is furnished by substitution for $\overline{C}_p$ of the relation given in equation (50) for single-wedge profiles, whence Z is found to be equal to θx between $x=0$ and $x=c/2$. In the same way, substitution of equation (53) for $\overline{C}_p$ leads directly to equation (52) for the ordinates of a circular-arc airfoil, etc.

Application to airfoils with constant pressure gradient.—An example that permits an additional comparison with an existing theoretical result given by Guderley in reference 41, is furnished by consideration of the problem of determining the shape of an airfoil having a constant negative pressure gradient at $M_\infty=1$, thus

$$C_p=\frac{dC_p}{d(x/c)}\left(\frac{x}{c}-\frac{x^*}{c}\right)=-\Lambda\left(\frac{x}{c}-\frac{x^*}{c}\right) \tag{70}$$

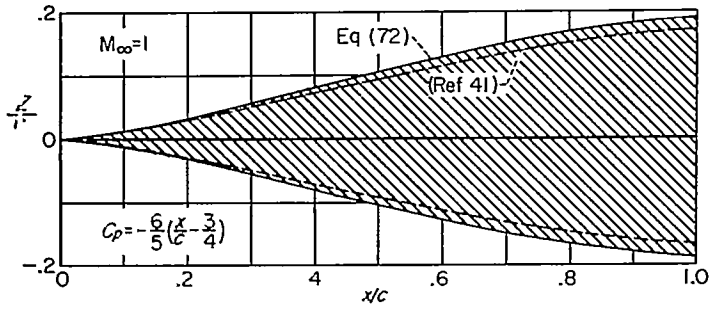

FIGURE 21.—Shape of the forward part of an airfoil having a constant pressure gradient at free-stream Mach number 1, as indicated by present theory and by Guderley.

where $\Lambda=-dC_p/d(x/c)$ is a positive constant. Substitution of this relation for C_p in equation (68) and integration leads directly to the following result:

$$\frac{Z}{c}=\frac{2}{3}\sqrt{\frac{\gamma+1}{2\pi}}\,\Lambda^{3/2}\left[\left(\frac{x}{c}\right)^{3/2}\left(\frac{x^*}{c}-\frac{2}{5}\frac{x}{c}\right)\right] \tag{71}$$

The special case considered by Guderley is obtained by insertion of the values $x^*/c=3/4$ and $\Lambda=6/5$, whence equation (71) reduces to

$$\frac{Z}{c}=\left(\frac{3}{5}\right)^{3/2}\sqrt{\frac{\gamma+1}{\pi}}\left[\left(\frac{x}{c}\right)^{3/2}\left(1-\frac{8}{15}\frac{x}{c}\right)\right] \tag{72}$$

Figure 21 shows a scale drawing of the profile calculated by use of equation (72) and of that given by Guderley. It is evident from the sketch that the present theory indicates larger values for the ordinates Z than are given by Guderley. Although the latter results are given only in graphical form, and are hence difficult to determine with precision, the two sets of values for Z appear to be related by a constant ratio of approximately 9 to 8.[6]

The case considered by Guderley and discussed above results in a shape that does not close at the stern. It can be seen immediately from equation (71), however, that a closed airfoil will result if x^*/c is equated to 2/5, in which case equation (71) reduces to

$$\frac{Z}{c}=\frac{4}{15}\sqrt{\frac{\gamma+1}{2\pi}}\,\Lambda^{3/2}\left[\left(\frac{x}{c}\right)^{3/2}\left(1-\frac{x}{c}\right)\right] \tag{73}$$

A plot of the results is shown in figure 22.

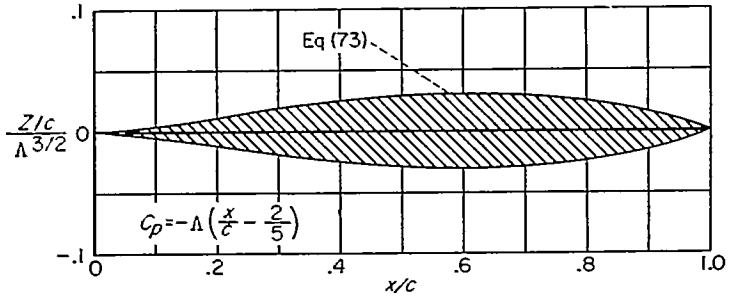

FIGURE 22.—Shape of complete airfoil having a constant pressure gradient at free-stream Mach number 1.

[6] This conclusion is confirmed by a new solution in closed analytic form given by Guderley on page 239 of his book "Theorie Schallnaher Strömungen" published by Springer-Verlag in 1957. Guderley's result has the same functional form as equation (72), but the coefficient in the latter result is greater by a factor $2/\sqrt{\pi}\approx 9.027/8$, after correcting an obvious slip in Guderley's final equation.

DECELERATING FLOWS

Although it is clear that the preceding relations are not appropriate for the analysis of flows with free-stream Mach number near 1 that decelerate smoothly through sonic velocity, it might appear that the proper expressions could be derived by formal application of the procedures described in the preceding section for positive λ_P to the approximate solution of equation (39) for negative λ_P. The analysis leads, in the absence of contributions from shock waves, to the following relation for u at the airfoil surface instead of equation (40)

$$u_P=-\frac{U_\infty}{\sqrt{-\pi\lambda_P}}\frac{d}{dx}\int_x^c\frac{dZ/d\xi}{\sqrt{\xi-x}}\,d\xi+\frac{1}{\lambda_P}\frac{\partial}{\partial x}\int_{-\infty}^{+\infty}d\zeta\int_x^\infty\sigma_P f\,d\xi \tag{74}$$

where

$$f=-(1-M_\infty^2)\varphi_{\xi\xi},\qquad \sigma_P=\sqrt{\frac{-\lambda_P}{4\pi(\xi-x)}}\,e^{\left[\frac{\lambda_P(x-\zeta)^2}{4(\xi-x)}\right]}$$

The principal difference between the results for the two cases is that the value of $u(x)$ indicated by equation (74) depends on conditions downstream of the point x, whereas that indicated by equation (40) for positive λ_P depends on conditions upstream of x. This difference is a fundamental property of equation (39) and necessitates a change in the argument required to disregard additional contributions from shock waves, because now it is the oblique shock waves situated downstream, rather than upstream of x, that furnish a contribution to $u(x)$. If, however, there are no oblique shock waves downstream of x, or if the contributions resulting from additional integrals over the shock surfaces are disregarded so that equation (74) can be used as a starting point in the analysis, the following result is obtained by proceeding in a fashion analogous to that employed in the derivation of equation (47) from (40):

$$\overline{C}_p=2\xi_\infty+2\left\{\frac{3}{\pi}\int_{x^*}^x\left[\frac{d}{dx_1}\int_{x_1}^c\frac{d(Z/\tau)/d\xi}{\sqrt{\xi-x_1}}\right]^2dx_1\right\}^{1/3} \tag{75}$$

The symbol x^* again refers to the location of the sonic point and is equal to the value for x for which

$$\frac{d}{dx}\int_x^c\frac{dZ/d\xi}{\sqrt{\xi-x}}\,d\xi=0 \tag{76}$$

The corresponding relation for the shape of an airfoil associated with a given pressure distribution at some free-stream Mach number near unity can also be found and is the following, again assuming that Z is zero at the leading edge:

$$Z=-\frac{\tau}{2\sqrt{2\pi}}\int_0^x dx_1\int_{x_1}^c\frac{(\overline{C}_p-2\xi_\infty)\sqrt{d\overline{C}_p/d\xi}}{\sqrt{\xi-x_1}}\,d\xi \tag{77}$$

No further use is made in this paper of equations (74) through (77) for decelerating flows at free-stream Mach numbers near 1. As will become more evident at a later point in the present discussion, it would appear necessary to use such formulas for the analysis of flows decelerating through sonic velocity, but the region of dependence in these relations is such as either to cast suspicions on their applicability or to require the occurrence of exceptional coincidences. On the other hand, two-dimensional flows that

decelerate smoothly through sonic velocity appear to be very exceptional physically. Further investigation is needed before additional remarks can be made regarding the role of the parabolic case with negative λ_P in the analysis of transonic flows.

The next section will be concerned with an alternative analysis of certain cases in which decelerating flows occur.

COMBINATION OF ACCELERATING AND DECELERATING FLOWS

The calculation of the pressure distribution at Mach numbers near 1 on an airfoil having such a shape that the velocity increases over part of the chord and decreases over the remainder cannot be accomplished by direct application of any of the relations developed in the preceding sections. On the one hand, the parabolic method described for flows with free-stream Mach number near 1 permits the analysis of flows that pass through sonic velocity, but fails when the velocity gradient is zero. On the other hand, the elliptic and hyperbolic methods described for subsonic and supersonic flows permit the analysis of flows with zero velocity gradient, but fail if the local velocity is sonic. The breakdown in each case is associated with the fact that the basic partial differential equation for each case, that is, equation (8), (21), or (39), assumes a degenerate form when λ is zero. Such cases are, nevertheless, interesting and important since they can occur in practical applications, and the present section is concerned with their discussion. The procedure adopted is based on the idea of joining together various of the results derived in the preceding sections in such a way that the failings associated with vanishing λ are avoided, rather than on a complete re-analysis of the problem from a sufficiently general point of view to encompass the entire problem in a single sweep.

In order to fix the ideas, consider the problem of calculating the pressure distribution at Mach number 1 on the airfoil with cusped trailing edge illustrated in figure 23 for which experimental data are available from reference 42 by Michel, Marchaud, and Le Gallo. The front half of this airfoil is the same as that of a biconvex circular-arc airfoil having a thickness ratio of 0.10, but the rear half is shaped in such a manner that an inflection point is located at 0.75 chord and that the trailing edge angle is zero. The ordinates

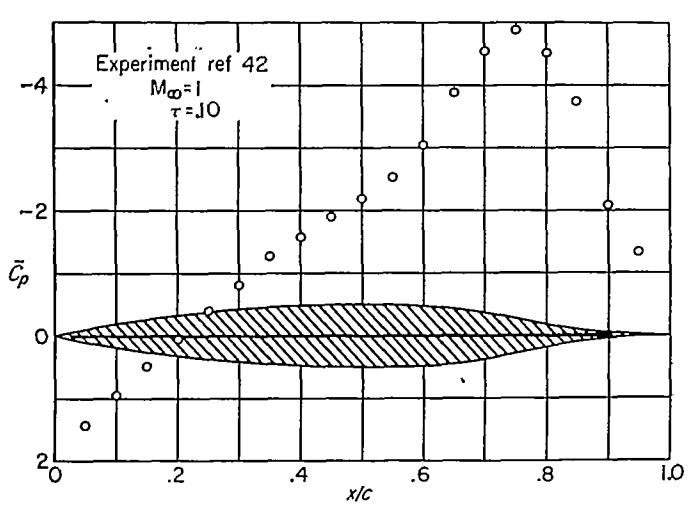

FIGURE 23.—Experimental pressure distribution for an airfoil with cusped trailing edge; $M_\infty=1$.

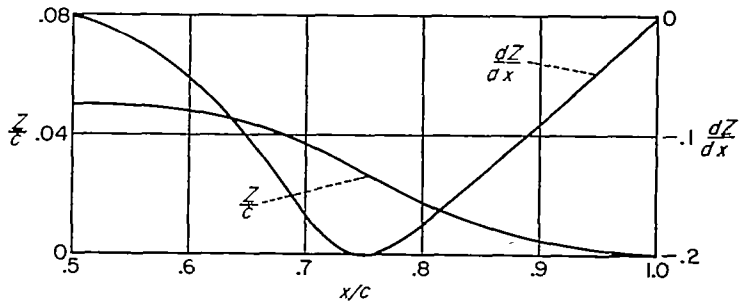

FIGURE 24.—Chordwise variation of ordinate, Z, and slope, $\frac{dZ}{dx}$, for the rear half of the airfoil shown in figure 23.

and slopes of the rear half of this airfoil are shown graphically in figure 24. No analytic expression is given in reference 42 for the ordinates of the rear half.

The pressure distribution on the front part of the airfoil where the passage through sonic velocity occurs can be calculated by use of equations (45) and (46), since it does not depend on the shape of the rear half of the airfoil. This means that the pressure distribution on the front half of the airfoil described above is given specifically by equation (53) for x/c between 0 and ½. It is clear that the pressure distribution on the entire rear half of the airfoil cannot be determined by use of equations (45) and (46) because the results so calculated indicate a point of zero pressure gradient in the vicinity of the inflection point. Although this detail, in itself, is not incorrect, it signals the breakdown of the parabolic method that occurs when λ is zero. Positive evidence of the breakdown is provided by the fact that the calculated pressures decrease downstream of the point of zero pressure gradient rather than increase as indicated by the experimental data shown on sketch (w) or by simple considerations of supersonic flow. These results, furthermore, cannot be joined to those obtained by use of equations (75) and (76) for the part of the airfoil downstream of the point of zero pressure gradient because the two sets of equations do not indicate the same location for this point. This situation should not be too surprising since the procedures should not be expected to fail abruptly when λ is precisely zero, but gradually as λ approaches zero.

There exists another possibility for the determination of the pressure distribution on the rear half of the present airfoil by joining together solutions. It is to use the formulas developed for supersonic flow, but with the final constant of integration adjusted so that the pressure is equal, at the point of connection, to that given by the solution for the forward part of the airfoil. This procedure corresponds to the use of simple wave theory for the calculation of the difference in pressure between an arbitrary point on the rear of the airfoil and the point of connection. In this way, the following equation results for the pressures on the rear of the airfoil at Mach numbers near unity:

$$\overline{C}_p-2\xi_\infty=-2\left\{\left[-\left(\frac{\overline{C}_p(X)-2\xi_\infty}{2}\right)\right]^{3/2}-\frac{3}{2\tau}\left[Z'(x)-Z'(X)\right]\right\}^{2/3} \tag{78}$$

where Z' refers to dZ/dx, and $\overline{C}_p(X)$ is the value of $\overline{C}_p$ at $x=X$.

The most convenient point for joining the two solutions in the application described in figures 23 and 24 is at $x/c=0.50$. Then the pressures on the forward half of the airfoil can be calculated directly by use of equation (53), the values of $(\overline{C}_p X)$ and $Z'(X)$ are

$$\overline{C}_p(X)=\overline{C}_p\left(\frac{c}{2}\right)=2\xi_\infty-2\left[\frac{6}{\pi}(-1+ln4)\right]^{1/3},\ Z'\left(\frac{c}{2}\right)=0 \quad (79)$$

and the following expression results for the pressures on the rear half of the airfoil at Mach numbers near unity:

$$\overline{C}_p\equiv\frac{[M_\infty^2(\gamma+1)]^{1/3}}{\tau^{2/3}}C_p=2\xi_\infty-2\left[\sqrt{\frac{6}{\pi}(-1+ln4)}-\frac{3}{2\tau}\frac{dZ}{dx}\right]^{2/3} \quad (80)$$

Figure 25 shows a comparison of the experimental pressure distribution for Mach number 1 given by Michel, Marchaud, and Le Gallo in reference 42 and the corresponding theoretical values calculated using equations (53) and (80) together with the values for dZ/dx given in figure 24. The theoretical and experimental results bear about the same relationship to each other as those shown previously for biconvex circular-arc airfoils although effects of boundary-layer shock-wave interaction extend over a larger fraction of the chord of the cusped airfoil. This difference is in agreement with the results obtained from schlieren photographs and given in reference 42 that indicate that the shock wave meets the airfoil, at Mach number 1, at 78-percent chord for the cusped airfoil and at 95-percent chord for the biconvex circular-arc airfoil of the same thickness ratio.

It is apparent that the pressures computed over the rear half of the airfoil by using equation (80) will tend to be somewhat too negative because the use of this relation corresponds to the use of simple wave theory and hence disregards the influence of a family of incoming compression waves arising from the sonic line. Some idea of the magnitude of this effect can be gained by examination of figure 26 which shows a comparison of the pressure distribution on biconvex circular-arc airfoils at Mach number 1 calculated using equation (53) for the entire airfoil, with those calculated using equation (78) for various fractions of the chord.

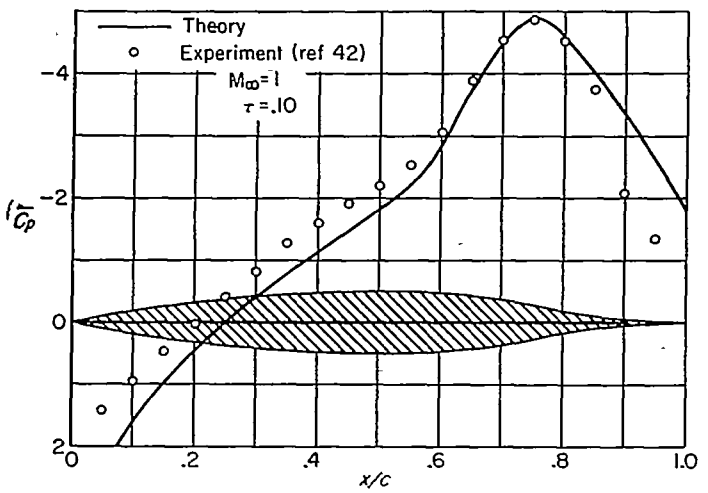

FIGURE 25.—Theoretical and experimental pressure distribution for the airfoil shown in figure 23; $M_\infty=1$.

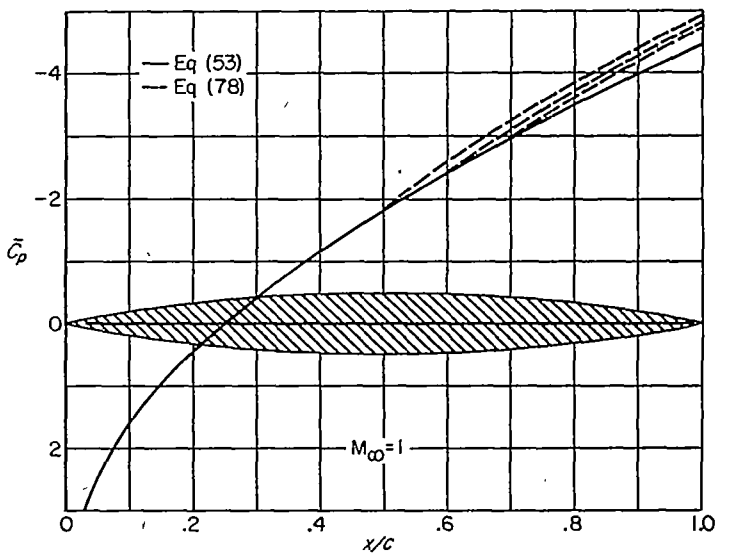

FIGURE 26.—Comparison of pressure distributions for the rear part of a circular-arc airfoil as indicated by the parabolic and hyperbolic methods; $M_\infty=1$.

A further example involving accelerating and decelerating flows at Mach number 1 is furnished by examining the case of the symmetrical double-wedge airfoil of arbitrary thickness ratio for which a solution has been given by Guderley and Yoshihara in reference 32. Figure 27 shows a plot of their result together with the corresponding result calculated by the procedures described above. The result for $0<x<c/2$ is calculated by use of equation (50). That for $c/2<x<c$ is calculated by use of the following equation which is obtained from equation (78) by equating $\overline{C}_p(X)$ to 0, $Z'(X)$ to τ, and $Z'(x)$ to $-\tau$.

$$\overline{C}_p=-2(3)^{2/3} \quad (81)$$

The difference between the two pressure distributions on the rear half of the airfoil is again the result of the neglect,

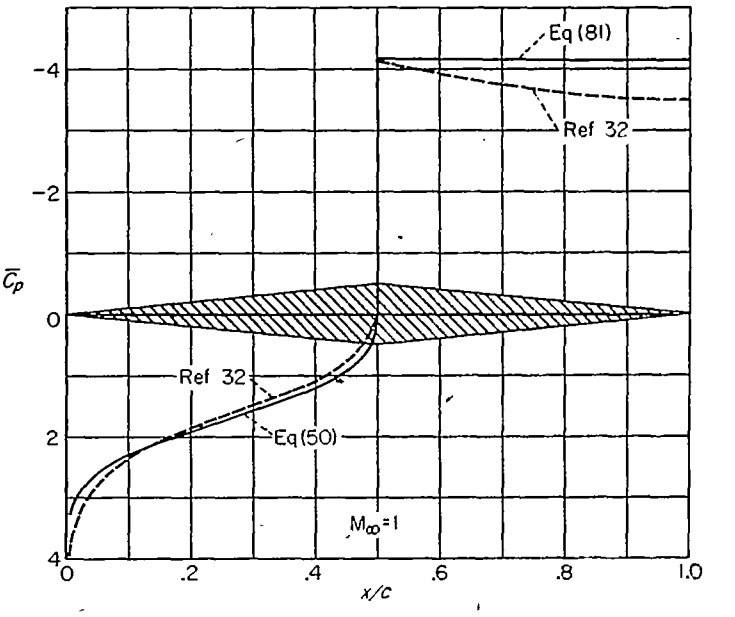

FIGURE 27.—Comparison of the pressure distributions for a double-wedge airfoil as indicated by the present theory and by Guderley and Yoshihara; $M_\infty=1$.

in the present analysis, of the contribution of the family of incoming compression waves arising from the sonic line.

It is evident from these three examples that the present procedure of joining solutions is capable of yielding results that are at least qualitatively correct and that, although somewhat greater accuracy is undoubtedly desired, this procedure may be useful until such time as a more general analysis of accelerating-decelerating flows is accomplished.

COMPARISON OF RESULTS FOR MACH NUMBER 1 WITH THOSE FOR OTHER MACH NUMBERS

The remainder of this report is concerned with the discussion of some selected examples that illustrate the relation between results for Mach number 1 and those for other Mach numbers. This discussion is divided into two parts. The first is concerned with comparisons of pressure distributions on the same airfoil at different Mach numbers, and the second with pressure drag.

PRESSURE DISTRIBUTION

Attention is directed in this section to comparisons, for a number of airfoils, of the theoretical pressure distribution for Mach number 1 with that for the highest Mach number for purely subsonic flow and that for the lowest Mach number for purely supersonic flow. Pressure distributions for these two Mach numbers, designated more briefly as the lower and upper critical Mach numbers, respectively, are of particular significance not only because they represent the results associated with the bounds of the transonic range, but also because they are typical of the pressure distributions for all purely subsonic or purely supersonic flows. All of the theoretical results shown are calculated by application of the general expressions derived in the present paper. The results for Mach number 1 are the same as discussed in detail in the preceding section. Subsonic pressure distributions are calculated by use of equation (28), and supersonic pressure distributions by use of equation (15). The lower critical Mach number is determined from equation (30) by replacing $C_{p_{t_{cr}}}$ with the most negative value of C_{p_i} that occurs in each case, and solving for M_∞. The upper critical Mach number is determined from equation (16) by replacing $(dZ/dx)_{cr}$ with the value of dZ/dx at the leading edge and solving for M_∞.

Consider, first, the single-wedge airfoil for which the pressure distribution at Mach number 1 is given by equation (50) and illustrated graphically in figure 10. Figure 28 shows a comparison of this result for the specific case of a wedge having a semiapex angle θ of 0.10 radians with those for the upper and lower critical Mach numbers. The lower critical Mach number is, of course, zero because the velocity is sonic at the corner for all free-stream Mach numbers less than the upper critical. The pressure distribution for Mach number 0 is given by

$$C_p = C_{p_i} = -\frac{2\theta}{\pi} \ln \frac{2x/c}{1-2x/c} \tag{82}$$

The three curves shown on figure 28 suffice to show that the pressure distribution on a single-wedge airfoil at Mach

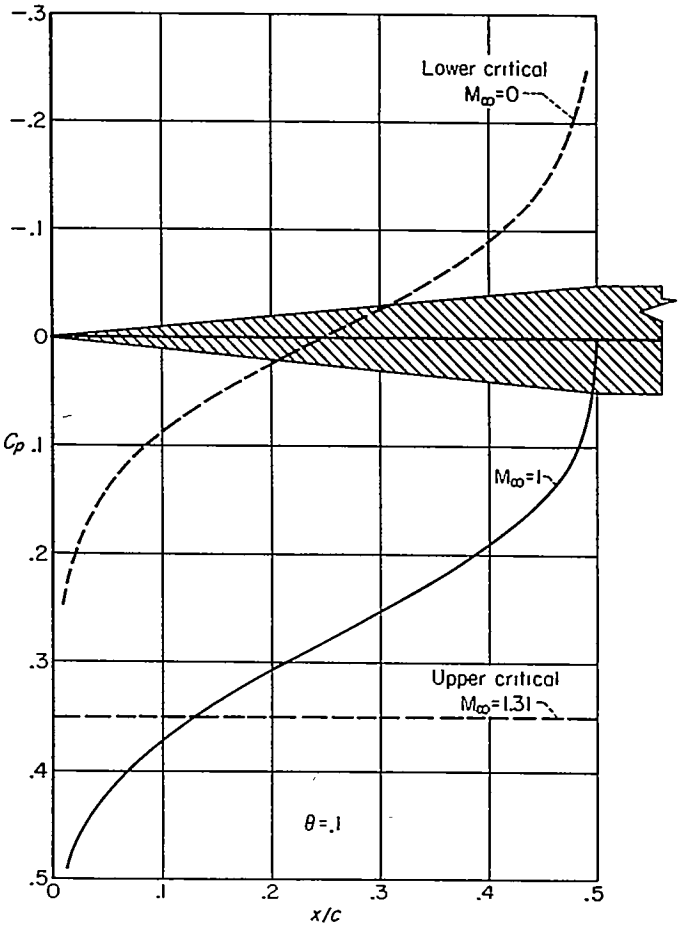

FIGURE 28.—Summary of pressure distributions for upper and lower critical Mach numbers and for Mach number 1. Single-wedge airfoil with a semiapex angle, θ, of 0.10 radian.

number 1 bears a much closer resemblance to that at the lower critical Mach number than to that at the upper critical Mach number. It is interesting to note, moreover, that the difference between the pressure distribution at Mach number 1 and that at Mach number 0 is very nearly constant across the chord.

Consider, next, the half circular-arc airfoil for which the pressure distribution at Mach number 1 is given by equation (53) and illustrated graphically in figure 15. Figure 29 shows a comparison of this result with those for the upper and lower critical Mach numbers. The computation of the pressure distribution for the lower critical Mach number involves the use of the following expression for C_{p_i} which is obtained by integration of the auxiliary relation of equation (28) with Z replaced by the expression given in equation (52) for $0<x<c/2$ and by $\tau c/2$ for $x>c/2$:

$$C_{p_i} = -\frac{4}{\pi}\tau\left[1+\left(1-\frac{2x}{c}\right)\ln\frac{2x/c}{1-2x/c}\right] \tag{83}$$

The results illustrated in figure 29 display a remarkable property that the subsonic part of the pressure distribution at Mach number 1 differs from the pressure distribution at the lower critical Mach number by nearly a constant, and that the supersonic part of the pressure distribution differs from the pressure distribution at the upper critical Mach number by nearly the same constant, although of opposite sign.

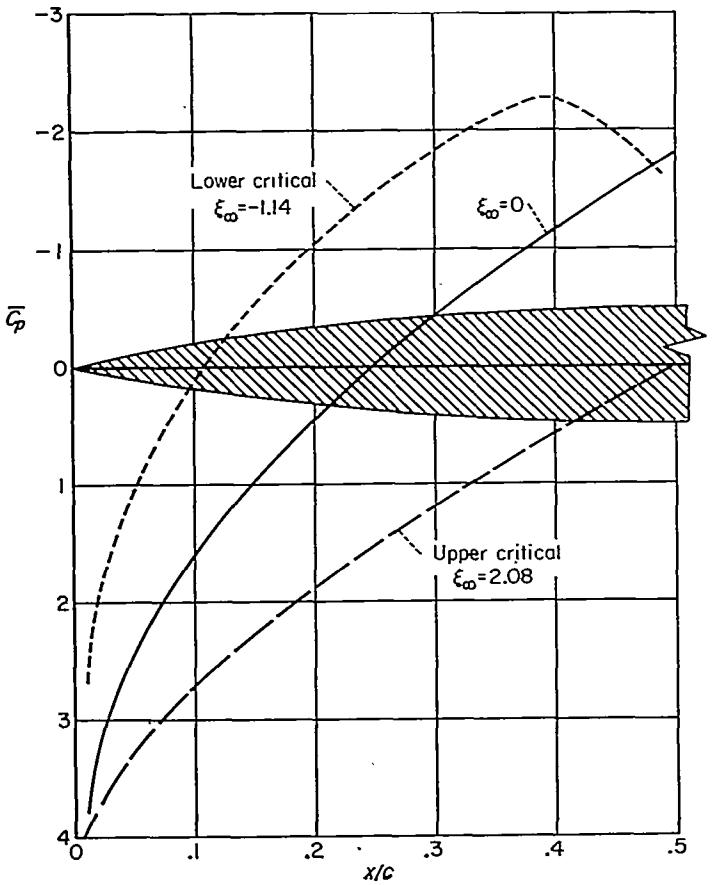

FIGURE 29.—Summary of pressure distributions for upper and lower critical Mach numbers and for Mach number 1 for half-circular-arc airfoils.

In order to investigate this difference further, the pressure distributions at the upper and lower critical Mach numbers have been calculated for the complete biconvex circular-arc airfoil and each of the four related airfoils having maximum thickness forward and aft of the midchord station for which the results for Mach number 1 are shown in figures 16 through 20. The results are shown in figure 30. It can be seen that the three pressure distributions for each airfoil bear the same general relationship to each other as noted above, although the difference between the pressure distributions is not always quite so constant as is observed for the wedge and circular-arc profiles.

PRESSURE DRAG

Once the pressure distribution is known for a given airfoil, the pressure drag can be obtained directly by integration of equation (48). The corresponding expression in terms of $\bar{c}_d$ and $\bar{C}_p$ is

$$\bar{c}_d \equiv \frac{[M_\infty^2(\gamma+1)]^{1/3}}{\tau^{5/3}} c_d \equiv 2\int_0^1 \bar{C}_p \frac{d(Z/t)}{d(x/c)}\, d\left(\frac{x}{c}\right) \qquad (84)$$

Although the present theoretical results only permit the calculation of pressure drag for Mach numbers near 1 and for Mach numbers greater than the upper critical, these results, together with existing theoretical and experimental results, can be used to sketch the variation of pressure drag with Mach number throughout the transonic range. The airfoil for which the most information is available is, of course, the single-wedge profile for which an approximate solution for Mach numbers less than 1 has been given by Cole (ref. 36) and improved recently by Yoshihara (ref. 35), that for Mach number 1 by Guderley and Yoshihara (ref. 32), and that for Mach numbers greater than 1 by Vincenti and Wagoner (ref. 34), and experimental data have been given by Liepmann and Bryson (refs. 30 and 31). Figure 31 shows a plot of these results, all in terms of the reduced parameters $\bar{c}_d$ and ξ_∞ and recast into the form consistent with the present formulation of the basic equations for transonic flow (see ref. 5, 6, or 9 for additional information on this point), together with the results computed by use of the present theory. The new results are indicated by the solid lines, the former by dashed lines and by data points. The short vertical lines on the data points indicate Bryson's estimate of the experimental accuracy of the data. As can be seen, the only point of difference between the present results and the previously existing results is at Mach numbers slightly in excess of the upper critical, and results from the error incurred in approximating the pressure jump through the bow shock wave by simple wave theory (i. e., by eq. (15) rather than eq. (6)). The positive slope of the drag curve at $\xi_\infty=0$, or Mach number 1 is in agreement with the result indicated by equation (51) and is typical for airfoils that do not close at the rear.

Figure 32 shows a summary of the comparable information for the front half of a biconvex circular-arc airfoil followed by a straight section, for which experimental data have been given by Bryson in reference 30. The theoretical values are again indicated by a solid line, and the experimental values by data points.[7] Although the amount of information available is much less than for the single-wedge airfoil, the results for both cases show striking similarity.

Results for half airfoils are not typical of those for complete airfoils, however, as can be seen by comparison of the preceding results with the corresponding theoretical and experimental results illustrated in figure 33 for complete biconvex circular-arc airfoils. The experimental results are those given by Michel, Marchaud, and Le Gallo in reference 37 and are obtained by integration of equation (48) together with experimental values for the pressure distribution. The most prominent difference concerns the slope of the curve of $\bar{c}_d$ versus ξ_∞ at $\xi_\infty=0$, or Mach number 1, for which the same procedures that led to positive values for a half airfoil, lead to zero slope for a complete airfoil. It can be seen that the experimental data support these values of the slope in both cases. Although the calculated values for drag are somewhat greater than those measured in the wind tunnel, most of the discrepancy can be attributed to the local effects of shock-wave boundary-layer interaction that occur near the trailing edge. Because this phenomenon depends on Reynolds number and may be of greatly diminished importance at full-scale conditions, Michel, Marchaud, and Le Gallo in-

[7] The experimental values shown in figure 32 differ somewhat from those given originally in figure 21 of reference 30 because of the correction of some inaccuracies in the calculation of the drag from the experimental pressure distributions given in figure 20 of reference 30. Although no explanation is known for the substantial negative drag indicated at subcritical Mach numbers and its existence must be indicative of some shortcomings of the experimental technique, its occurrence is an unmistakable consequence of the measured pressure distribution. That this is so can be seen at a glance by comparison of the measured pressure distribution with that indicated by linearized compressible flow theory, for which the drag is zero.

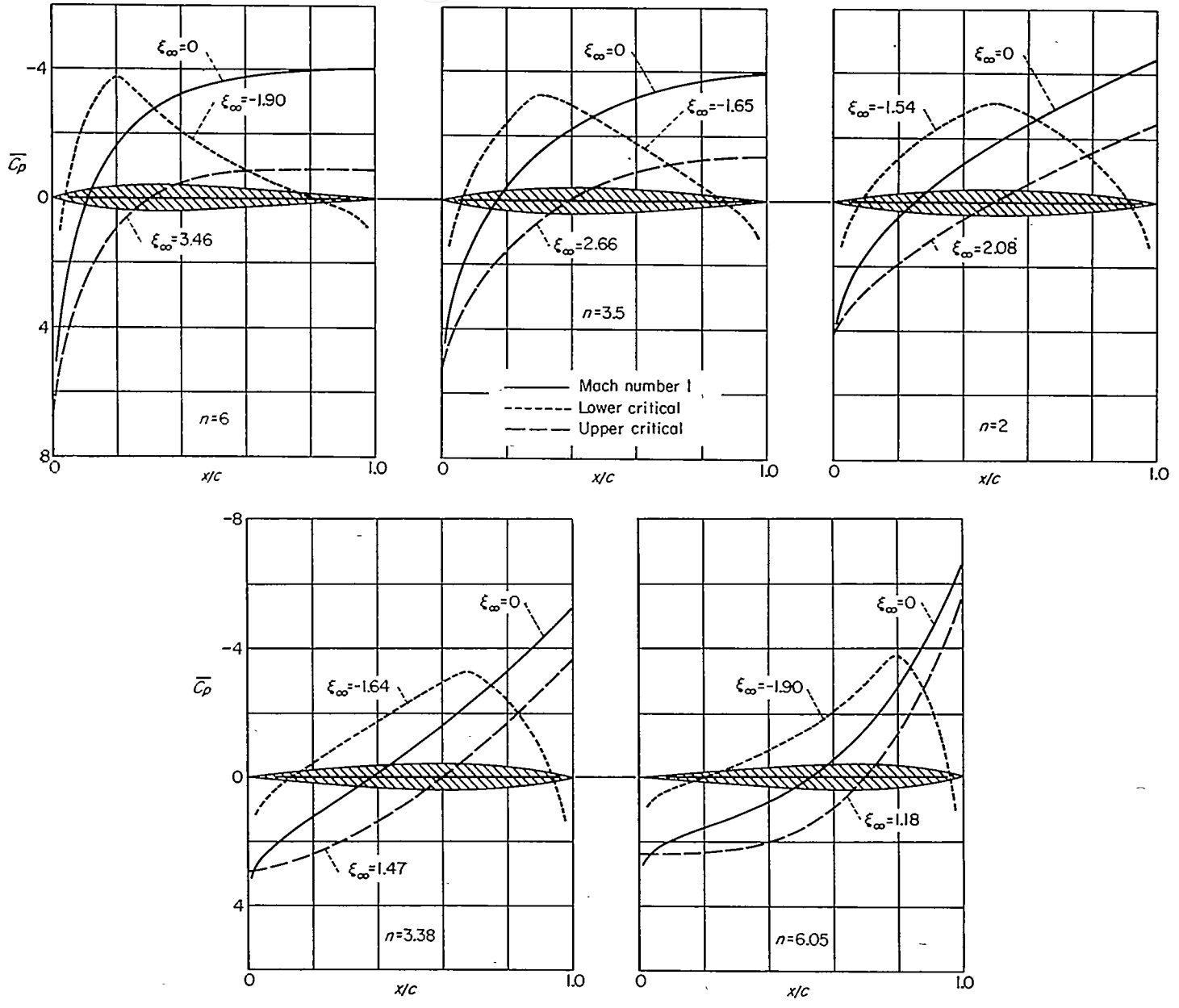

FIGURE 30.—Summary of pressure distributions for upper and lower critical Mach numbers and for Mach number 1 for a series of airfoils with different positions of maximum thickness.

troduced, in the discussion of their experimental results, the concept of "extrapolated drag" to represent the drag that would occur in the absence of separation. This quantity is calculated by consideration of a pressure distribution that differs from the experimental pressure distribution in the vicinity of the trailing edge as a result of the replacement of the pressures actually measured by those obtained by extrapolation of the trends indicated at stations upstream of the separation point. Accordingly, the values for "extrapolated drag" given by Michel, Marchaud, and Le Gallo are also shown on figure 33. As might be expected, the theoretical values for drag are in better agreement with the values for "extrapolated drag" than with those obtained directly from the actual measurements.

The results for biconvex circular-arc airfoils are typical of those for other complete airfoils. Attention is called, however, to the fact that the experimental values given by Michel, Marchaud, and Le Gallo in reference 39 for the airfoils that have the point of maximum thickness located forward of the midchord station are not so reliable as those they give for airfoils that have a more rearward location of the point of maximum thickness. This reduction in accuracy results from the facts that the method of testing and the fixed spacing of the orifices tend to diminish the accuracy with which the contribution of the region near the leading edge can be evaluated, and that the contribution of this region is, at the same time, of increased importance.

Figure 34 shows a summary of the calculated results for the pressure drag of the two families of airfoils described by equations (56) and (61) with values for n ranging from 1.5 to 6. For this range of n the airfoils described by equation (61) have a range of location for the point of maximum thickness that extends from about 0.30 to 0.55 chord, and those described by equation (56) have a range of locations extending from about 0.45 to 0.70 chord. In addition to lines for

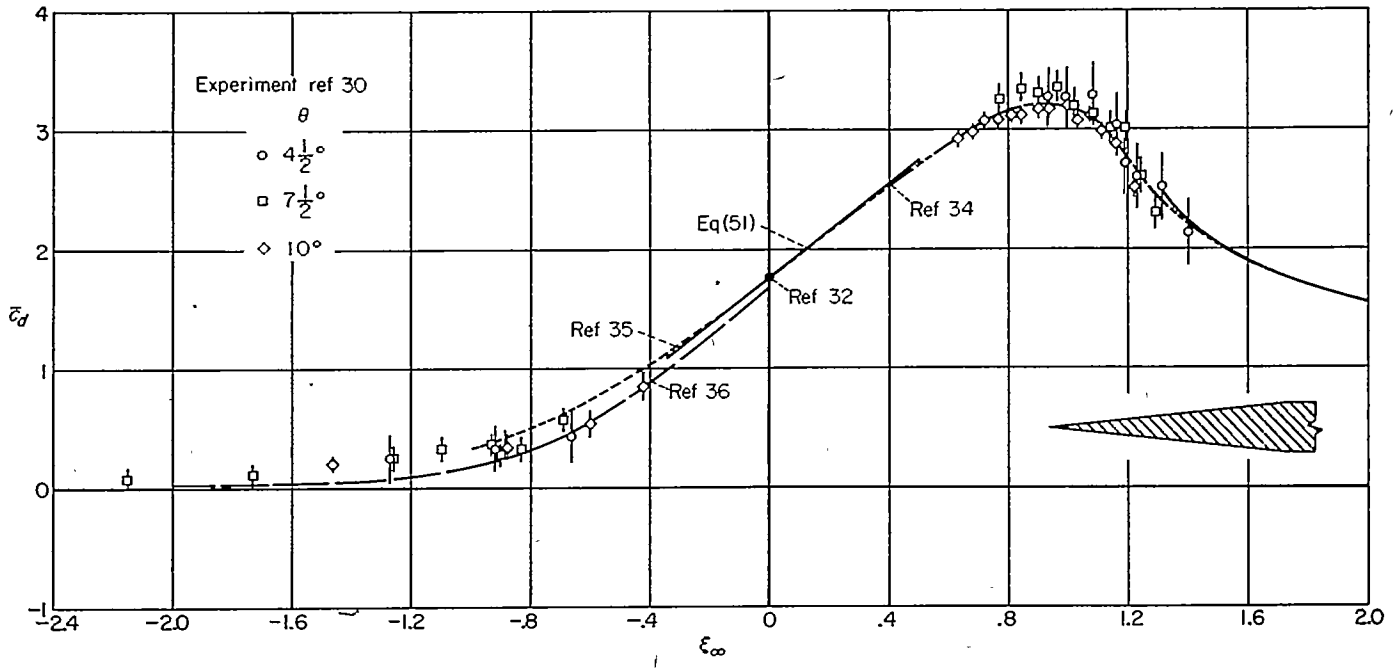

FIGURE 31.—Summary of theoretical and experimental results for the drag of single-wedge airfoils.

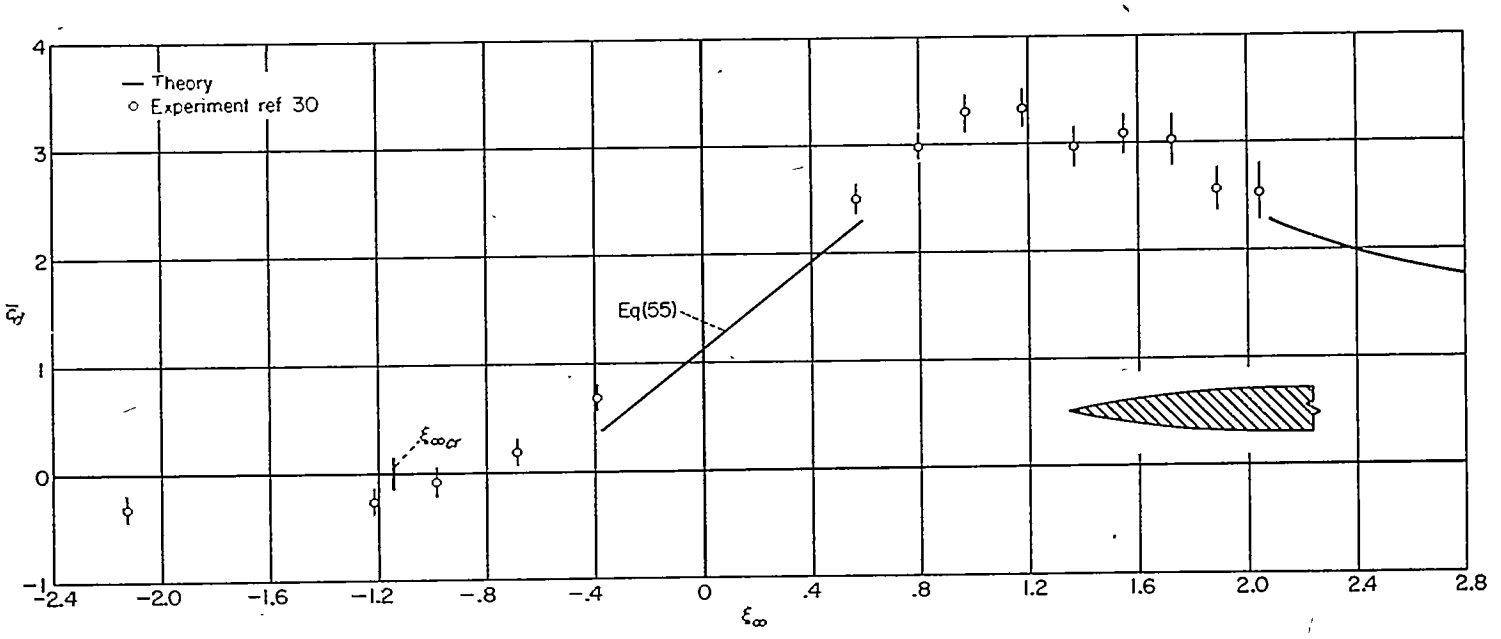

FIGURE 32.—Summary of theoretical and experimental results for the drag of half-circular-arc airfoils.

constant ξ_∞, which correspond to lines of constant Mach number for a group of airfoils having the same thickness ratio, a line is also shown for $\xi_{\infty cr}$, which corresponds to the line for the lowest Mach number for which the flow is purely supersonic. It can be seen that the variation of pressure drag with the location of the point of maximum thickness at Mach number 1 is quite different from that indicated by lines of constant ξ_∞, or Mach number, for purely supersonic flows, but is rather similar to that indicated by the line for $\xi_{\infty cr}$. An interesting feature of the results for purely supersonic flow is that the drag is not the same in forward and reverse flow, as is indicated by linearized compressible flow theory (see ref. 43 or 44).

CONCLUDING REMARKS

It appears worthwhile, in conclusion, to summarize and contrast the alternative discussions presented in the main text and in the Appendix of the general procedures involved in the approximate solution of all the problems treated in this paper. The arguments presented in the Appendix are based essentially on the idea of diminishing the importance of the higher order terms, and hence concentrate on the

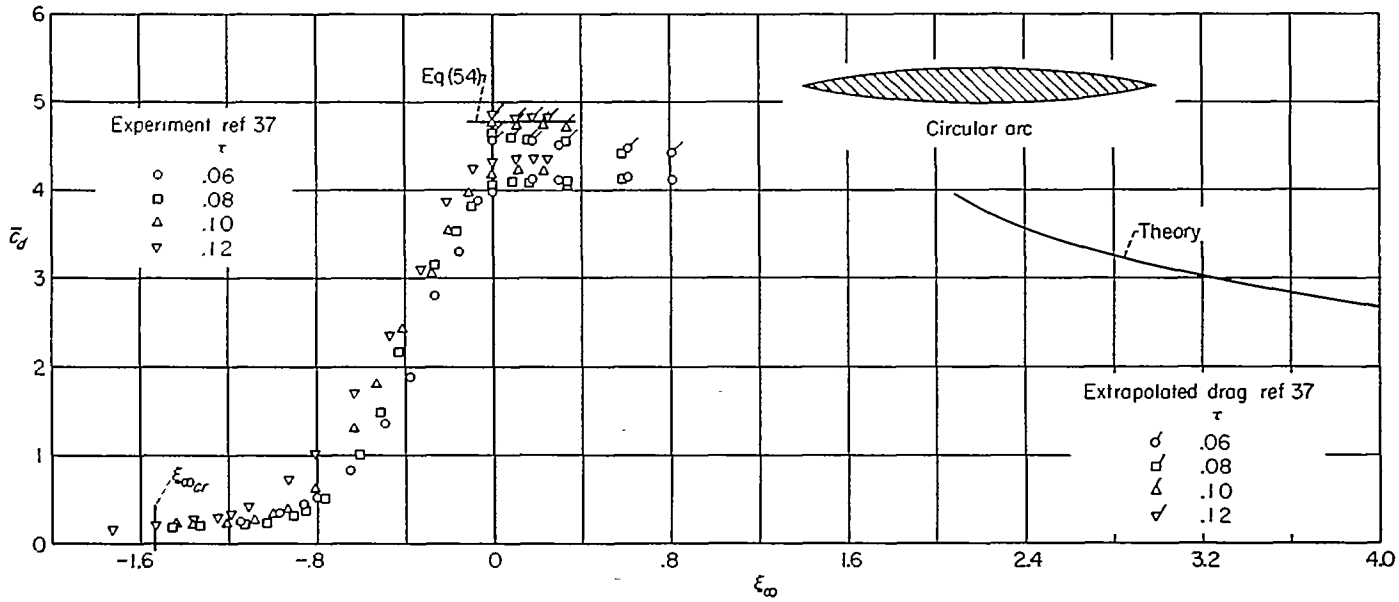

FIGURE 33.—Summary of theoretical and experimental results for the drag of complete circular-arc airfoils.

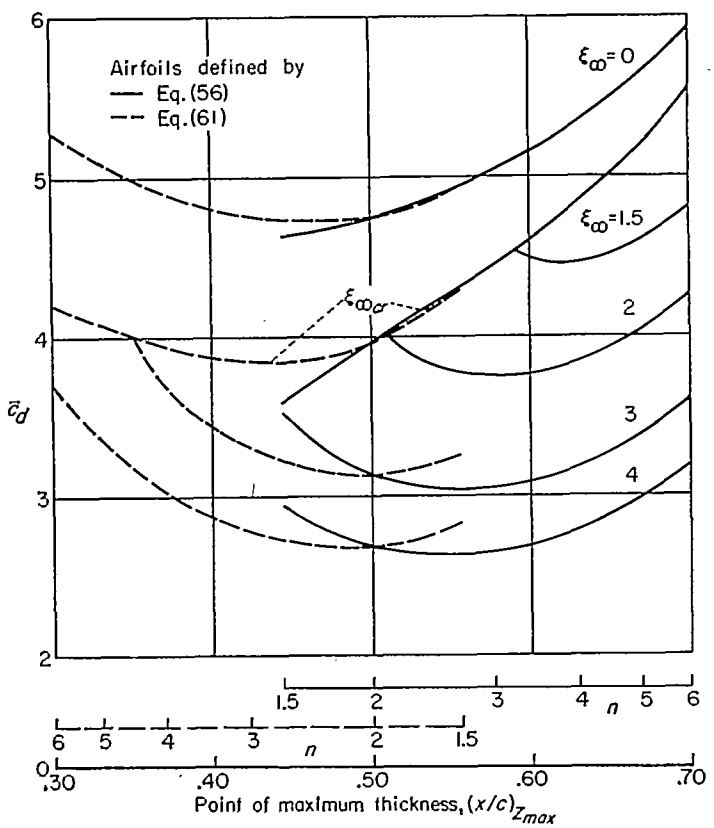

FIGURE 34.—Summary of theoretical results for the drag of two families of airfoils having various positions for the point of maximum thickness.

contributions stemming from the double integral of the integral equation appropriate for each case. The arguments presented in the main text lead to the same conclusions, but are based essentially on the idea of linearizing the transonic equation in a small region by replacing part of the nonlinear term by a constant λ, and then introducing different values for λ for different points in the field. This procedure might be considered equivalent, in some sense, to the replacement of the original nonlinear equation by a different linear differential equation for each point. Results obtained by solution of the equations at this stage depend, of course, on the choice of λ and must be assembled in order to determine the final results. This step is accomplished in each case by putting the results into such a form that a first-order nonlinear ordinary differential equation is obtained upon substituting for λ the quantity it originally replaced. At this point, the equations encountered coincide with those obtained following the procedures described in the Appendix and the remainder of the analysis proceeds in identical manner. In the cases considered herein, the differential equation is always of sufficiently simple form that it can be integrated analytically and the result expressed in closed analytic form. This integration implicitly introduces the assumption of continuity of the velocity or pressure distribution and leads, upon evaluation of a single constant of integration, to the final result.

AMES AERONAUTICAL LABORATORY
NATIONAL ADVISORY COMMITTEE FOR AERONAUTICS
MOFFETT FIELD, CALIF., *Mar. 11, 1957*

APPENDIX A

REINSPECTION AND ANALYSIS OF METHOD OF APPROXIMATION

INTRODUCTION

The methods used in the main text of this paper are appealing for their brevity and for the efficiency with which approximate solutions of the nonlinear equations of transonic flow theory are found. These methods are not entirely satisfying to the critical reader, however, because certain elements appear to be arbitrary and there is no a priori way in which the accuracy of the approximations can be judged. Both the virtue and weakness of these procedures are the result of introducing the essential simplifications at the beginning of the analysis. If the introduction of approximations is deferred to the end, the relations that occur in the initial stages of the analysis are, of course, more complicated than those presented in the main text. Consideration of these relations is, however, essential for an understanding of the basis for the method of approximation.

The following discussion of the approximate solution of problems of transonic flow theory is based on consideration of integral equations derived from the differential equations of transonic flow theory by standard application of Green's theorem. Since the details of each of the three cases, hyperbolic, elliptic, and parabolic, are somewhat different, each case is considered separately. In each case, exact relations are retained as long as possible and the approximations, when introduced, are seen to be closely related to those employed in the method of successive approximations commonly used in the determination of higher approximations in compressible flow theory. The following paragraphs will be concerned at the outset with the derivation of integral equations for each of the three cases, and subsequently with the discussion of the simplification and approximate solution of these equations.

DERIVATION OF INTEGRAL EQUATIONS

All of the subsequent analysis proceeds from Green's theorem. There are many forms of Green's theorem, but a sufficiently general form for all of the present purposes is that associated with the linear operator $\overline{L}(\Omega)$ defined as follows (ref. 45, pp. 244–247):

$$\overline{L}(\Omega)=\overline{A}\Omega_{xx}+\Omega_{zz}+\overline{B}\Omega_x \tag{A1}$$

where $\overline{A}$ and $\overline{B}$ are constants. Green's theorem states that the following relation holds between any two arbitrary functions Ω and ψ having continuous first and second derivatives:

$$\iint_{\overline{R}}[\psi\overline{L}(\Omega)-\Omega\overline{M}(\psi)]\,d\overline{R}=-\oint_{\overline{C}}\left[\overline{\Lambda}\left(\psi\frac{\partial\Omega}{\partial\nu}-\Omega\frac{\partial\psi}{\partial\nu}\right)+\overline{B}\psi\Omega\cos(n,x)\right]ds \tag{A2}$$

in which $\overline{R}$ refers to the interior of an arbitrary region bounded by the curve $\overline{C}$, as shown in figure 35, $\overline{M}$ is called the adjoint differential operator

$$\overline{M}(\psi)=\overline{A}\psi_{xx}+\psi_{zz}-\overline{B}\psi_x$$

$\overline{\Lambda}$ represents the quantity

$$\Lambda=\sqrt{\overline{A}^2\cos(n,x)+\cos^2(n,z)}$$

and $\partial/\partial\nu$ stands for a derivative in the direction ν, and can be written as a linear differential operator.

$$\frac{\partial\Omega}{\partial\nu}=\Omega_x\cos(\nu,x)+\Omega_z\cos(\nu,z)$$

The direction ν is called the conormal, and its direction cosines are related to those of the normal n according to

$$\overline{\Lambda}\cos(\nu,x)=\overline{A}\cos(n,x)$$

$$\overline{\Lambda}\cos(\nu,z)=\cos(n,z)$$

HYPERBOLIC CASE

The initial step in the present derivation of the integral equation appropriate for the discussion of the hyperbolic case is to subtract $\lambda_H\varphi_{xx}$ from both sides of equation (3), and to write the resulting equation as follows:

$$-\lambda_H\varphi_{xx}+\varphi_{zz}=(M_\infty{}^2-1+ku-\lambda_H)\varphi_{xx}=f_H \tag{A3}$$

The symbol λ_H refers to any positive finite constant. The form of Green's theorem associated with the linear operator

$$\overline{L}(\varphi)=\overline{L}_H(\varphi)=-\lambda_H\varphi_{xx}+\varphi_{zz} \tag{A4}$$

will now be applied, whence

$$\overline{A}=-\lambda_H,\qquad \overline{B}=0,\qquad \overline{M}_H(\varphi)=\overline{L}_H(\varphi) \tag{A5}$$

The quantity Ω is now identified with the perturbation potential φ, and ψ with an elementary solution of $\overline{M}_H(\psi)=0$,

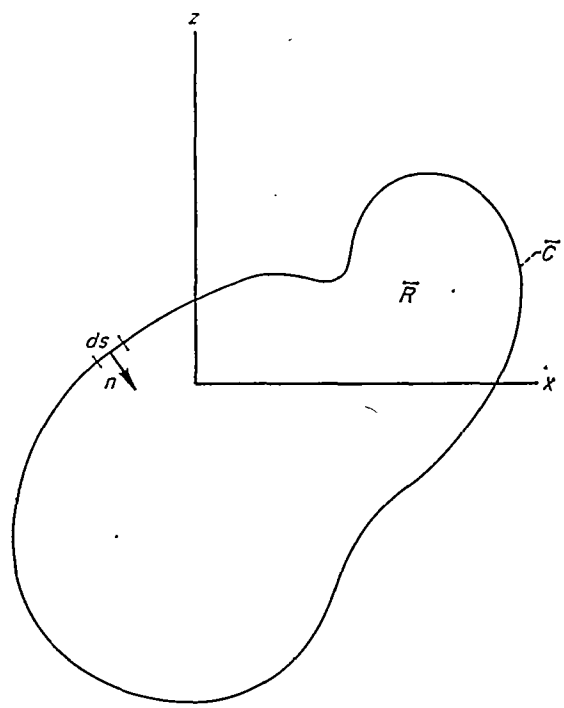

FIGURE 35.—Region of integration.

in particular with the unit supersonic source σ_H defined as follows:

$$\psi=\sigma_H=\begin{cases}-\dfrac{1}{2\sqrt{\lambda_H}} & \text{for } (x-\xi)^2\geq\lambda_H(z-\zeta)^2 \quad \text{(A6a)}\\ 0 & \text{for } (x-\xi)^2<\lambda_H(z-\zeta)^2 \quad \text{(A6b)}\end{cases}$$

If the region $\overline{R}$ is so selected that the inequality expressed in equation (A6a) holds throughout, equation (A2) reduces to

$$-\int_{\overline{C}}\overline{\Lambda}_H\frac{\partial\varphi}{\partial\nu_H}ds=\iint_{\overline{R}}\overline{L}_H(\varphi)d\overline{R}=\iint_{\overline{R}}f_Hd\overline{R} \qquad \text{(A7)}$$

in which $\overline{\Lambda}_H$ and ν_H refer to the special forms of $\overline{\Lambda}$ and ν consistent with equation (A4) or (A5), the running coordinates of integration are ξ,ζ, and the field point at which φ is to be evaluated is x,z. Equation (A7) is now applied to the region indicated in figure 36. Note that the wing, wake, and shock waves must be excluded from the region of integration. It should be noted that figure 36 is only a schematic illustration to help define the quantities involved in equation (A7), and that the shock wave, indicated as a detached bow wave, might instead be attached to the leading edge, to the trailing edge, or situated somewhere along the chord. The single shock wave illustrated in figure 36 could, moreover, be replaced by a complicated system of shock waves. The region $\overline{R}_H$ may likewise be considered to consist of a single region, or as the sum of a number of regions as typified by adding to $\overline{R}_H$ the region situated upstream of the bow wave

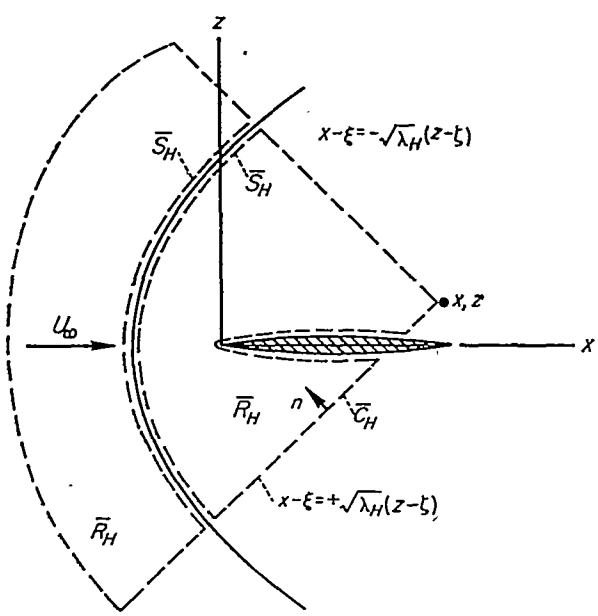

FIGURE 36.—Region of integration for the hyperbolic case.

and within the dotted lines of figure 36. In any case, the general considerations remain the same, and the following integral equation is obtained for φ at an arbitrary point x,z:

$$\varphi(x,z)=\left[\frac{1}{-2\sqrt{\lambda_H}}\int_0^{x-\sqrt{\lambda_H}|z|}\Delta\frac{\partial\varphi}{\partial\zeta}d\xi+\frac{\Delta\varphi(x-\sqrt{\lambda_H}|z|)}{2}\right]-\frac{1}{2\sqrt{\lambda_H}}\int_{\overline{S}_H}\overline{\Lambda}_H\delta\frac{\partial\varphi}{\partial\nu_H}d\overline{S}_H-\frac{1}{2\sqrt{\lambda_H}}\iint_{\overline{R}_H}f_Hd\overline{R}_H \qquad \text{(A8)}$$

where

$$\Delta\frac{\partial\varphi}{\partial\zeta}=\frac{\partial\varphi_u}{\partial\zeta}-\frac{\partial\varphi_l}{\partial\zeta}, \qquad \Delta\varphi=\varphi_u-\varphi_l$$

in which u and l refer to conditions on the upper and lower sides of the wing and wake, where

$$\delta\frac{\partial\varphi}{\partial\nu_H}=\frac{\partial\varphi_a}{\partial\nu_H}+\frac{\partial\varphi_b}{\partial\nu_H}$$

in which a and b refer to conditions on the two sides of the shock wave $\overline{S}_H$, and where

$$\overline{\Lambda}_H\frac{\partial\varphi}{\partial\nu_H}=-\lambda_H\frac{\partial\varphi}{\partial\xi}\cos(n,x)+\frac{\partial\varphi}{\partial\zeta}\cos(n,z)$$

ELLIPTIC CASE

The integral equation appropriate for the discussion of the elliptic case can be derived by use of procedures analogous to those described in the preceding paragraph for the hyperbolic case. The initial step is to add $\lambda_E\varphi_{xx}$ to both sides of equation (3), and to write the resulting equation as follows:

$$\lambda_E\varphi_{xx}+\varphi_{zz}=[\lambda_E-(1-M_\infty{}^2-ku]\varphi_{xx}=f_E \qquad \text{(A9)}$$

As in the hyperbolic case, the symbol λ_E refers to any positive finite constant. The form of Green's theorem associated with the linear operator

$$\overline{L}(\varphi)=\overline{L}_E(\varphi)=\lambda_E\varphi_{xx}+\varphi_{zz} \qquad \text{(A10)}$$

will now be applied, whence

$$\overline{A}=\lambda_E, \qquad \overline{B}=0, \qquad \overline{M}_E(\varphi)=\overline{L}_E(\varphi) \qquad \text{(A11)}$$

The quantity Ω is now identified with φ, and ψ with an elementary solution of $\overline{M}_E(\psi)=0$, in particular the unit subsonic source defined by the function

$$\psi=\sigma_E=\frac{1}{2\pi\sqrt{\lambda_E}}ln\sqrt{(x-\xi)^2+\lambda_E(z-\zeta)^2} \qquad \text{(A12)}$$

In this way equation (A2) reduces to

$$-\int_{\overline{C}}\overline{\Lambda}_E\left(\sigma_E\frac{\partial\varphi}{\partial\nu_E}-\varphi\frac{\partial\sigma_E}{\partial\nu_E}\right)ds=\iint_{\overline{R}}\sigma_E\overline{L}_E(\varphi)d\overline{R}=\iint_{\overline{R}}\sigma_Ef_Ed\overline{R} \qquad \text{(A13)}$$

in which $\overline{\Lambda}_E$ and ν_E refer to the special forms of $\overline{\Lambda}$ and ν consistent with equation (A10) or (A11), the running coordinates of integration are ξ,ζ, and the field point at which φ is to be determined is x,z. If equation (A13) is now applied to the region $\overline{R}_E$ surrounding the wing, wake, and shock waves, as illustrated in figure 37, and the a priori assumption is made that the perturbation field attenuates sufficiently fast with distance to negate the contribution of the surface integral over the large circle in the limit as the radius goes to infinity, the following integral equation is obtained for φ at an arbitrary point x,z:

$$\varphi(x,z)=\int_0^\infty\left(\sigma_E\Delta\frac{\partial\varphi}{\partial\zeta}-\Delta\varphi\frac{\partial\sigma_E}{\partial\zeta}\right)d\xi+\int_{\overline{S}_E}\sigma_E\overline{\Lambda}_E\delta\frac{\partial\varphi}{\partial\nu_E}d\overline{S}_E+\iint_{\overline{R}_E}\sigma_Ef_Ed\overline{R}_E \qquad \text{(A14)}$$

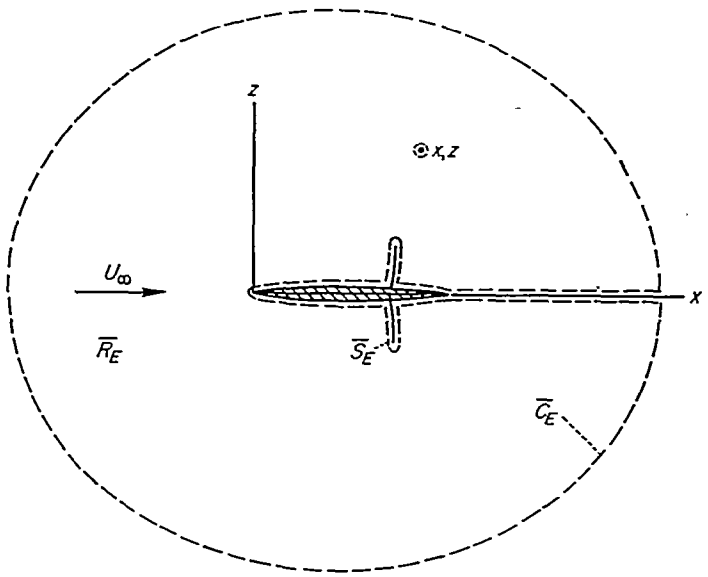

FIGURE 37.—Region of integration for the elliptic case.

where $\Delta\varphi$ and $\Delta(\partial\varphi/\partial\zeta)$ have the same meaning as in equation (A8), but where

$$\delta\frac{\partial\varphi}{\partial\nu_E}=\frac{\partial\varphi_a}{\partial\nu_E}+\frac{\partial\varphi_b}{\partial\nu_E}$$

in which a and b refer to conditions on the two sides of the shock wave $\bar{S}_E$, and where

$$\bar{\Lambda}_E\frac{\partial\varphi}{\partial\nu_E}=\lambda_E\frac{\partial\varphi}{\partial\xi}\cos(n,x)+\frac{\partial\varphi}{\partial\zeta}\cos(n,z)$$

PARABOLIC CASE

The initial step in the derivation of the integral equations appropriate for the discussion of the parabolic case is to subtract $\lambda_P\varphi_x$ from both sides of equation (3), and to write the resulting equation as follows:

$$\varphi_{xz}-\lambda_P\varphi_x=(M_\infty^2-1)\varphi_{xx}+(k\varphi_{xx}-\lambda_P)\varphi_x=f_P \qquad \text{(A15)}$$

The symbol λ_P refers again to a finite constant, which may be either positive or negative. The form of Green's theorem associated with the linear operator

$$\bar{L}(\varphi)=\bar{L}_P(\varphi)=\varphi_{xz}-\lambda_P\varphi_x \qquad \text{(A16)}$$

will now be applied, whence

$$\bar{A}=0, \quad \bar{B}=-\lambda_P, \quad \bar{M}_P(\varphi)=\varphi_{xz}+\lambda_P\varphi_x \qquad \text{(A17)}$$

The quantity Ω is again identified with φ, and ψ with an elementary solution of $\bar{M}_P(\psi)=0$, in particular with the function

$$\psi=\sigma_P=\begin{cases}\sqrt{\dfrac{\lambda_P}{4\pi(x-\xi)}}\,e^{\left[-\frac{\lambda_P(z-\zeta)^2}{4(x-\xi)}\right]} & \text{for } \dfrac{\lambda_P}{x-\xi}\geq 0 \qquad \text{(A18a)}\\ 0 & \text{for } \dfrac{\lambda_P}{x-\xi}<0 \qquad \text{(A18b)}\end{cases}$$

This function assumes a role in the analysis of the parabolic case that is analogous to that of the unit subsonic and supersonic sources in the elliptic and hyperbolic cases. In mathematical literature, the linear partial differential equation $\bar{L}_P(\varphi)=0$ with positive λ_P arises in the study of heat conduction, and the function σ_P is often referred to as a unit heat source. If the region $\bar{R}$ is so selected that the inequality expressed in equation (A18a) holds throughout, equation (A2) reduces to

$$-\int_{\bar{C}}\left[\bar{\Lambda}_P\left(\sigma_P\frac{\partial\varphi}{\partial\nu_P}-\varphi\frac{\partial\sigma_P}{\partial\nu_P}\right)-\lambda_P\sigma_P\varphi\cos(n,x)\right]ds$$
$$=\iint_{\bar{R}}\sigma_P\bar{L}_P(\varphi)d\bar{R}=\iint_{\bar{R}}\sigma_P f_P d\bar{R} \qquad \text{(A19)}$$

in which $\bar{\Lambda}_P$ and ν_P refer to the special forms of $\bar{\Lambda}$ and ν consistent with equation (A16) or (A17), the running coordinates of integration are ξ,ζ, and the field point at which φ is to be determined is x,z. It is apparent from the condition imposed on $\bar{R}_P$, that $\lambda_P/(x-\xi)$ is greater than or equal to zero, that two distinct subcases result depending on the sign of λ_P.

Positive λ_P.—If λ_P is positive, the region $\bar{R}_P$ appropriate for the application of equation (A19) is that part of space upstream from the point x,z. Again the wing, wake, and shock must be excluded from the region of integration, as illustrated schematically in figure 38. If equation (A19) is

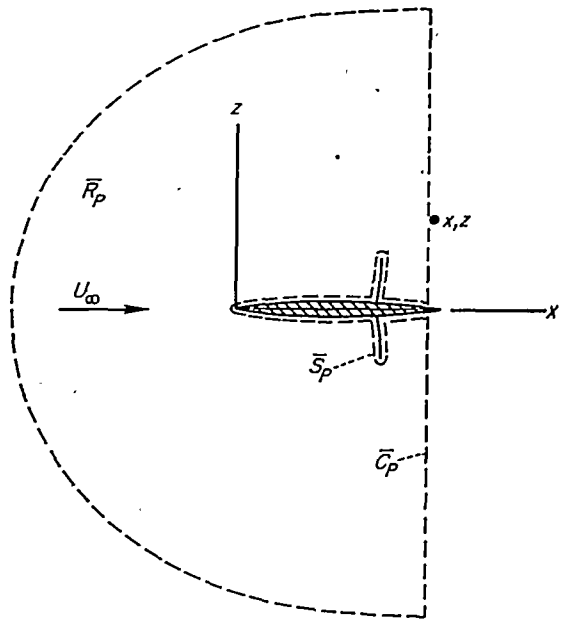

FIGURE 38.—Region of integration for the parabolic case with $\lambda_P>0$.

now applied to the region $\bar{R}_P$, and it is assumed that the perturbation field attenuates sufficiently fast with distance to negate the contribution of the surface integral over the outer boundary in the limit as the radius is increased to infinity, the following integral equation is obtained for φ at an arbitrary point x,z:

$$\varphi(x,z)=-\frac{1}{\lambda_P}\int_0^z\left(\sigma_P\Delta\frac{\partial\varphi}{\partial\zeta}-\Delta\varphi\frac{\partial\sigma_P}{\partial\zeta}\right)d\xi-\frac{1}{\lambda_P}\int_{\bar{S}_P}\sigma_P\bar{\Lambda}_P\delta\left(\frac{\partial\varphi}{\partial\nu_P}\right)d\bar{S}_P-$$
$$\frac{1}{\lambda_P}\iint_{\bar{R}_P}\sigma_P f_P d\bar{R}_P \qquad \text{(A20)}$$

where $\Delta\varphi$ and $\Delta(\partial\varphi/\partial\zeta)$ have the same meaning as in equation (A8), but where

$$\delta\frac{\partial\varphi}{\partial\nu_P}=\frac{\partial\varphi_a}{\partial\nu_P}+\frac{\partial\varphi_b}{\partial\nu_P}$$

in which a and b refer to conditions on the two sides of the shock wave $\overline{S}_P$, and where

$$\overline{\Lambda}_P\frac{\partial\varphi}{\partial\nu_P}=\frac{\partial\varphi}{\partial\zeta}\cos(n,z)$$

Negative λ_P.—If λ_P is negative, the region $\overline{R}_P$ appropriate for the application of equation (A19) is that part of space downstream from the point x, z. If equation (A19) is applied to the region $\overline{R}_P$ surrounding the appropriate part of the wing, wake, and shock waves, as illustrated in figure 39, and the contribution of the surface integral over the outer boundary vanishes as the radius is increased to infinity, the following integral equation is obtained for φ at an arbitrary point x,z:

$$\varphi(x,z)=\frac{1}{\lambda_P}\int_x^\infty\left(\sigma_P\Delta\frac{\partial\varphi}{\partial\zeta}-\Delta\varphi\frac{\partial\sigma_P}{\partial\zeta}\right)d\xi+\frac{1}{\lambda_P}\int_{\overline{S}_P}\sigma_P\overline{\Lambda}_P\delta\left(\frac{\partial\varphi}{\partial\nu_P}\right)d\overline{S}_P+\frac{1}{\lambda_P}\iint_{\overline{R}_P}\sigma_P f_P d\overline{R}_P \qquad \text{(A21)}$$

where the symbols have the same meaning as in equation (A20), except that $\overline{S}_P$ and $\overline{R}_P$ now refer to those portions of the shock waves and space situated downstream from x,z.

SOME PROPERTIES OF THE INTEGRAL EQUATIONS

Although the four integral equations derived in the preceding paragraphs and written explicitly in equations (A8), (A14), (A20), and (A21) are quite different in most respects, they do possess a number of properties in common that are of concern in the present discussion. Perhaps the most obvious similarity is that each integral equation consists of a term that involves integration over the wing and wake, another term that involves integration over the shock waves, and a third term that involves integration over the surrounding space. The integrals extend over all space in the elliptic case, but only over part of space in the parabolic and hyperbolic cases. It is important to realize that there is no direct connection between the region of integration in each of the integral equations and the region of dependence in the solution, or in the physical flow, and that these two regions may, in fact, be distinctly different in some applications.

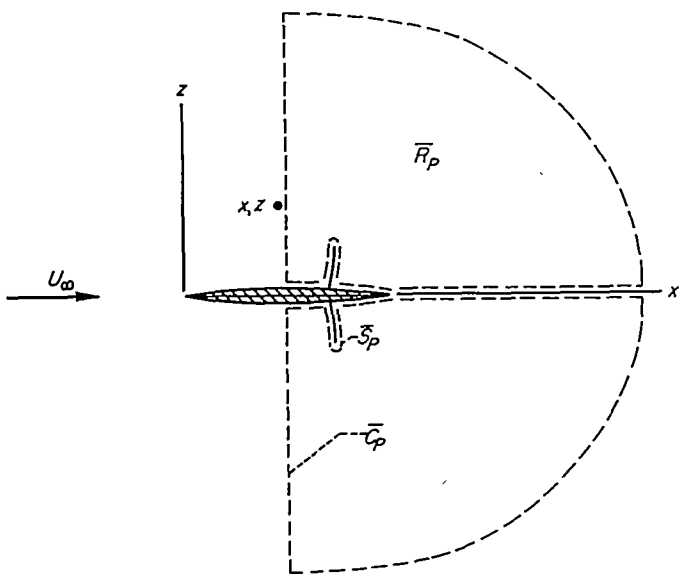

FIGURE 39.—Region of integration for the parabolic case with $\lambda_P<0$.

The first term in each integral equation involves a distribution of sources σ proportional to $\Delta(\partial\varphi/\partial\zeta)$ and doublets $\partial\sigma/\partial\zeta$ proportional to $\Delta\varphi$. Since $\Delta(\partial\varphi/\partial\zeta)$ is equal, according to the boundary condition given in equation (1), to $U_\infty\Delta(dZ/dx)$ and $\Delta\varphi$ is proportional to an x-wise integration of the lift, it follows that the part of the term containing sources is associated with the thickness distribution, and that part containing doublets, with the effects of camber and angle of attack. The latter part of the first term is zero for all of the nonlifting airfoils discussed in the main text of this paper. The first term in the elliptic and hyperbolic cases is familiar in compressible flow theory because, upon equating λ_E to $1-M_\infty^2$ or λ_H to M_∞^2-1, it reduces to the well-known solution for φ in the linearized theory of subsonic and supersonic flow around thin airfoils.

The second term in each integral equation involves a distribution of sources σ proportional to $\overline{\Lambda}\delta(\partial\varphi/\partial\nu)$ over any part of the shock waves that is situated in what otherwise would be part of the region of integration $\overline{R}$. There is no doublet distribution on the shock wave, as on the wing and wake, because φ is continuous across the shock wave. Although the contribution of the integral over the shock waves is often difficult to evaluate because $\delta(\partial\varphi/\partial\nu)$ is unknown and must be determined as part of the solution, there are a number of important applications in which this term either vanishes completely, or contributes nothing to the values for φ along the chord of the airfoil. The simplest class of problems for which this term vanishes is, of course, that in which the flow is subsonic everywhere and is hence shock-free. The contribution of this term will also vanish in parts of the field even if shock waves are present, provided they are situated entirely downstream of the region of integration in the hyperbolic case or the parabolic case with positive λ_P, or entirely upstream of the region of integration in the parabolic case with negative λ_P. The contributions of the shock wave vanish in the above situations because the complete term disappears from the integral equation. If the term remains, however, each element of the shock wave provides a contribution to φ that depends upon its strength and orientation. There are, moreover, certain directions in which an element of a shock wave can be oriented that result in no contribution to φ in the parabolic and hyperbolic cases. Thus, in the parabolic case, the contribution vanishes when the element of the shock wave extends perpendicular to the x axis, so that $\cos(n,z)$ in the second term of equation (A20) or (A21) is zero. It is similarly evident from equation (A8) that an element of a shock wave contributes nothing to φ in the hyperbolic case if the direction cosines and velocity components on the two sides of the shock wave satisfy the relationship

$$\frac{\cos(n_b,z)}{\cos(n_b,x)}=\lambda_H\frac{u_a-u_b}{w_a-w_b} \qquad \text{(A22)}$$

This relation can be expressed completely in geometric terms by combining it with the following equation that can be derived from consideration of the fact that φ is continuous across the shock

$$\frac{\cos(n_b,z)}{\cos(n_b,x)}=\frac{w_a-w_b}{u_a-u_b} \tag{A23}$$

Thus, the contribution to φ vanishes if the element of the shock wave is oriented so that

$$\left[\frac{\cos(n_b,z)}{\cos(n_b,x)}\right]^2=\tan^2(n_b,x)=\lambda_H \tag{A24}$$

If the same line of reasoning is applied to the elliptic case, relations analogous to equations (A22) through (A24) occur in which λ_H is replaced by $-\lambda_E$. From such considerations it would appear that the contribution to φ vanishes if the element of the shock wave is oriented so that

$$\left[\frac{\cos(n_b,z)}{\cos(n_b,x)}\right]^2=-\lambda_E \tag{A25}$$

Since λ_E is required to be a positive quantity, however, it is clear that there is no orientation for which the contribution vanishes. In the hyperbolic case, on the other hand, λ_H is required to be positive and there are always two particular orientations for which an element of a shock wave contributes nothing to φ. It is interesting to note, before leaving the discussion of the second term of each of the integral equations, that the particular orientation for which an element of a shock wave provides no contribution to φ coincides in all three cases, elliptic, parabolic, and hyperbolic, with the directions of the characteristic lines of the associated form of the linear partial differential equation, $\overline{L}(\varphi)=0$. The reader should observe, however, that these characteristic lines have no particular physical significance, inasmuch as their existence and direction depend on an arbitrary choice of a value for λ.

The third term in each integral equation involves integration of the effects of a distribution of sources σ proportional to f over that part of space surrounding the airfoil that is enclosed within the region of integration $\overline{R}$. The contribution of this term does not vanish, except in almost trivial circumstances such as occur, for example, in the hyperbolic case for points upstream of a bow wave provided λ_H is equated to M_∞^2-1 so that f_H is zero. Discussion of the contribution of the third term in each integral equation will consequently constitute the subject of much of the remainder of this Appendix. An interesting property of each of the integral equations that is worth noting before proceeding to the more specific discussion of each case is that the integrated strength of the sources in all space exterior to the airfoil, including those distributed along the shock waves, is equal, but opposite in sign, to the integrated strength of the sources distributed along the entire chord of the airfoil.

SIMPLIFICATION AND APPROXIMATE SOLUTION OF THE INTEGRAL EQUATIONS

No general methods are known for the analytical solution of the integral equations given in equations (A8), (A14), (A20), and (A21). Although certain simplifications can be made by restricting attention to nonlifting cases, and to cases in which the shock waves are not in the region of dependence, the essential difficulties remain because the integral equations are nonlinear, just as is the differential equation from which they are derived. The principal method that has been employed in the past for the solution of similar problems is that of successive approximation in which φ is expanded in a power series of some parameter such as the thickness ratio, and the coefficients in this series are determined as the solution develops. The first approximation in these methods is generally either the solution for linearized compressible flow theory or for incompressible flow, and the second and higher approximations are determined by iteration procedures in which linear equations are solved at every step. In practice, these methods have been found very difficult to apply to problems of compressible flow, and calculations of higher approximations than the second have, in most cases, proved prohibitively lengthy. (See ref. 3 for a résumé.) Serious questions of convergence remain in the existing solutions of this type, and it is doubtful if the results apply when mixed subsonic-supersonic flow occurs.

Another type of successive approximation procedure which involves the solution of quadratic equations with every iteration step is described in reference 9 and applied to the calculation of pressure distributions on circular-arc airfoils for all Mach numbers up to unity. Although the calculations could only be accomplished after the introduction of certain approximations, whose influence on the result is difficult to ascertain, the general procedure appears to succeed even with the occurrence of mixed flow.

The methods applied in the main text of this paper can be considered as the first step of still another type of successive approximation procedure in which certain nonlinear features are incorporated into even the first approximation. This procedure possesses the advantage of yielding results that disclose much of the nonlinear effects in the first approximation, and of making unnecessary, in many applications, the difficult task of iteration to determine higher approximations. A simple heuristic description of the analysis is given in the main text. The following paragraphs are concerned with a more detailed examination of the approximations involved in the analysis, and of the relationship between the present approximation and the approximations previously employed in the solution of problems of compressible flow. Although it is apparent that much of the discussion could be applied to lifting airfoils, attention is confined, as in the main text, to symmetrical nonlifting airfoils for which the following relations are to be applied in the first term of each integral equation:

$$\Delta\varphi=0, \qquad \Delta\frac{\partial\varphi}{\partial\zeta}=2U_\infty\frac{dZ}{d\xi} \tag{A26}$$

HYPERBOLIC CASE

The first problem to be discussed is the approximate solution of the integral equation given in equation (A8) for the hyperbolic case under the restrictions that the flow is purely supersonic so that

$$M_\infty^2-1+ku>0 \tag{A27}$$

Equation (A8) contains both a line integral over the shock wave $\bar{S}_H$ and a double integral over the surrounding region $\bar{R}_H$. The double integral can be integrated x-wise, however, because the integrand is a perfect differential. This partial integration results in a term that exactly cancels the line integral on the shock wave and equation (A8) can be rewritten as follows:

$$\varphi(x,z)=-\frac{U_\infty}{\sqrt{\lambda_H}}\int_0^{x-\sqrt{\lambda_H}|z|}\frac{dZ}{d\xi}\,d\xi-\frac{1}{2\sqrt{\lambda_H}}\int_>u\left(M_\infty{}^2-1+\frac{ku}{2}-\lambda_H\right)d\zeta \qquad \text{(A28)}$$

The symbol $>$ below the integral sign of the second term indicates that the integration is to be carried over the lines $\xi=x-\sqrt{\lambda_H}(|z-\zeta|)$ extending upstream from x,z. Differentiation yields the following relations for u and $\partial u/\partial x$:

$$u(x,z)=-\frac{U_\infty}{\sqrt{\lambda_H}}Z'(x-\sqrt{\lambda_H}|z|)-\frac{1}{2\sqrt{\lambda_H}}\frac{\partial}{\partial x}\int_>u\left(M_\infty{}^2-1+\frac{ku}{2}-\lambda_H\right)d\zeta \qquad \text{(A29)}$$

$$\frac{\partial u(x,z)}{\partial x}=-\frac{U_\infty}{\sqrt{\lambda_H}}Z''(x-\sqrt{\lambda_H}|z|)-\frac{1}{2\sqrt{\lambda_H}}\frac{\partial^2}{\partial x^2}\int_>u\left(M_\infty{}^2-1+\frac{ku}{2}-\lambda_H\right)d\zeta \qquad \text{(A30)}$$

It should be noted that equations (A28), (A29), and (A30) are all integral equations and that each is an exact relation valid for any positive value of λ_H.

The results of linearized supersonic flow theory, as well as those of the counterpart, in the small disturbance theory of transonic flow, of higher approximations can be reproduced from any of the above equations upon equating λ_H to $M_\infty{}^2-1$. In this way, all contributions of first order are included in the first term on the right and the contribution of the second term on the right is, at most, of second order. Thus, the familiar expression of linearized supersonic flow theory follows immediately upon disregarding the contribution of the second term

$$u(x,z)=-\frac{U_\infty}{\sqrt{M_\infty{}^2-1}}Z'\,(x-\sqrt{M_\infty{}^2-1}|z|)+0(u^2) \qquad \text{(A31)}$$

Its counterpart, correct to second order in Z', can be determined by application of the method of successive approximations in which the contribution of the second term is approximated by replacing the unknown u by the first-order approximation provided by equation (A31) and integrating. In this way, the following result is obtained for points on the airfoil.

$$u(x,0)=-\frac{U_\infty}{\sqrt{M_\infty{}^2-1}}\frac{dZ}{dx}-\frac{kU_\infty{}^2}{4(M_\infty{}^2-1)^2}\left(\frac{dZ}{dx}\right)^2+0\left(\frac{dZ}{dx}\right)^3 \qquad \text{(A32)}$$

Note that although the first- and second-order approximations for u are different in general, first-order theory is sufficient to determine to second-order accuracy the point where u vanishes, that is where $dZ/dx=0$. First-order theory, moreover, provides the exact location for the point of zero u in the absence of shock waves, but this simple result is true only to second order if there are shock waves situated within the Mach forecone of the point $(x,0)$. Although the difficulties of integration are such that only the first few steps of the method of successive approximation can be evaluated in all but the simplest examples, the method can, in principle at least, be repeated indefinitely to establish the result accurate to any desired order. The result for u on the airfoil surface appears in the form of a power series involving ascending powers of $(dZ/dx)/(M_\infty{}^2-1)^{3/2}$. It is clear that a valid approximation is obtained provided the absolute value of dZ/dx is sufficiently small at all points, and the Mach number is not too close to unity. The failure associated with excessive positive values for dZ/dx usually occurs near the leading edge of the airfoil and is associated physically with detachment of the bow wave and the occurrence of local regions of subsonic flow. The failure associated with excessive negative values for dZ/dx, and clearly illustrated in figure 3 of the main text, usually occurs near the trailing edge of the airfoil and is purely mathematical in origin. In actual practice where only the first term or two may be evaluated, the result fails to provide adequate information regarding the ultimate convergence or divergence of the series and the question must be settled in each application by appeal to more exact solutions. It is important to realize that these uncertainties are not inherent in the integral equations given in equations (A28) through (A30), but enter the analysis with the assumption that the solution can be approximated satisfactorily by application of the particular form of the method of successive approximation described above.

The method of analysis employed throughout the main text is equivalent, from the present point of view, to the first step of a slightly different method of successive approximation that proceeds from consideration of the infinite set of relations that result if different values are selected for λ_H in the determination of conditions at different points in space. Analyses based on such a system of equations are more complex, in general, than those based on a single equation, but this increase in complexity is counterbalanced, in the present applications, by the fact that approximations can be introduced on the basis of local, rather than global, considerations. This fact makes possible the incorporation of some of the higher order or nonlinear contributions, as well as all of the first-order contributions, into the first term on the right in each relation of the infinite set, thereby reducing the contribution of the term containing the unknown u (ξ,ζ). If a rule for the selection of λ_H can be found that achieves this effect and if it can be expressed in analytic form, the infinite set of relations can be expressed once again in the form of a single equation; and the remainder of the analysis can proceed in a manner analogous to that described in the preceding paragraph for the classical method of successive approximation.

The method employed in the analysis of the hyperbolic case in the main text of this paper is equivalent to the first step of a successive approximation procedure based on the infinite set of equations for $\partial u/\partial x$ typified by equation (A30)

with λ_H equated to the local value of $M_\infty^2-1+ku(x,z)$ in each relation. Although it would appear from cursory examination of equation (A30) that the error incurred in so doing would be of second order, it will be demonstrated below that the result is actually accurate to second order and that the error is, at most, of third order. Although equations (A29) and (A30), upon which the remainder of the discussion of the hyperbolic case is based, are exact within the approximations of transonic flow theory, they are not in the most advantageous form for the following discussion because of the presence of the integral in the second term of each relation. If, however, attention is confined to the evaluation of the result at the airfoil surface to second-order accuracy, and to cases for which λ_H is restricted to values that differ from M_∞^2-1 by, at most, a quantity proportional to $u(x,z)$, that is $\lambda_H=M_\infty^2-1+au(x,z)$, the integrals can be integrated and the following relations result:

$$u(x,0)=-\frac{U_\infty}{\sqrt{\lambda_H}}\frac{dZ}{dx}-\frac{u\left(M_\infty^2-1+\frac{ku}{2}-\lambda_H\right)}{2(M_\infty^2-1)}+0(u^3) \quad \text{(A33)}$$

$$\frac{\partial u(x,0)}{\partial x}=-\frac{U_\infty}{\sqrt{\lambda_H}}\frac{d^2Z}{dx^2}-\frac{u_x(M_\infty^2-1+ku-\lambda_H)}{2(M_\infty^2-1)}+0(u^3) \quad \text{(A34)}$$

It is now clear that the substitution of M_∞^2-1+ku for λ_H in equation (A34) yields

$$\frac{\partial u(x,0)}{\partial x}=-\frac{U_\infty}{\sqrt{M_\infty^2-1+ku}}\frac{d^2Z}{dx^2}+0(u^3) \quad \text{(A35)}$$

This result corresponds to equation (11) of the main text and leads, upon integration and insertion of the auxiliary relation that u vanishes where dZ/dx is zero, to equation (15) relating C_p and dZ/dx. This relationship is commonly designated as that of simple wave theory. From the above discussion, it is clear that equation (15) must be correct to at least second order, as indeed simple wave theory is known to be for the pressures on the surface of an airfoil. If there are no shock waves in the region influencing conditions at the point $(x,0)$, the flow field is characterized by a single family of waves; and it can be shown that the error term indicated in equation (A35) vanishes completely. The resulting relation is thus exact within the approximation of transonic flow theory. It is interesting to observe that the use of the same relation for λ_H in equation (A29) for u leads to

$$u=-\frac{U_\infty}{\sqrt{M_\infty^2-1+ku}}\frac{dZ}{dx}+\frac{ku^2}{4(M_\infty^2-1)}+0(u^3) \quad \text{(A36)}$$

and results in errors of second order if only the first term is used.

There is another choice for λ_H that is not mentioned in the main text that will remove the second-order error if only the first term of equation (A29) or (A33) for u is used and that is $\lambda_H=M_\infty^2-1+(ku/2)$, since then

$$u=-\frac{U_\infty}{\sqrt{M_\infty^2-1+\frac{ku}{2}}}\frac{dZ}{dx}+0(u^3) \quad \text{(A37)}$$

This result is not the same as that of simple wave theory, but is recognized upon rearranging so that

$$u\sqrt{M_\infty^2-1+\frac{ku}{2}}=-U_\infty\frac{dZ}{dx} \quad \text{(A38)}$$

as being the square root, with appropriate choice of sign, of the shock relation given in equation (6) with u_a and w_a equated to zero. The result obtained by use of equation (A38) is thus equivalent to that obtained by equating the pressure at each point of the airfoil surface to that on a tangent wedge. Such a procedure has been proposed previously and is sometimes called "tangent-wedge theory." Although the first two terms of the formal expansion of either equation (A38) of tangent-wedge theory or equation (14) of simple wave theory agree with the second-order result obtained by use of the method of successive approximations and given in equation (A32), the results of either simple wave theory or tangent-wedge theory are to be preferred in applications because they approximate the proper termination of the solution when dZ/dx becomes too large, and do not fail spuriously at larger negative values of dZ/dx.

ELLIPTIC CASE

The second problem to be discussed is the approximate solution of the integral equation given in equation (A14) under the restriction that the flow is purely subsonic so that

$$1-M_\infty^2-ku>0 \quad \text{(A39)}$$

This restriction implies that the integral over $\overline{S}_E$ is zero, since there are no shock waves in a purely subsonic flow. Thus, equation (A14) reduces to

$$\varphi(x,z)=2U_\infty\int_0^c\sigma_E\frac{dZ}{d\xi}d\xi+\int_{-\infty}^{+\infty}\int f_E\sigma_E d\xi\,d\zeta \quad \text{(A40)}$$

Differentiation yields the following relations for u and $\partial u/\partial x$

$$u(x,z)=2U_\infty\int_0^c\frac{\partial\sigma_E}{\partial x}\frac{dZ}{d\xi}d\xi+\int_{-\infty}^{+\infty}\int f_E\frac{\partial\sigma_E}{\partial x}d\xi\,d\zeta \quad \text{(A41)}$$

$$\frac{\partial u(x,z)}{\partial x}=2U_\infty\int_0^c\frac{\partial^2\sigma_E}{\partial x^2}\frac{dZ}{d\xi}d\xi+\int_{-\infty}^{+\infty}\int f_E\frac{\partial^2\sigma_E}{\partial x^2}d\xi\,d\zeta \quad \text{(A42)}$$

where

$$\sigma_E=\frac{1}{2\pi\sqrt{\lambda_E}}ln\sqrt{(x-\xi)^2+\lambda_E(z-\zeta)^2}$$

$$\frac{\partial\sigma_E}{\partial x}=\frac{1}{2\pi\sqrt{\lambda_E}}\frac{x-\xi}{[(x-\xi)^2+\lambda_E(z-\zeta)^2]}$$

$$\frac{\partial^2\sigma_E}{\partial x^2}=-\frac{1}{2\pi\sqrt{\lambda_E}}\frac{(x-\xi)^2-\lambda_E(z-\zeta)^2}{[(x-\xi)^2+\lambda_E(z-\zeta)^2]^2}$$

$$f_E=\left\{\lambda_E-[1-M_\infty^2-ku(\xi,\zeta)]\right\}\frac{\partial u}{\partial\xi}$$

Equations (A40), (A41), and (A42) are all integral equations and each is exact for any positive value for λ_E. The solution of any of these integral equations is complicated not only because the relations are nonlinear, but also because the kernel, designated by σ_E or its derivative, is infinite at the point $\xi=x$, $\zeta=z$.

The familiar result of linearized subsonic flow theory can be obtained from any of the above equations by replacing λ_E by $1-M_\infty^2$ and disregarding the contribution of the double integral as being of higher order. The corresponding result, correct to second order, can be obtained by application of the method of successive approximations in which the contribution of the double integral is approximated by means of the first-order result to evaluate f_E at each point. Higher approximations can be obtained, at least in principle, by repeated application of the same procedure except that f_E is evaluated at each step by use of the results of the next lower approximation. In this way, an approximate expression for the solution is determined in the form of a truncated power series. Although the difficulties of integration are so great that few cases have been evaluated beyond the second approximation, it appears that the process converges to the desired solution for thin airfoils provided that certain well-known difficulties associated with stagnation points are properly accounted for and that, as in the hyperbolic case, the Mach number is not too close to unity. Again the results provided by the method of successive approximation indicate no definite limit for the Mach number. Comparison with experimental results shows that the trends displayed by the results are generally confirmed for Mach numbers less than the critical Mach number, but are essentially refuted for greater Mach numbers.

It is interesting and informative to compare the results obtained in the manner described above with those obtained by application of an alternative version of the method of successive approximations described in reference 9 that involves the solution of quadratic rather than linear algebraic equations at each step of the iteration process. The equation fundamental to this discussion is obtained from equation (A41) by again equating λ_E to $1-M_\infty^2$ and integrating the double integral by parts. In this way the following integral equation is determined for u:

$$u-\frac{k}{1-M_\infty^2}\frac{u^2}{2}=2U_\infty\int_0^c\frac{\partial\sigma_E}{\partial x}\frac{dZ}{d\xi}\,d\xi-k\int_{-\infty}^{+\infty}\int\frac{u^2(\xi,\zeta)}{2}\frac{\partial^2\sigma_E}{\partial x^2}\,d\xi\,d\zeta \tag{A43}$$

Although equation (A43) is completely equivalent to equation (A41), it is, in certain respects, superior from the point of view of obtaining approximate solutions. This is because the predominant effects of the region near the point x,z, which form a major contribution to the value of the integral in equation (A41), are furnished in equation (A43), by the term involving the square of u standing outside the integral. Although the difficulties of integration are as great or greater than encountered in the classical method of successive approximations and only the first few steps can be evaluated without approximation in any specific application, certain general features of the solution are clearly defined. In particular, it is shown in the report version of reference 9 that the results obtained for flows that are subsonic everywhere converge, in the limit of an infinite number of iteration steps, to the same result as ultimately obtained by application of the classical method of successive approximation. Whereas there is considerable doubt about the precise range of convergence of the latter result, the result obtained by application of the quadratic method of successive approximation clearly terminates with the occurrence of sonic velocity somewhere in the flow. The termination of the solution is recognized by the disappearance of real roots of the quadratic equation and is apparent at every step of the iteration process. It is evident, moreover, from comparison of the two sets of results that the series expansion for the solution obtained by the classical method of successive approximation converges only for purely subsonic flows and that the results indicated for mixed or transonic flows are false. These properties of the result obtained by the quadratic method of successive approximation are consistent with the numerous arguments and proofs for the nearly nonexistence of continuous shock-free transonic flows that have been advanced in recent years. (See ref. 46 for a brief résumé.)

This difference in behavior can be readily illustrated if one considers the expressions for the pressure coefficient at the midpoint of a symmetrical circular-arc airfoil that are obtained following the completion of the first two steps of each iteration process. The result provided by use of the classical method can be readily obtained from the third-order result quoted in equation (37) of the main text and is

$$C_p=-\frac{8}{\pi}\frac{\tau}{\sqrt{1-M_\infty^2}}-\left(\frac{10}{\pi^2}-\frac{1}{2}\right)\frac{(\gamma+1)M_\infty^2}{(1-M_\infty^2)^2}\tau^2+0(\tau^3) \tag{A44}$$

The first term represents the result obtained if one considers equation (A41) and disregards completely the contribution of the double integral. The result is precisely that of linearized compressible flow theory for the particular point under discussion. The second term represents an approximation for the contribution of the double integral obtained by replacing f_E for each point in space with the result provided by linearized theory. The results obtained by application of equation (A44) indicate that $-C_p$ increases indefinitely with increasing value of $\tau/(1-M_\infty^2)^{3/2}$ and appear to apply for mixed, or transonic, flows as well as for purely subsonic flows. The corresponding results obtained by use of the quadratic method of successive approximation are found by consideration of equation (A43). A first approximation obtained by disregarding completely the contribution of the double integral is

$$C_p=-\frac{2(1-M_\infty^2)}{M_\infty^2(\gamma+1)}\left[1-\sqrt{1-\frac{8}{\pi}\frac{M_\infty^2(\gamma+1)}{(1-M_\infty^2)^{3/2}}\tau}+0(\tau^2)\right] \tag{A45}$$

and a second approximation obtained from the evaluation of the contribution of the double integral by use of the result provided by linearized theory for f_E at each point is

$$C_p=-\frac{2(1-M_\infty^2)}{M_\infty^2(\gamma+1)}\left[1-\sqrt{1-\frac{8}{\pi}\frac{M_\infty^2(\gamma+1)}{(1-M_\infty^2)^{3/2}}\tau+\left(\frac{6}{\pi^2}+\frac{1}{2}\right)\frac{M_\infty^4(\gamma+1)^2}{(1-M_\infty^2)^3}\tau^2+0(\tau^3)}\right] \tag{A46}$$

The results obtained by application of either equation (A45) or (A46) also indicate that $-C_p$ increases with increasing values of $\tau/(1-M_\infty^2)^{3/2}$, but that this trend terminates when C_p reaches the critical value associated with the occurrence of sonic velocity, that is, when

$$C_p=-\frac{2(1-M_\infty^2)}{M_\infty^2(\gamma+1)}=C_{p_{cr}} \tag{5}$$

At this point, the slope of a curve representing the variation of C_p with M_∞ is infinite. In spite of these distinct differences in behavior, it is important to note that a formal power series expansion of equation (A46) in terms of τ agrees to second order with equation (A44), and that this agreement increases by one order of τ upon the completion of each additional iteration step. Results obtained following completion of additional iteration steps continue to follow the same trends. Those indicated by the classical method never provide any information regarding the precise range of convergence, and those indicated by the quadratic method always terminate with the occurrence of sonic velocity.

The method employed in the main text can be considered as an alternative procedure devised in any attempt to improve the quality of the first approximation and to diminish thereby some of the necessity for the evaluation of higher approximations. Before proceeding, it is important to recall that equations (A40), (A41), and (A42) are all integral equations valid for any positive value for λ_E; and that each can be considered, in the same way as described for the hyperbolic case, as a typical member of an infinite set of relations that result if different values are selected for λ_E in the determination of conditions at different points in space. It appears plausible that an increase in the accuracy, although not the mathematical order, of the first approximation might occur if λ_E is equated not to simply $1-M_\infty^2$, but to $1-M_\infty^2-ku(x,z)$ because then the function f_E in the double integral of each integral equation reduces to $k[u(x,z)-u(\xi,\zeta)](\partial u/\partial\xi)$ and hence vanishes at the point $\xi=x$, $\zeta=z$ where σ_E, $\partial\sigma_E/\partial x$, or $\partial^2\sigma_E/\partial x^2$ are infinite. If this procedure is applied to equation (A40) or (A41) for φ or u, and only the contribution of the single integral is retained, it is clear that the desired improvement will not be obtained for all Mach numbers up to the critical because the function $\sqrt{1-M_\infty^2-ku}$ that appears in the denominator of each term vanishes with the occurrence of sonic velocity, and the numerator does not vanish simultaneously. It is interesting to note, nevertheless, that the result for the pressure coefficient on the airfoil surface that is obtained in this way from equation (A41), that is,

$$C_p(x,0)=\frac{C_{p_i}(x,0)}{\sqrt{1-M_\infty^2+\frac{kU_\infty}{2}C_p}}=\frac{C_{p_i}(x,0)}{\sqrt{1-M^2}} \tag{A47}$$

corresponds to the use of the local, rather than free-stream, Mach number in the Prandtl-Glauert rule; and that this result is the counterpart, in transonic small disturbance theory, of an approximation proposed by Laitone, Szebehely, and Truitt (refs. 47 through 51). It is immediately apparent that although this result differs from the Prandtl-Glauert rule in the same direction as the higher order approximations, the effects of compressibility are greatly overestimated at points where the local velocity approaches sonic velocity. A typical set of results illustrating this statement is shown in figure 40 in which are repeated the curves of figure 8 showing the variation of C_p with M_∞ at the midpoint of a 10-percent-thick circular-arc airfoil together with the corresponding curve calculated by use of equation (A47).

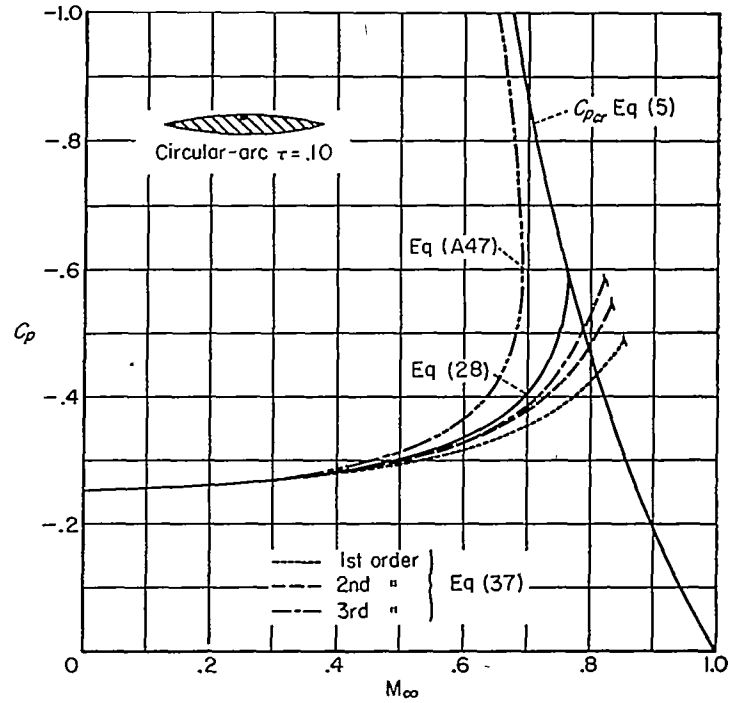

FIGURE 40.—Variation of C_p with M_∞ at the midpoint of a circular-arc airfoil, as indicated by equation (A47), by present theory, and by the method of successive approximations.

The relations developed in the discussion of the elliptic case in the main text do not encounter any such difficulties as the local Mach number approaches unity. The difference in behavior is a consequence of the fact that the latter results are based on the equation for $\partial u/\partial x$ rather than that for φ or u. That such a difference might occur can be seen by examination of equation (A42). The denominator again approaches zero as the local Mach number approaches 1, but the numerator is always zero at the point of maximum velocity. Since sonic velocity is first encountered with increasing Mach number at the point of maximum velocity, it is apparent that an indeterminate form occurs at the critical Mach number and the possibility at least exists that the gain sought by forcing f_E to be zero at the point where $\partial^2\sigma_E/\partial x^2$ is infinite will be realized. That a gain in accuracy, although not the mathematical order, of the solution is actually attained by this procedure is shown in the main text by comparison with existing higher approximations. Further confirmation of this conclusion is shown by the comparison illustrated in figure 41 in which the curves of figure 8 showing the variation with M_∞ of C_p at the midpoint of a 10-percent-thick circular-arc airfoil are repeated together with the curves calculated by use of equations (A45) and (A46) representing the first two approximations furnished by the quadratic method of successive approximations.

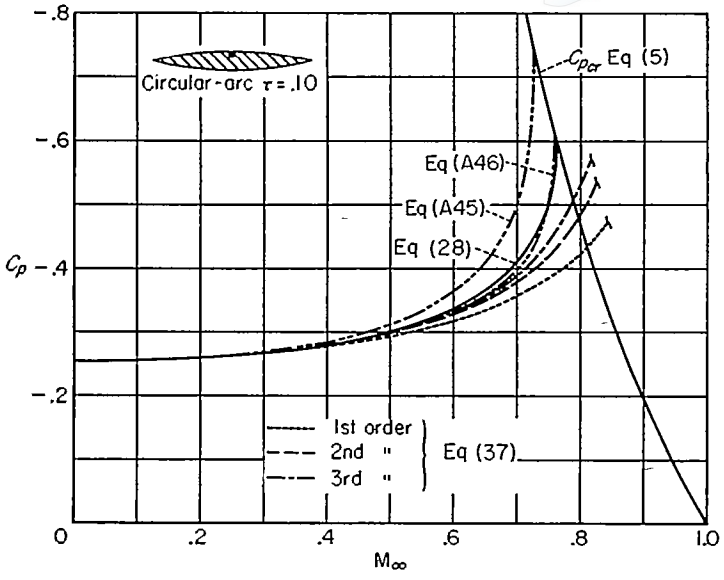

FIGURE 41.—Variation of C_p with M_∞ at the midpoint of a circular-arc airfoil, as indicated by present theory and by two alternative methods of successive approximations.

PARABOLIC CASE

The third problem to be discussed is the approximate solution of the integral equations for the parabolic case under the restriction that the free-stream Mach number is near unity. Two integral equations are given depending on whether λ_P is positive or negative. Inasmuch as no use is made in the main text of the equation for negative λ_P, the following remarks will be confined to the case for positive λ_P, for which the integral equation is given by equation (A20):

$$\varphi(x,z)=-\frac{2U_\infty}{\lambda_P}\int_0^x \sigma_P \frac{dZ}{d\xi}d\xi-\frac{1}{\lambda_P}\iint_{\overline{R}_P}\sigma_P f_P d\overline{R}_P-$$

$$\frac{1}{\lambda_P}\int_{\overline{S}_P}\sigma_P\left(\frac{\partial\varphi_b}{\partial\zeta}-\frac{\partial\varphi_a}{\partial\zeta}\right)\cos(n_b,z)dS \quad \text{(A48)}$$

where

$$\sigma_P=\sqrt{\frac{\lambda_P}{4\pi(x-\xi)}}\,e^{\left[-\frac{\lambda_P(z-\zeta)^2}{4(x-\xi)}\right]}$$

$$f_P=(M_\infty^2-1)\varphi_{\xi\xi}+(k\varphi_{\xi\xi}-\lambda_P)\varphi_\xi$$

The third term of equation (A48) represents the contribution of sources distributed along the surface of any part of the shock system that is situated upstream of the point x,z. This term has the property of effectively continuing the source distribution of the first term smoothly through a concave corner when the adjacent flow is supersonic. In this way, the singularities in the velocity and pressure that occur at such corners when the adjacent flow is subsonic are replaced, when the adjacent flow is supersonic, by the discontinuous, but finite, jump associated with an oblique shock wave. The contribution of this term vanishes if no part of the shock system is situated upstream of x,z or if the shock wave is parallel to the z axis. In that which follows attention is confined to cases in which it is presumed that one or both of these conditions are satisfied for all points situated upstream of the trailing edge. The integral over the shock waves thus contributes nothing to φ at any point on the airfoil surface, and the remainder of the discussion will proceed with considerations involving only the first two terms of equation (A48), and with the corresponding equation for u obtained therefrom by differentiation with respect to x. These two equations reduce to the following forms for points on the airfoil surface (i. e., $z=0$):

$$\varphi(x,0)=-\frac{U_\infty}{\sqrt{\pi\lambda_P}}\int_0^x\frac{dZ/d\xi}{\sqrt{x-\xi}}d\xi-\frac{1}{\lambda_P}\iint_{\overline{R}_P}\sigma_P f_P d\overline{R}_P \quad \text{(A49)}$$

$$u(x,0)=-\frac{U_\infty}{\sqrt{\pi\lambda_P}}\frac{\partial}{\partial x}\int_0^x\frac{dZ/d\xi}{\sqrt{x-\xi}}d\xi-\frac{f_P}{\lambda_P}-\frac{1}{\lambda_P}\iint_{\overline{R}_P}f_P\frac{\partial\sigma_P}{\partial x}d\overline{R}_P \quad \text{(A50)}$$

where

$$\sigma_P=\sqrt{\frac{\lambda_P}{4\pi(x-\xi)}}\,e^{\left[-\frac{\lambda_P\zeta^2}{4(x-\xi)}\right]}$$

$$\frac{\partial\sigma_P}{\partial x}=\sqrt{\frac{\lambda_P}{4\pi(x-\xi)^3}}\left[\frac{1}{2}+\frac{\lambda_P\zeta^2}{4(x-\xi)}\right]e^{\left[-\frac{\lambda_P\zeta^2}{4(x-\xi)}\right]}$$

It can be seen from examination of the preceding relations that the integral equations for the parabolic case are nonlinear and singular just as are the integral equations for the elliptic case. The following discussion of the approximate solution of the equations for the parabolic case will proceed, therefore, through applications of considerations that are very similar to those described in the discussion of the elliptic case in the preceding section.

The results found by application of the linearized theory for sonic flow described in references 23 through 28 follow from equation (A49) or (A50) by equating f_P to zero so that

$$u(x,0)=-\frac{U_\infty}{\sqrt{\pi\lambda_P}}\frac{\partial}{\partial x}\int_0^x\frac{dZ/d\xi}{\sqrt{x-\xi}}d\xi \quad \text{(A51)}$$

and selecting a value for λ_P. Various means have been proposed for the selection of an appropriate value for λ_P. In reference 28, the only one of the above references that pertains directly to two-dimensional flows, Maeder and Thommen suggest that λ_P be determined by equating it to the value for $k\partial u/\partial x$, obtained by differentiating equation (A51), that occurs at the point along the chord at which u is a maximum in incompressible flow. As noted in the main text in the discussion of the solution for the wedge, the results obtained by application of this linearized theory for sonic flow past thin airfoils may be at considerable variance with other theoretical and experimental results. A further illustration of this statement is provided in figure 42 in which the results given in figures 16, 18, and 19 for the circular-arc airfoil and the two related airfoils that have the point of maximum thickness at 30- and 70-percent chord are repeated together with the corresponding results obtained by application of the procedures described in reference 28. It can be seen upon comparison of these results with the experimental results shown in figures 16, 18, and 19 that the agreement between the pressure distribution calculated by application of the linearized theory for sonic flow and that measured experimentally deteriorates as the pressure gradient departs from a constant. It is apparent from equation (A51) that the accuracy cannot be improved

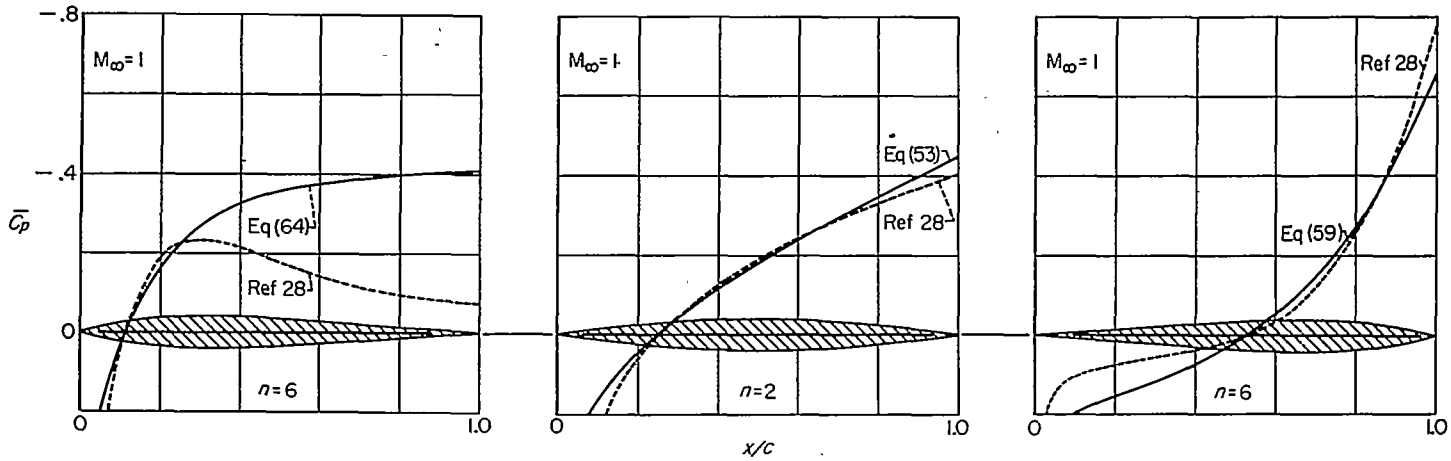

FIGURE 42.—Comparison of pressure distributions as indicated by present theory and by linearized transonic flow theory; $M_\infty = 1$.

in any essential manner by the adoption of a different rule for the selection of an appropriate value for λ_P. This follows from the fact that the entire curve representing the pressure distribution is proportional to $1/\sqrt{\lambda_P}$ and can be altered in scale, but not in form, by use of other values for λ_P. Possibilities for iteration always exist, and it is conceivable that improvements in accuracy could be attained by inserting the solution of linearized sonic flow theory into the terms involving f_P in equation (A49) or (A50) to obtain a second approximation, etc. To do so would be a laborious task and there is always present a grave danger that the process will diverge, or not converge sufficiently rapidly to be useful, when the first approximation is as far from the proper solution as may be inferred from figure 42 for the airfoil with maximum thickness at 30-percent chord.

The procedures employed in the main text for the approximate solution of the equations for the parabolic case closely parallel those used for the approximate solution of the equations for the hyperbolic and elliptic cases. It is, consequently, not surprizing that the following discussion of these procedures from the point of view of the integral equations given in equations (A49) and (A50) is very similar to that in the preceding sections of the Appendix. The general considerations are the same in all three cases, but the parabolic case more closely resembles the elliptic case than the hyperbolic case because of the singular nature of the kernel in the double integral; that is, σ_P and σ_E approach infinity at the point $\xi=x$, $\zeta=z$. The expressions applied in the main text follow from consideration of equation (A50) as a typical member of an infinite set of relations that result if λ_P is replaced with the local value of $k\partial u/\partial x$ and the contribution of the double integral is disregarded. At free-stream Mach number 1, the function f_P thus reduces to zero at the point where σ_P is infinite, and it again appears plausible that less loss in accuracy is incurred by disregarding the contribution of the double integral than in alternative procedures in which f_P is not zero at this point. At free-stream Mach numbers different from unity, f_P is not zero although it can be made as small as desired by approaching sufficiently closely to free-stream Mach number 1. The results obtained by solution of the remaining relation, which is a first-order nonlinear ordinary differential equation, are completely consistent with the above remarks. The pressure distributions calculated by use of only the first approximation are indeed in good accord with existing theoretical and experimental results, and the initial variation of C_p with M_∞ at free-stream Mach number 1 is given exactly; but no indication is provided of the subsequent variation of C_p with M_∞ at Mach numbers considerably removed from unity.

If, on the other hand, the pressure distribution is calculated by substitution of $k\varphi_{xx}$ for λ_P in equation (A49) and differentiation of the resulting expression to obtain an equation for u, the function in the double integral that corresponds to f_P in the above discussion does not vanish at the point $\xi=x$, $\zeta=z$ where the kernel is infinite. If the preceding discussion can be considered to imply that the effective removal of the singularity is important in the approximate solution of singular integral equations, it may be anticipated that the results obtained using equation (A49) will not, in general, be so good as those obtained following the procedure employed in the main text.

REFERENCES

1. Heaslet, Max. A., and Lomax, Harvard: Supersonic and Transonic Small Perturbation Theory. Sec. D of General Theory of High Speed Aerodynamics. Vol. VI of High Speed Aerodynamics and Jet Propulsion, W. R. Sears, ed., Princeton Univ. Press, 1954.
2. Ward, G. N.: Linearized Theory of Steady High-Speed Flow. Cambridge Univ. Press, 1955.
3. Lighthill, M. J.: Higher Approximations. Sec. E of General Theory of High Speed Aerodynamics. Vol. VI of High Speed Aerodynamics and Jet Propulsion, W. R. Sears, ed., Princeton Univ. Press, 1954.
4. von Kármán, Th.: On the Foundation of High Speed Aerodynamics. Sec. A of General Theory of High Speed Aerodynamics. Vol. VI of High Speed Aerodynamics and Jet Propulsion, W. R. Sears, ed., Princeton Univ. Press, 1954.
5. Spreiter, John R.: On Alternative Forms for the Basic Equations of Transonic Flow Theory. Jour. Aero. Sci., vol. 21, no. 1, Jan. 1954, pp. 70–72.
6. Spreiter, John R.: On the Application of Transonic Similarity Rules to Wings of Finite Span. NACA Rep. 1153, 1953.
7. Vincenti, Walter G., Dugan, Duane W., and Phelps, E. Ray: On Experimental Study of the Lift and Pressure Distribution on a Double-Wedge Profile at Mach Numbers Near Shock Attachment. NACA TN 3225, 1954.
8. Heaslet, Max. A., and Fuller, Franklyn B.: Particular Solutions for Flows at Mach Number 1. NACA TN 3868, 1956.

9. Spreiter, John R., and Alksne, Alberta Y.: Theoretical Predictions of Pressure Distributions on Nonlifting Airfoils at High Subsonic Speeds. NACA Rep. 1217, 1955. (Formerly NACA TN 3096.)
10. Heaslet, Max A., and Spreiter, John R.: Three-Dimensional Transonic Flow Theory Applied to Slender Wings and Bodies. NACA TN 3717, 1956.
11. Spreiter, John R.: Theoretical and Experimental Analysis of Transonic Flow Fields. NACA—University Conference on Aerodynamics, Construction and Propulsion. Vol. II, Aerodynamics. A compilation of the papers presented, Lewis Flight Propulsion Laboratory, Cleveland, Ohio, Oct. 20–22, 1954.
12. Sauer, Robert: Instroduction to Theoretical Gas Dynamics. J. W. Edwards, Ann Arbor, Mich., 1947.
13. Liepmann, Hans Wolfgang, and Puckett, Allen E.: Introduction to Aerodynamics of a Compressible Fluid. John Wiley and Sons, Inc., 1947.
14. Donov, A. E.: Ploskoe Krylo s Ostrymi Kromkami v Sverkhzvukovom Potoke. Izvestiia Akademii NAUK, USSR, 1939, pp. 603–626.
15. Donov, A. E.: A Flat Wing with Sharp Edges in a Supersonic Stream. NACA TM 1394, 1956.
16. Kuo, Y. H., and Sears, W. R.: Plane Subsonic and Transonic Potential Flows. Sec. F of General Theory of High Speed Aerodynamics. Vol. VI of High Speed Aerodynamics and Jet Propulsion. W. E. Sears, ed., Princeton Univ. Press, 1954.
17. Garrick, I. E., and Kaplan, Carl: On the Flow of a Compressible Fluid by the Hodograph Method. I—Unification and Extension of Present-Day Results. NACA Rep. 789, 1944.
18. Van Dyke, Milton D.: Second-Order Subsonic Airfoil Theory Including Edge Effects. NACA Rep. 1274, 1956.
19. Hantzsche, W., and Wendt, H.: Der Kompressibilitätseinfluss für dünne wenig gekrümmte Profile bei Unterschallgeschwindigkeit. Z. a. M. M., Bd. 22, Nr. 2, Apr. 1942, pp. 72–86.
20. Asaka, Saburo: On the Velocity Distribution over the Surface of a Symmetrical Airfoil at High Speeds, II. National Science Report of the Ochanomizu University, vol. 5, no. 1, 1954, pp. 59–78.
21. Asaka, Saburo: Application of the Thin-Wing-Expansion Method to the Flow of a Compressible Fluid Past a Symmetrical Circular Arc Aerofoil. Jour. Phy. Soc. Japan, vol. 10, no. 6, June 1955, pp. 482–492.
22. Asaka, Saburo: Errata: Application of the Thin-Wing-Expansion Method to the Flow of a Compressible Fluid Past a Symmetrical Circular Arc Aerofoil. Jour. Phy. Soc. Japan, vol. 10, no. 7, July 1955, p. 593.
23. Behrbohm, H.: Näherungstheorie des unsymmetrischen Schalldurchgangs in einer Lavaldüse. Z. a. M. M., Bd. 30, Nr. 4, Apr. 1950, pp. 101–112.
24. Behrbohm, H.: Schalldurchgang in zwei-und dreidimensionalen Düsenstromungen. Z. a. M. M., Bd. 30, Nr. 8/9, Aug./Sept. 1950, pp. 268–269.
25. Oswatitsch, K., and Kuene, F.: The Flow Around Bodies of Revolution at Mach Number 1. Proc. Conf. on High-Speed Aeronautics, Polytechnic Institute of Brooklyn, Brooklyn, N. Y., Jan. 20–22, 1955, pp. 113–131.
26. Keune, F.: Bericht über eine Näherungstheorie der Strömung um Rotationskörper ohne Anstellung bei Machzahl Eins. DVL Bericht Nr. 3. Westdeutscher Verlag, Köln und Opladen, 1955.
27. Keune, F.: Über den Kompressibilitätseinfluss bei und nahe Machzahl Eins für Körper kleiner Streckung und schlanke Rotationskörper. Zs. f. Flugwiss. 4 Jahr., Heft 1/2, Jan./Feb. 1956, pp. 47–53.
28. Maeder, P. F., and Thommen, H. U.: Some Results of Linearized Transonic Flow About Slender Airfoils and Bodies of Revolution. Jour. Aero, Sci., vol. 23, no. 2, Feb. 1956, pp. 187–188.
29. Miles, John W.: On Linearized Transonic Flow Theory for Slender Bodies. Jour. Aero. Sci., vol. 23, no. 7, July 1956, pp. 704–705.
30. Bryson, Arthur Earl, Jr.: On Experimental Investigation of Transonic Flow Past Two-Dimensional Wedge and Circular-Arc Sections Using a Mach-Zehnder Interferometer. NACA Rep. 1094, 1952. (Formerly NACA TN 2560.)
31. Liepmann, H. W., and Bryson, A. E., Jr.: Transonic Flow Past Wedge Sections. Jour. Aero. Sci., vol. 17, no. 12, Dec. 1950, pp. 745–755.
32. Guderley, Gottfried, and Yoshihara, Hideo: The Flow Over a Wedge Profile at Mach Number 1. Jour. Aero. Sci., vol. 17, no. 11, Nov. 1950, pp. 723–735.
33. Habel, Louis W., Henderson, James H., and Miller, Mason F.: The Langley Annular Transonic Tunnel. NACA Rep. 1106, 1952.
34. Vincenti, Walter G., and Wagoner, Cleo B.: Transonic Flow Past a Wedge Profile With Detached Bow Wave. NACA Rep. 1095, 1952. (Supersedes NACA TN's 2339 and 2588)
35. Yoshihara, Hideo: On the Flow Over a Finite Wedge in the Lower Transonic Region. WADC Tech. Rep. 56–268, June 1956.
36. Cole, Julian D.: Drag of Finite Wedge at High Subsonic Speeds. Jour. Math. and Phys., vol. 30, no. 2, July 1951, pp. 79–93.
37. Michel, R., Marchaud, F., and Le Gallo, J.: Étude des écoulements transsoniques autour des profils lenticulaires, a incidence nulle. O. N. E. R. A. Pub. No. 65, 1953.
38. Carroll, James B., and Anderson, Gordon F.: Boundary-Layer Effect on Local Mach Number Measurements on a Circular Arc Half Profile. Jour. Aero. Sci., vol. 23, no. 6, June 1956, pp. 604–605.
39. Michel, R., Marchaud, F., and Le Gallo, J.: Influence de la position du maitre-couple sur les écoulements transsoniques autour de profils a pointes. O. N. E. R. A. Pub. No. 72, 1954.
40. Frank, Philip, and v. Mises, Richard: Die Differential-und Integralgleichungen der Mechanik und Physik. Mary S. Rosenberg, New York, 1943.
41. Guderley, K. Gottfried: Singularities at the Sonic Velocity. Tech. Rep. F–TR–1171–ND, Air Materiel Command, U. S. Air Force, June 1948.
42. Michel, R., Marchaud, F., and Le Gallo, J.: Influence d'un point d'inflexion a l'arriere d'un profil en écoulement transsonique. La Recherche Aéronautique, No. 40, Juillet, Aout, 1954, pp 15–19.
43. von Kármán, Th.: Supersonic Aerodynamics—Principles and Applications. Jour. Aero. Sci., vol. 14, no. 7, July 1947, pp. 373–409.
44. Heaslet, Max. A., and Spreiter, John R.: Reciprocity Relations in Aerodynamics. NACA Rep. 1119, 1953.
45. Webster, Arthur Gordon: Partial Differential Equations of Mathematical Physics. G. E. Stechert and Co., New York, 1933.
46. von Kármán, Theodore: Solved and Unsolved Problems of High Speed Aerodynamics. Proc. Conf. on High-Speed Aeronautics, Polytechnic Institute of Brooklyn, Brooklyn, N. Y., Jan. 20–22, 1955, pp. 11–39.
47. Laitone, E. V.: New Compressibility Correction for Two-Dimensional Subsonic Flow. Jour. Aero. Sci., vol. 18, no. 5, May 1951, p. 350.
48. Szebehely, V. G.: Local Compressible Pressure Coefficient. Jour. Aero. Sci., vol. 18, no. 11, Nov. 1951, pp. 772–773.
49. Laitone, E. V.: Use of the Local Mach Number in the Prandtl-Glauert Method. Jour. Aero. Sci., vol. 18, no. 12, Dec. 1951, pp. 842–843.
50. Truitt, Robert Wesley: Analogy of the Special Theory of Relativity to the Study of Compressible Fluid Flow. Bulletin No. 44, Dept. of Engineering Research, North Carolina State College, June 1949.
51. Truitt, Robert Wesley: Prediction of Subsonic Pressure Distributions by the Sound-Space Theory. Bulletin No. 47, Dept. of Engineering Research, North Carolina State College, Sept. 1950.